School of Chemical and Petroleum Engineering

Department of Chemical Engineering

Surface modified nanocarbons for photodegradation of organic pollutants

Li Zhou

This thesis is presented for Degree of

Master of Philosophy

of

Curtin University

April 2016

Declaration

To be best of my knowledge and belief this thesis contains no material previously published by any other person except where due acknowledgement has been made. This thesis contains no material which has been accepted for the award of any other degree of diploma in any university.

Signature:  Date: 02/04/2016

Li Zhou

Acknowledgments

I would like to express my most sincere gratitude to my supervisor, Professor Shaobin Wang, for his warmest and continuous support during my study. He is always supportive, inspirational and patient. I cannot complete this thesis without his intelligence and warm encouragement.

I must also present my deep gratitude to my co-supervisor, Professor Shaomin Liu, whose supports, kindness and knowledge always help me make everything go smoothly during my study.

I am also grateful to all of my group members, especially to Dr. Xiaoguang Duan, and PhD students, Huayang Zhang, Xiaochen Guo, Wenjie Tian, Ping Liang and Jian Kang, who are always ready to help me at various occasions.

I also thank the laboratory technical staff, Jason Wright, Roshanak Doroushi, Anja Werner and Xiao (Jimmy) Hua, for their kindly technical supports during my lab work.

I am also thankful to those undergraduate students who have worked with me on this research.

Lastly and most importantly, I would like to express my gratitude to my family. My special thanks must go to my husband, Dr. Hongqi Sun, and my lovely daughter, Emma Sun. They give me the invaluable support and encouragement during my study. I have no chance to go back to my study without their selfless support.

Abstract

Photocatalysis is a green and powerful technology and the key factor is the efficiency of the photocatalysts. Graphitic carbon nitride (g-C_3N_4), possessing an excellent high thermal stability and unique electronic structure, is a promising metal-free photocatalyst. Great efforts have been made to synthesize g-C_3N_4-based photocatalysts with enhanced photocatalytic activities. This study aims to develop metal-free, visible-light-responsive photocatalysts for water remediation and solar energy conversion based on graphitic carbon nitride. Surface modification and hybridization with metal-free nanocarbons (nanodiamonds and single-walled carbon nanotubes) were employed to extend the absorbance threshold and enhance the photocatalytic efficiency of the prepared photocatalysts.

Various characterization methods were used, such as X-ray diffraction (XRD), UV-vis diffusion, photoluminescence (PL), scanning electron microscopy (SEM), thermogravimetric analysis/differential temperature gradient (TGA/DTG) and N_2 sorption isotherms. The photocatalytic activities of these prepared composites were investigated for photodegradation of organic pollutants in water. The test of photoelectrochemical activity was carried out on an electrochemical workstation. The mechanism was also discussed.

Papers in preparation

Li Zhou, Huayang Zhang, Xiaochen Guo, Hongqi Sun, Shaomin Liu, and Shaobin Wang, Recent advances in development of metal-free photocatalysts, (In preparation).

Li Zhou, Huayang Zhang, Xiaoguang Duan, Hongqi Sun, Shaomin Liu, and Shaobin Wang, Metal-free hybrid photocatalyst of nanodiamond/g-C_3N_4 for photocatalysis and photoelectrochemical applications, (In preparation).

Contents

1

Chapter 1: Introduction and Overview

1.1 Motivation

In recent years, with the rapid development of modern society, water pollution from industrial processes and domestic households has become serious public health concern [1, 2]. Photocatalysis, employment of an additional substance (called photocatalyst) to facilitate the rate of photochemical reactions, has led to a great level of contributions in field of environmental remediation [3]. It can be used for reduction of heavy metals in water, and decomposition of organic compounds in air or water to carbon dioxide, water and other non-toxic ions/groups, with the potential utilization of solar energy.

Currently, the majority of photocatalysts that have been applied widely in research are metal oxides [4], metal sulfides [5], and plasmonic noble metals [6]. During the reactions, metal ions of these photocatalysts might be discharged into water which may induce the secondary water pollution[7], while the metal-free photocatalysts will completely avoid this problem. Hence, this study tends to find some green and eco-friendly photocatalysts based on metal-free materials.

Graphitic carbon nitride, as a promising metal-free photocatalyst, has drawn extensive researchers' interests [8-12], though its photocatalytic efficiency is still at a low level. In the meantime, great efforts have been done to tackle this drawback, while coupling with other nanocarbons appears to be more interesting because the metal-free nature is remained [1, 3].

In this study, different precursors, including melamine, urea, thiourea and D-glucose, were used to synthesize graphitic carbon nitride via a simple method (thermal condensation). The different precursors and reaction parameters were expected to offer a feasible control to the characteristics of graphitic carbon nitride. Afterwards, in order to enhance the photocatalytic activity of graphitic carbon nitride, two kinds of nanocarbons, nanodiamonds (NDs) and single-walled carbon nanotubes (SWCNTs), were used to couple with the graphitic carbon nitride, because both of them exhibited many merits, such as high thermal stability, large specific surface areas, and unique physical properties [13-15].

1.2 Objectives of this research

This research aims at the development of some novel metal-free photocatalysts based on graphitic carbon nitride for photodegradation of organic pollutants in water and solar energy conversion by photoelectrochemical applications. The detailed objectives are defined as below:

a) Investigating the effect of precursors on the photocatalysis and photoelectrochemistry of graphitic carbon nitride;
b) Developing a novel approach for preparation of surface modified graphitic carbon nitride as a metal-free photocatalyst using a solvothermal route;
c) Preparing hybrid photocatalysts based on graphitic carbon nitride and different nanocarbons, such as nanodiamonds and single-walled carbon nanotubes;
d) Comprehensive characterizing the newly prepared photocatalysts; and
e) Applying the prepared hybrid photocatalysts for photodegradation of methylene blue solutions and photoelectrochemical applications under UV-visible light irradiations.

1.3 Thesis structure

This thesis structure is defined as below:

Chapter 1: This chapter briefly introduced the motivations on the metal-free photocatalysts, objectives of this study and the overall thesis structure.

Chapter 2: This chapter presented a comprehensive literature review on the green and sustainable technology of photocatalysis which played an increasingly important role in environmental remediation. It mainly focused on the development of photocatalysts, including both metal and metal-free based materials. And great attentions were paid on the metal-free photocatalysts. Furthermore, it also summarized and discussed the various modification techniques of g-C_3N_4.

Chapter 3: This chapter reported that a series of g-C_3N_4 were prepared by a thermal condensation method using different ratios of combinational precursors including

melamine, urea, thiourea and D-glucose. The photocatalytic activities of these obtained g-C_3N_4 were tested for photodegradation of two aqueous contaminant solutions.

Chapter 4: In this chapter, naodiamond (ND), a kind of nanocarbon, was employed to develop an effective metal-free photocatalyst based on graphitic carbon nitride via a solvothermal method. The synthesis, characterisations, photocatalytic activity and photoelectrochemical performance were illustrated and discussed.

Chapter 5: In this chapter, a series of hybrid photocatalysts derived from graphitic carbon nitride (g-C_3N_4) and single-walled carbon nanotubes (SWCNTs) were synthesized. The prepared samples were investigated for photodegradation of methylene blue solutions and photocurrent generation.

Chapter 6: This chapter concluded the overall work of this research and briefly analyzed the effect of parameters on surface modification of graphitic carbon nitride and nanocarbons as studied in Chapters 4 and5. At last, some perspective applications of g-C_3N_4/NDs and g-C_3N_4/SWCNTs for the future work were proposed.

References

[1] B. Ai, X.G. Duan, H.Q. Sun, X. Qiu, S.B. Wang, Metal-free graphene-carbon nitride hybrids for photodegradation of organic pollutants in water, Catalysis Today, 258 (2015) 668-675.

[2] Y.X. Wang, L. Zhou, X.G. Duan, H.Q. Sun, E.L. Tin, W.Q. Jin, S.B. Wang, Photochemical degradation of phenol solutions on Co_3O_4 nanorods with sulfate radicals, Catalysis Today, 258 (2015) 576-584.

[3] H.Q. Sun, G.L. Zhou, Y.X. Wang, A. Suvorova, S.B. Wang, A New Metal-Free Carbon Hybrid for Enhanced Photocatalysis, Acs Applied Materials & Interfaces, 6 (2014) 16745-16754.

[4] H.Q. Sun, Y. Bai, H.J. Liu, W.Q. Jin, N.P. Xu, Photocatalytic decomposition of 4-chlorophenol over an efficient N-doped TiO_2 under sunlight irradiation, Journal of Photochemistry and Photobiology a-Chemistry, 201 (2009) 15-22.

[5] Z. Khan, T.R. Chetia, A.K. Vardhaman, D. Barpuzary, C.V. Sastri, M. Qureshi, Visible light assisted photocatalytic hydrogen generation and organic dye degradation by CdS-metal oxide hybrids in presence of graphene oxide, Rsc Advances, 2 (2012) 12122-12128.

[6] Z.G. Xiong, L.L. Zhang, J.Z. Ma, X.S. Zhao, Photocatalytic degradation of dyes over graphene-gold nanocomposites under visible light irradiation, Chemical Communications, 46 (2010) 6099-6101.

[7] X.G. Duan, Z.M. Ao, H.Q. Sun, L. Zhou, G.X. Wang, S.B. Wang, Insights into N-doping in single-walled carbon nanotubes for enhanced activation of superoxides: a mechanistic study, Chemical Communications, 51 (2015) 15249-15252.

[8] Y. Zheng, L.H. Lin, B. Wang, X.C. Wang, Graphitic Carbon Nitride Polymers toward Sustainable Photoredox Catalysis, Angewandte Chemie-International Edition, 54 (2015) 12868-12884.

[9] S.W. Cao, J.X. Low, J.G. Yu, M. Jaroniec, Polymeric Photocatalysts Based on Graphitic Carbon Nitride, Advanced Materials, 27 (2015) 2150-2176.

[10] J.J. Zhu, P. Xiao, H.L. Li, S.A.C. Carabineiro, Graphitic Carbon Nitride: Synthesis, Properties, and Applications in Catalysis, Acs Applied Materials & Interfaces, 6 (2014) 16449-16465.

[11] X.C. Wang, S. Blechert, M. Antonietti, Polymeric Graphitic Carbon Nitride for Heterogeneous Photocatalysis, Acs Catalysis, 2 (2012) 1596-1606.

[12] Q.H. Liang, Z. Li, X.L. Yu, Z.H. Huang, F.Y. Kang, Q.H. Yang, Macroscopic 3D Porous Graphitic Carbon Nitride Monolith for Enhanced Photocatalytic Hydrogen Evolution, Advanced Materials, 27 (2015) 4634-4639.
[13] V.N. Mochalin, O. Shenderova, D. Ho, Y. Gogotsi, The properties and applications of nanodiamonds, Nature Nanotechnology, 7 (2012) 11-23.
[14] A. Peigney, C. Laurent, E. Flahaut, R.R. Bacsa, A. Rousset, Specific surface area of carbon nanotubes and bundles of carbon nanotubes, Carbon, 39 (2001) 507-514.
[15] A.A. Kane, K. Loutherback, B.R. Goldsmith, P.G. Collins, High temperature resistance of small diameter, metallic sngle-walled carbon nanotube devices, Applied Physics Letters, 92 (2008).

2

Chapter 2: Literature Review

Abstract

Photocatalysis is a green, feasible and versatile technology that has been widely applied for energy and environmental applications. Bearing the potential for solar energy utilization, extensive investigations have been carried out in the last decades. The fundamental mechanism and most applications were well established in the last century. Currently, the major focus in photocatalysis research is the design and development of photocatalyst materials. This chapter firstly introduces the historic milestones in photocatalysis studies, then a comprehensive survey is made on the various photocatalysts, including TiO_2-based photocatalysts, ZnO and other metal oxides, metal sulfides, metal nitrides, and plasmon photocatalysts. After that, a particular attention is paid on metal-free graphitic carbon nitride (g-C_3N_4), a novel visible light photocatalyst. Various modification techniques of g-C_3N_4 are summarized and analyzed. Some emerging photocatalysts are mentioned. At last, perspectives on photocatalyst design and development are provided.

2.1 Introduction

Human beings have had a long history to utilize solar energy since the discovery of solar energy drying by ancient people. As one of the green, clean and sustainable energy resources inducing no global warning and any contaminations, solar energy has attracted worldwide attention providing about 120,000 TW annually to the Earth. Such an enormous energy source might, at least partially, be the solution to the increasing energy consumption, which would be 27 TW by 2050 and highly likely to reach 43 TW by 2100, as comparison to the current level of 15 TW[1, 2]. The energy crisis, along with the environmental deterioration and climate change from fossil fuel combustion, has propelled the technological developments for versatile solar energy applications. Two main categories, e.g. solar thermal system and photovoltaic system have been operated in industrial processes. The first system includes solar water heating, steam generation, solar drying and dehydration, solar refrigeration and air-conditioning, while the latter one is represented by building-integration photovoltaic, solar electricity for industry, and solar powered water desalination industry[3, 4]. It can be seen that the above applications are mainly based on physical processes.

It is anticipated that solar energy driven chemical processes would be able to greatly extend the application fields. This assumption can be verified by natural photosynthesis, which has literally populated the creatures on the Earth by converting carbon dioxide and water to green plants via harvesting sunlight[5]. Mimicking natural photosynthesis, i.e. artificial photosynthesis, led to the discovery of photocatalysis at the beginning of 1970s. Japanese scientists, Fujishima and Honda, reported that water can be splitted to produce hydrogen and oxygen under irradiations when TiO_2 was used as a semiconductor electrode[6]. Once semiconductor particles are used, on the surface numerous micro photoelectrochemical cells are formed to carry out the chemical reactions based on the effective separation of photoinduced electron-hole pairs[7]. As a result, heterogeneous photocatalysis appeared to be able to play a significant role in the fields.

In typical photocatalysis processes, semiconductor photocatalysts such as TiO_2, ZnO, Fe_2O_3, CdS and ZnS, are firstly activated by incoming photons, provided by either ultraviolet (UV) or visible light irradiations. Once the photon energy equals to or is

higher than that of band gap energy of the semiconductor photocatalyst, an electron can be activated from the valence band (VB) to the conduction band (CB) of the semiconductor, leaving a positively charged hole in the VB. The photoinduced electron-hole pairs will migrate to the surface of the particle, undergoing bulk and surface recombination, and then reacting with the reactants on the surface. The redox potentials of the carriers are determined by the band structure, i.e. the positions of the VB (oxidation potential) and CB (reduction potential) [8]. Such a principle for heterogeneous photocatalysis process has derived a variety of applications.

The historical milestones in photocatalysis are summarized here. Photocatalysis was firstly discovered in 1972 for artificial photosynthesis by splitting of water for hydrogen production.[6] The photocatalytic oxidation ability was then utilized for oxidation or decomposition of organics in contaminated water[9, 10]. Following the idea of water reduction, photocatalytic reduction of carbon dioxide was reported in 1979, demonstrating a novel route for converting CO_2 to hydrocarbons[11]. In 1988, Yamagata et al. reported the photocatalytic oxidation of alcohols on TiO_2 in which oxygen participated in a radical chain mechanism in the oxidation of ethanol to acetaldehyde, opening the venue for selective oxidation of organics[12]. In 1991 photocatalytic gas-phase oxidation of hydrocarbons on TiO_2 and ZnO surfaces was reported by Anpo and co-workers[13]. Inorganic ions or metal ions were also able to be removed by photocatalysis [14, 15]. The photo-induced hydrophilicity has enabled the application of photocatalysis as self-cleaning technology for developing building materials[16]. In fact, this field is the only one that has been commercialized at a reasonable scale. It can be seen that most historical applications were observed on the classical photocatalyst of titanium dioxide[17].

The wide applications of photocatalysis in hydrogen production, CO_2 reduction, degradation, synthesis and self-cleaning in 1970s and 1980s had paved sound fundamentals, leading to a number of excellent review papers published in 1990s. Legrini et al.[18] reviewed different photochemical processes for water treatment, and indicated that the presence of TiO_2 under UV can lead to similar degradation to those with oxidants such as H_2O_2 or O_3. Kamat [19] discussed the photochemistry on nonreactive and reactive surfaces of semiconductors, providing the surface activation

and charge transfer processes and the induced photocatalytic degradation mechanism. Fox and Dulay [20] discussed the mechanism of heterogeneous photocatalysis with particular attention on catalyst preparation, surface group conversion and surface reactions in photocatalysis. Using TiO_2 as a typical photocatalyst, more comprehensive mechanism discussion was reviewed by Linsebigler et al. [8]. The band structure, photoexcitation, separation and migration of photoinduced charges, surface adsorption, photochemistry and modification of TiO_2 surface were introduced. Hoffmann et al[21]. presented an excellent review on the environmental applications of semiconductor photocatalysis with concentration on reaction kinetics of photocatalysis for removal of aqueous and gaseous pollutants. Later on, more review papers focusing on environmental applications of photocatalysis appeared [22-24]. With abovementioned reviews, knowledge base and application implications had been well established.

The practical application of photocatalysis was believed to be restricted by the low efficiency of photocatalysts, i.e. TiO_2. Thereafter, the adventure of photocatalysis was navigated to the development of photocatalyst materials. In this chapter, a comprehensive survey on the photocatalyst materials was made. Particular attention was paid on novel metal-free photocatalyst of graphitic carbon nitride, and its modifications for visible light photocatalysis.

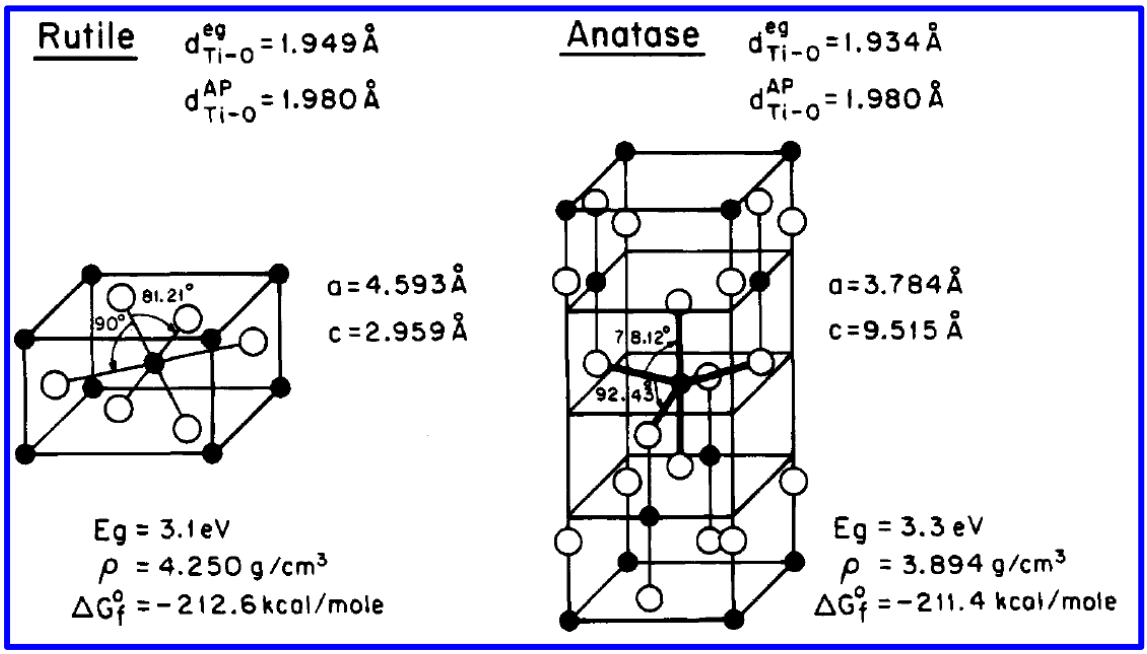

(A)

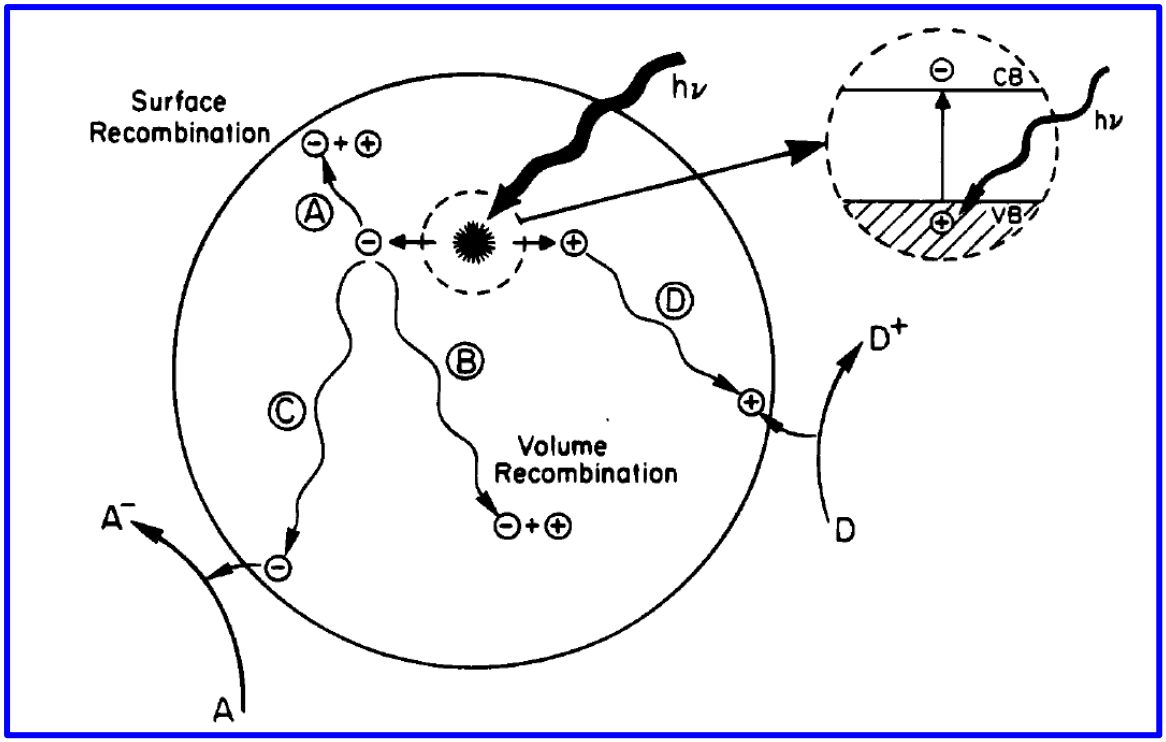

(B)

Fig.2.1 (A) The crystal structures of rutile and anatase TiO_2, and (B) Typical photocatalysis processes on TiO_2[8].

2.2 Metal oxide photocatalysts

2.2.1 TiO_2 and its modified counterparts

Titanium dioxide (TiO_2) is a typical semiconductor having three main crystallographic structures, e.g. brookite, anatase and rutile. Anatase TiO_2, with a band-gap energy of 3.2 eV, has been believed to possess higher photocatalytic activity than rutile, while brookite shows the lowest efficiency. Fig.2.1 (A) shows the two different crystal structures (rutile and anatase) of TiO_2 and Fig. 2.1(B) displays the typical photocatalytic processes on TiO_2 [8]. It is known that the most milestones in photocatalysis were made on TiO_2 [6, 9-12, 14, 15]. Same to any other semiconductor photocatalyst, TiO_2 undergoes photoexcitation, charge separation and surface reactions for a typical photocatalysis process. As a result, enhanced TiO_2 photocatalysis can be achieved by modulating the material for controlling each steps. A variety of modifications have been undertaken.

Surface modification was firstly proven to be effective. Noble metals such as Pt, Au, Pd, Rh and Ag can be deposited on TiO_2 surface [25-27], therefore the charge separation can be promoted for enhanced photocatalysis. Surface sensitization inspired another route which applies an organic dye sensitizer to absorb more photons followed by charge transfer to a semiconductor for photocatalysis. It was reported that some dyes, such as erythrosin B, thionines and different kinds of $Ru(bpy)_3^{2+}$ can be used as efficient sensitizers to harvest visible light for photocatalysis [28-30]. Coupling another lower band-gap semiconductor to TiO_2 could integrate the advantages of surface modification and sensitization by harvesting more photons and inhibiting photoinduced charge recombination. Spanhel et al. [31] reported that illuminated CdS can inject electrons to attached TiO_2, indicating the enhanced activity in photocatalytic applications. It has been demonstrated that metal sulfides such as CdS [32], MoS_2 and WS_2 [33], and some metal oxides [34] can help the TiO_2 composites visible light responsive and more efficient as a photocatalyst.

Compositional modification, i.e. heteroatom doping is also expected to bring out profound influence to TiO_2 photocatalysis. Initially, transition metal ions were extensively employed as a dopant for TiO_2. The introduction of metal ions can lead to formation of new energy levels in the band gap, and sometimes reduce the recombination of the electron-hole pairs[14, 35]. Though extensive studies on transition metal [36-38] or rare earth [39-41] -doped titania had been conducted and reported, some disadvantages of metal doping cannot be avoided. For example, thermal stability of the doped ions is poor. Also the newly created energy bands can also act as recombination centres leading to lower quantum efficiency.

Non-metal doped TiO_2 has attracted extensive attention in TiO_2-based photocatalysis due to the visible light response, which can utilize 42% solar spectrum energy compared to less than 4% from ultraviolet light. In 2001, Asahi et al.[42] reported their synthesis of nitrogen-doped TiO_2 and the application in visible light photocatalysis. Inspired by this excellent work, numerous studies on nitrogen doping have been conducted and reported [43-48]. Based on heteroatom doping, co-doping with nitrogen by metals [49, 50] or non-metals [51-53] have been also investigated. Carbon doped titania was also developed. In 2002, Khan et al. [54] found that carbon doped titania can also show

strong visible light response and enhanced photocatalysis. Carbon-doped TiO_2 prepared by different methods and their different applications were then reported [55-58], as well as its co-doping studies with other elements [52, 59-61]. In addition to nitrogen or carbon doping, other elements, such as sulfur [62-64], phosphorus [65-67], boron [68-71], and halogen elements [72-74] were also used to synthesize visible-light-driven TiO_2 photocatalysts.

With extensive studies, TiO_2 was proposed to be the most suitable candidate for practical applications [17, 75].

2.2.2 ZnO and other metal oxide photocatalysts

ZnO has a similar band-gap energy of 3.2 eV as anatase TiO_2, and has also demonstrated as an efficient photocatalyst. [13, 31, 76-78] In fact ZnO could show a higher photocatalytic activity than TiO_2 [76, 78], yet the stability is poor due to photo-corrosion [79, 80]. For improving the stability, enhancing the photocatalytic activity, and extending the absorption to visible light region, a variety of modification methods, such as semiconductor coupling [81-84], noble metal-[85-88] or transition metal-doping [89-91], and non-metal doping [92-94], have been employed to modify the physicochemical properties of zinc oxide.

Besides TiO_2 and ZnO, some other semiconductor metal oxides have demonstrated effective photocatalysis. Hou et al.[95] reported that β-Ga_2O_3 shows efficient photodegradation of gaseous benzene in air under UV light, with one order of magnitude higher than that over P25. Wang et al. [96] found the photocatalytic activity of Ga_2O_3 for water splitting, which can be significantly enhanced by tailored α-β junction. Faust et al. [97] firstly reported that α-Fe_2O_3 can act as an efficient photocatalyst for photocatalytic oxidation of SO_2 in water. Further studies showed that it can be promising photocatalysts for water splitting and organics degradation via photocatalysis.[98-100] Due to the lower band-gap energy and more negative conduction band position, Cu_2O has been employed as an efficient photocatalyst for photoreduction, i.e. splitting of water for hydrogen production [101, 102]. Other metal oxides such Ta_2O_5 [76, 103], Bi_2O_3 [104, 105], and WO_3 [106, 107] have demonstrated photocatalytic activity in various applications.

2.2.3 Complex metal oxides and single-site photocatalysts

Two or more metals would make it easier to modulate the band structures, e.g. band-gap energy and the positions of VB and CB of the oxides, therefore complex metal oxides have attracted extensive attention in photocatalysis. In 2001, Zou et al.[108] reported that $In_{1-x}Ni_xTaO_4$ (x=0-0.2) can induce direct water splitting into stoichiometric amounts of O_2 and H_2 under visible light irradiations with a quantum yield of 0.66%. Some other oxides, such as $AgInW_2O_8$, $CaBi_2O_4$, $BiWO_6$ and Zn_2GeO_4 were also developed by their group.[109-112] Our group have prepared $BiTaO_4$, $InTaO_4$ and other bi-metallic oxides for photodegradation of gas organic pollutants [113-115].

Once the isolated and tetrahedrally coordinated metal oxide moieties, for example Ti, W, Cr, Mo, or V oxides are located in the silica or silica-based zeolites and similar porous materials, a single-site photocatalyst can be produced[116]. Anpo et al. [117, 118] prepared Ti-, V- Cr-oxide single-site photocatalysts and isolated them within zeolite frameworks. Their photocatalytic activities were evaluated in the decomposition of NO_x or CO_2 conversion. The novel photocatalysis mechanism was also discussed.

2.3 Metal sulfides and nitrides (oxynitrides)

In pursuit of visible light photocatalysis that cannot be realized on TiO_2 and ZnO, metal sulfides were employed as alternatives. CdS has a band-gap energy of around 2.4 eV and can respond to visible light with a absorption threshold at about 520 nm[119]. In 1983, Aruga et al. [120] reported that CdS can produce hydrogen from water under visible light photocatalysis using sulfite anion as a hole scavenger. For a stable photocatalytic activity, CdS has been frequently applied to fabricate hybrid photocatalysts for hydrogen production [121-124]. With proper modification or hybridization, CdS has been also used for photodegradation of organic pollutants in water [125-127]. ZnS has been proven to be a good photocatalyst owing to the rapid generation of electron-hole pairs and its excellent reduction potential for hydrogen production and CO_2 conversion [128, 129]. Photodegradation of organic pollutants in water has been also investigated.[130, 131] Bulk MoS_2 is not a good photocatalyst while nanoscaled MoS_2 can exhibit an excellent photocatalytic activity[132]. Other

metal sulfides, such as WS_2 [133], NiS [134], CuS [135], In_2S_3 [135], Ag_2S [136] and some complex sulfides, such as $A_2(I)$-Zn-A(IV)-S_4 (A(I) = Cu and Ag; A(IV) = Sn and Ge) [137], $CuInS_2$ [138], and $Zn_{1-x}Cd_xS$ [139] have demonstrated their photocatalytic activity in a variety of photocatalytic reactions.

Hitoki et al.[140] reported that Ta_3N_5 can be an efficient photocatalyst responding to visible light and produce hydrogen and oxygen from water splitting. Ma et al.[141] observed enhanced water oxidation on a Ta_3N_5 photocatalyst which was modified by alkaline metal salts. Lee et al.[142] reported that Ge_3N_4 can be used for overall water splitting. Metal oxynitrides, such as TaON [143] and $Zn_xTiO_yN_z$ [144] have been also investigated as visible light photocatalysts.

2.4 Noble metal-based plasmonic photocatalysts

Some novel photocatalysts appeared to initiate further exploration of photocatalysis mechanism. In 2005, Tian and Tatsuma [145] investigated the plasmon-induced photo-electrochemistry in the visible region on Au-TiO_2 composites, and found that gold nanoparticles can be photo-excited due to surface plasmon resonance (SPR). The charge separation can occur when the electrons are transferred from gold nanoparticles to the TiO_2 conduction band, and then the induced photocatalysis can oxidize organics. The associated mechanism is schematically shown in Fig.2.2 [145].

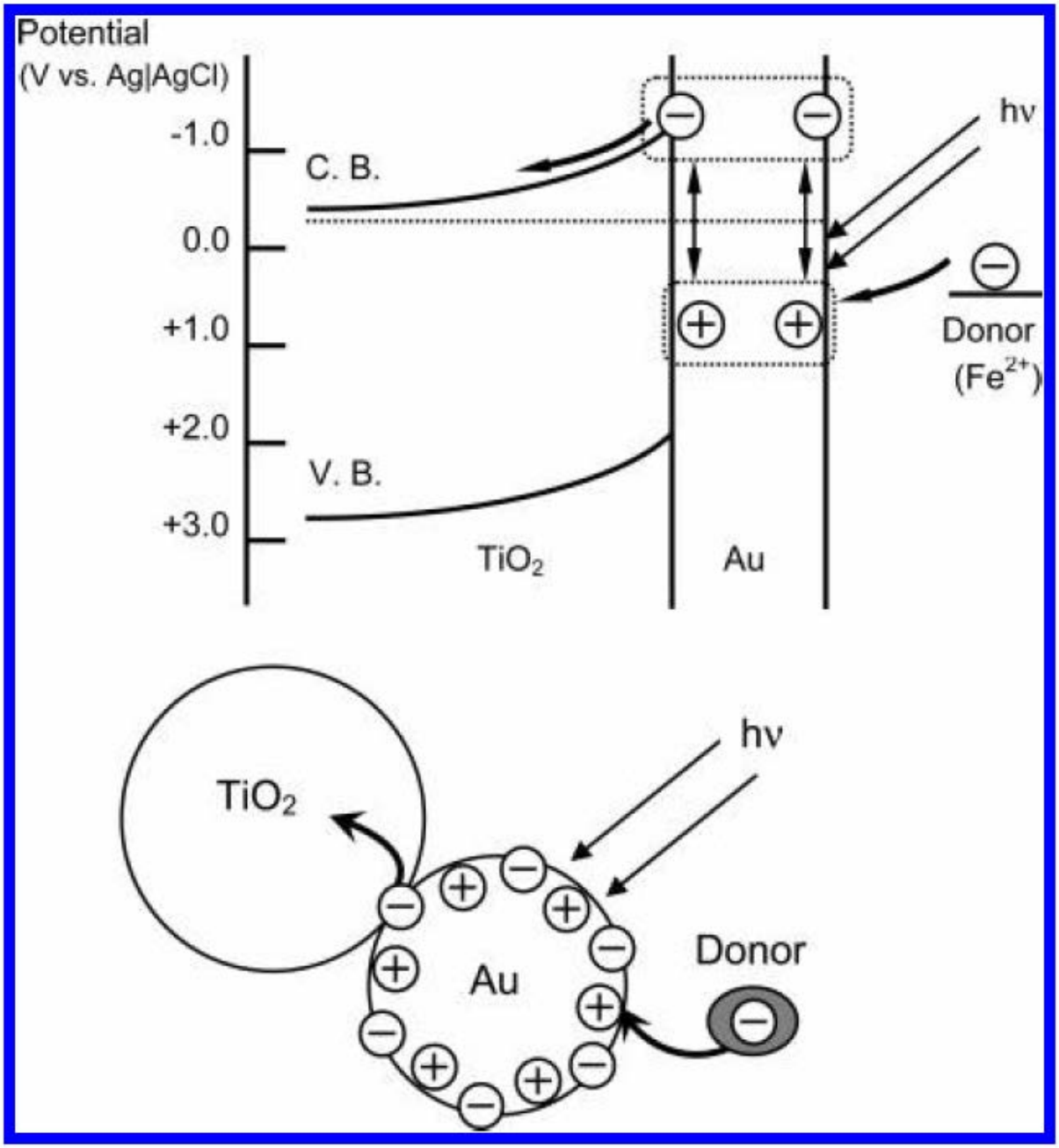

Fig. 2.2 Photoelectrochemistry of gold nanoparticle-TiO_2 system under visible light irradiations [145].

Chen et al.[146] prepared several metal oxide supported Au nanoparticles, such as Au/ZrO_2, Au/Fe_2O_3, Au/CeO_2, and Au/SiO_2, and observed efficient photodegradation of gas pollutants under sunlight. In 2008, Awazu et al. [147] proposed that the photocatalytic performance of TiO_2 might be improved by the assistance of the near-field amplitudes of localized surface plasmon (LSP) of silver nanoparticles. Wang et al. [148] described the synthesis and Ag@AgBr and proposed it as a highly active

plasmonic photocatalyst with visible light response. An et al. [149] reported the facile synthesis of AgCl:Ag plasmonic nanoparticles as photocatalysts. The prepared materials showed efficient degradation of organics under sunlight, and the activity was ascribed to the strong SPR of metallic Ag components. The plasmonic photocatalysis can be used for degradation, hydrogen production, and chemical synthesis [150, 151].

The plasmonic photocatalysis has offered new opportunities for this field, and more mechanistic aspects can be found in review papers [152, 153].

2.5 Metal-free photocatalysts

2.5.1 Graphitic carbon nitride

Scarcity in nature and toxic metal leaching from photo-corrosion can be significant barriers of metal-based photocatalysts to practical applications[154]. A metal-free photocatalyst, for example, graphitic carbon nitride (g-C_3N_4) has been proposed to be a promising candidate. Polymeric graphitic carbon nitride consisting of metal-free compositions of carbon, nitrogen and hydrogen, has been believed to be the most stable allotrope among C_xN_y, due to the layered structure similar to graphene. g-C_3N_4 is a polymeric semiconductor with a band-gap energy of 2.7 eV and unique structure and remarkable physicochemical properties[155]. In 2009, Wang et al.[156] for the first time observed efficient hydrogen production from visible light photocatalysis on g-C_3N_4 and the quantum efficiency was 0.1% under the irradiations in 420 – 460 nm. The crystal structure and optical property of g-C_3N_4 are shown in Fig. 2.3. The low activity can be ascribed to several aspects, such as the high excitation energy, the low charge mobility of a polymer compared to metals or oxides, the low surface area (2 -10 m^2/g), and poor absorption in longer wavelength[157]. Therefore, a number of modification approaches have been applied to improve the photocatalytic activity. Shalom et al. [158] reported an ordered, hollow carbon nitride structures using a cyanuric acid-melamine complex as the precursors. Enhanced photocatalysis for degradation of organic pollutants was achieved.

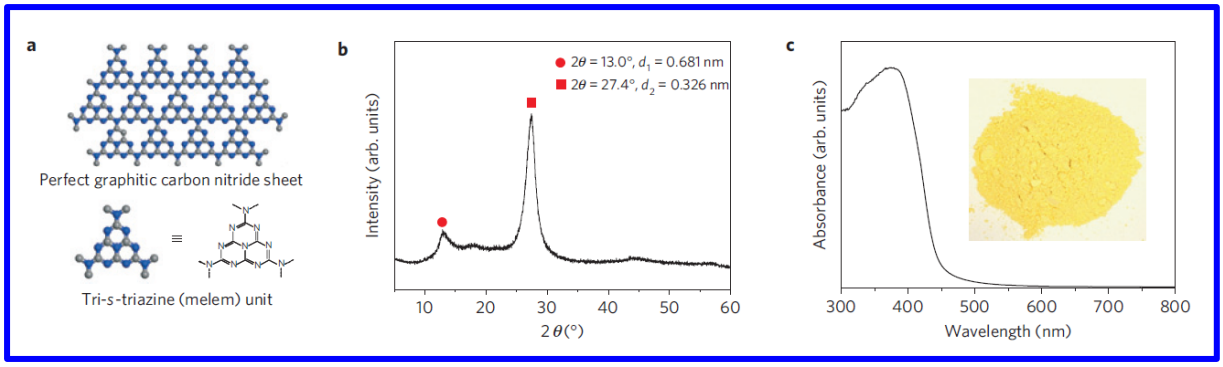

Fig. 2.3 (a) Construction of graphitic carbon nitride from melem unit, (b) XRD pattern of g-C_3N_4, and (c) UV-visible diffuse reflectance spectrum and image (inset) of g-C_3N_4. [156]

2.5.1.1 Structural modification

It is well known that for the catalysts a higher specific surface area (SSA) can provide more active sites on the surface for enhanced catalysis. Modification on g-C_3N_4 began with the creation of porous structure and the increase of SSAs. Hong et al. [159] employed SiO_2 nanoparticles as the hard template and obtained mesoporous g-C_3N_4 with a high surface area of 128 m^2/g, while unmodified one had a low BET around 12 m^2/g. Pluronic P123 was applied as a soft template to prepare g-C_3N_4 of worm-like pore and narrow pore size distribution and the BET surface area was increased to 90 m^2/g [160].

Zhang et al.[161] prepared porous g-C_3N_4 by direct polymerization of urea and found that it had a BET surface area of 69.6 m^2/g, compared to 11.3 and 12.3 m^2/g of g-C_3N_4 derived from thiourea and dicyandiamide. Han et al. [162] reported that the BET surface area of g-C_3N_4 can be increased to ca. 210 m^2/g by a facile template-free method controlling the reaction of polymer according to Le Chatelier's principle. Sano et al. [163] reported that the BET surface area of pristine g-C_3N_4 prepared by heating melamine at 550 ^oC was only 7.7 m^2/g, which can be increased to 65 m^2/g by hydrothermally treating the sample with NaOH solution at 90 – 150 ^oC. Niu et al. [164] reported that BET of g-C_3N_4 can be increased to 306 m^2/g when it was exfoliated to nanosheets by a simple top-down method of thermal oxidation etching of bulk g-C_3N_4 in air.

2.5.1.2 Heteroatom doping

Doping heteroatoms into TiO_2 has been extensively proven to be an effective strategy to extend the light absorption and enhance the photocatalytic performance [47, 48, 61]. This technique has been also employed to modify g-C_3N_4.

Fe-doped graphitic carbon nitride (g-C_3N_4) nanosheets were prepared by Tonda et al. [165] using ferric chloride as the Fe-precursor. The dopant of Fe appeared to be +3 oxidation state and could significantly influence the electronic and optical properties of g-C_3N_4. It was reported that 2 mol% Fe-doped g-C_3N_4 showed almost 7-time and 4.5-time higher activity than unmodified g-C_3N_4 and g-C_3N_4 nanosheets, respectively. Potassium-doped g-C_3N_4 was prepared by thermal polymerization of dicyandiamide and KI. It was found that the doped potassium can enhance the photocatalytic activity by lowering the valence band and increasing charge separation rate.[166] Besides, Zr-doped and W-doped g-C_3N_4 were also developed for enhanced photocatalysis [167, 168].

In consideration of the metal-free nature of the modified g-C_3N_4, non-metal doping has attracted more extensive attention. Fluorinated g-C_3N_4 was prepared by directly incorporating NH_4F into the thermal condensation process in g-C_3N_4 synthesis.[169] The doped F can shift both VB and CB to higher energy values, which were beneficial for the redox properties and enhanced heterogeneous photocatalysis. In photocatalytic hydrogen evolution, F-g-C_3N_4 with 3 wt% Pt as the co-catalyst demonstrated about 2.7 times higher activity than the unmodified g-C_3N_4. Boron-doped g-C_3N_4 was prepared by heating a mixture of melamine and boron oxide.[170] It was found that boron doping for g-C_3N_4 can improve the efficiency of photodegradation of Rh B owing to the increased dye adsorption and light absorption of the catalyst.

Zhang et al. [157] developed sulfur-mediated synthesis to stimulate carbon nitride bulk condensation by trithiocyanuric as the precursor in which the –SH groups were supposed to play a key role in adjusting the physicochemical properties of the prepared g-C_3N_4. Trace amount of sulfur doping showed effective modifications of the texture, optical and electronic properties, as a result the activity in water oxidation reactions were improved. Liu et al.[171] reported that sulfur-doping can induce a unique

electronic structure that shows an increased VB along with an elevated CB minimum and minor declined absorbance. Fig. 2.4 shows the changes of band structure induced by sulfur doping and various properties of the modified g-C_3N_4[171]. Significant changes in optical properties and electronic structures would lead to the enhanced photocatalysis in hydrogen evolution over sulfur-doped g-C_3N_4, with 7.2 and 8.0 times higher than unmodified one under $\lambda > 300$ and 420 nm, respectively.

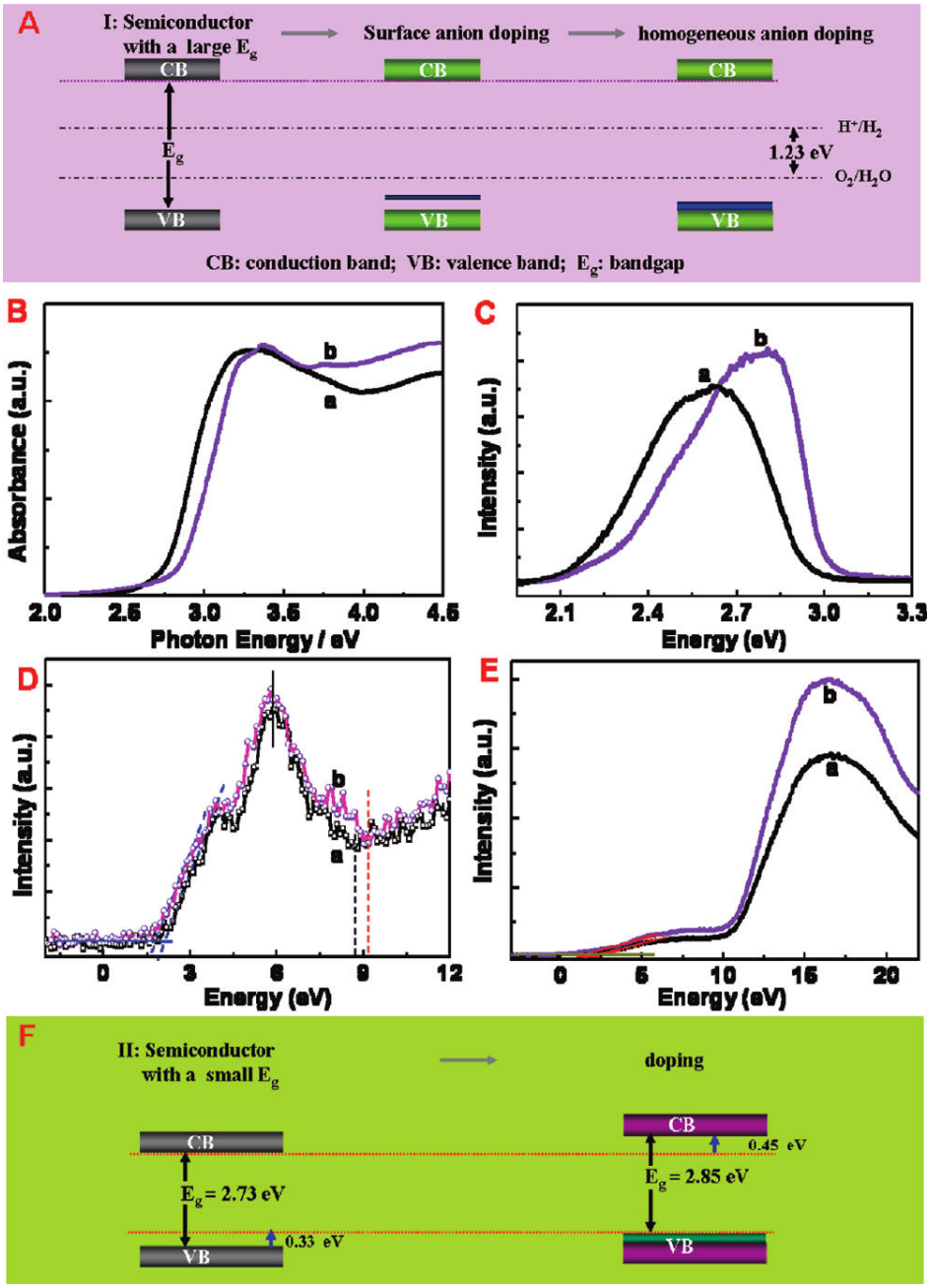

Fig. 2.4 (a) Band structure changes over surface and homogeneous anion doping, (b) optical properties, (c) fluorescence spectra, (d) the total densities of states (DOSs) of

the samples, (e0 ultraviolet photoelectron spectra, and (f) electronic structure of the samples [171].

Phosphorus-doped g-C_3N_4 was prepared by poly-condensation of a mixture with the precursor of g-C_3N_4 (dicyandiamide) and a heteroatom source namely a phosphorus-containing ionic liquid. The modification can provide a much better electric conductivity and an improvement in photocurrent generation[172]. Phosphorus doping and structure modification were integrated by Ran et al.[173], who prepared porous P-doped g-C_3N_4 nanosheets by combining P doping and thermal exfoliation of bulk material. The P-doping and novel macroporous nanosheets morphology can significantly increase the visible light photocatalytic H_2-production compared to pristine g-C_3N_4. The newly formed mid-gap states (-0.16 V vs. SHE) were observed due to the P-doping. With a similar strategy of simultaneous tailoring of texture and electro-/optical- properties, mesoporous P-doped g-C_3N_4 nanostructured flowers were prepared by a co-condensation method in the absence of any templates. [174] Improved hydrogen evolution under visible light irradiation was observed due to the promoted light trapping, mass transfer and charge separation.

Iodinated g-C_3N_4 nanosheets were prepared by a simple and scalable physical method using ball-milling technique [175]. Both photoelectrochemical and photocatalytic properties were changed by I-doping. Fig. 2.5 shows photoelectrochemical tests of pristine and I-doped g-C_3N_4 samples. The electrochemical impedance spectroscopy (EIS) of three samples, bulk g-C_3N_4 (GCN), I-free GCN (modified g-C_3N_4 by ball-milling) and $IGCNS_{S1/2}$ (the mass ratio of iodine to bulk GCN is ½ in ball-milling process) was measured in a 0.2 M Na_2SO_4 aqueous solution in the dark. The Nyquist plots in Fig. 2.5(a) suggest that electrons of $IGCNS_{S1/2}$ can be more freely transferred to the protons than other two samples. Moreover, the I-doped sample also demonstrated the highest photocurrent density among all the samples under visible light irradiations as shown in Fig. 2.5(c). Such an enhanced photoelectrochemical performance also led to the best hydrogen evolution rate of 44.5 μmol/h on $IGCNS_{S1/2}$, as compared to 4.9 and 19.5 μmol/h on bulk GCN and I-free GCN, respectively.

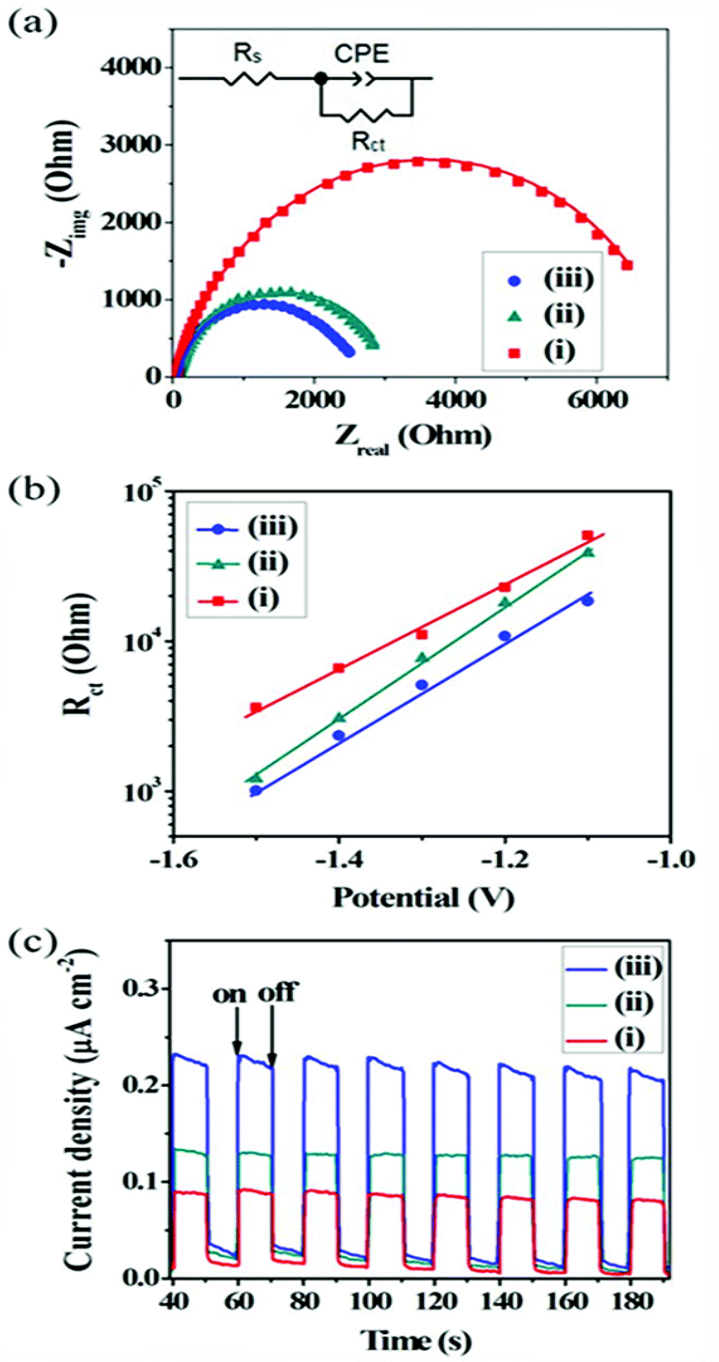

Fig. 2.5 (a) Nyquist plots and electrical equivalent-circuit model (inset) of IGCNSs$_{1/2}$. (b) Dependence of R_{ct} on applied biases. (c) Transient photocurrents responses under visible light irradiation. Samples: bulk GCN (i), I-free GCNSs (ii) and IGCNSs$_{1/2}$ (iii).[175]

Porous O-doped g-C_3N_4 was prepared by a precursor pre-treatment method forming hydrogen bond-induced supramolecular aggregates for creation of porous structure and tailored O-doping.[176] The porous structure and O-doping worked together to achieve 6.1 and 3.1 times higher hydrogen evolution than bulk and porous g-C_3N_4 (non-doping).

Nitrogen-doped g-C_3N_4 was fabricated by the co-thermal condensation of the precursor of melamine with a nitrogen-rich additive of hydrazine hydrate [177]. The band structure of C_3N_{4+x} was changed compared to pristine g-C_3N_4. Fig. 2.6 shows the modified band structure determined by the integration of UV-vis DRS, XPS, Mott-schotty plots. Fig. 2.6(a) shows that N-doping can lower the band gap of 2.72 eV of pristine g-C_3N_4 to 2.65 eV of C_3N_{4+x}. Fig. 2.6(b) indicates that the valence band maximum of pristine g-C_3N_4 is at 1.84 eV. Mott-Schotty plots in Figs. 2.6 (c) and (d) show the typical n-type characteristic and a flat band potential of -0.98 and -1.13 eV vs. Ag/AgCl for C_3N_{4+x} and g-C_3N_4 respectively. With above analysis, the band structure can be shown in Fig. 2.6(e). The modified band structure can improve the photocatalytic activity. In hydrogen evolution, the rate of C_3N_{4+x} was 1.8 times higher than pristine g-C_3N_4 photocatalysts.

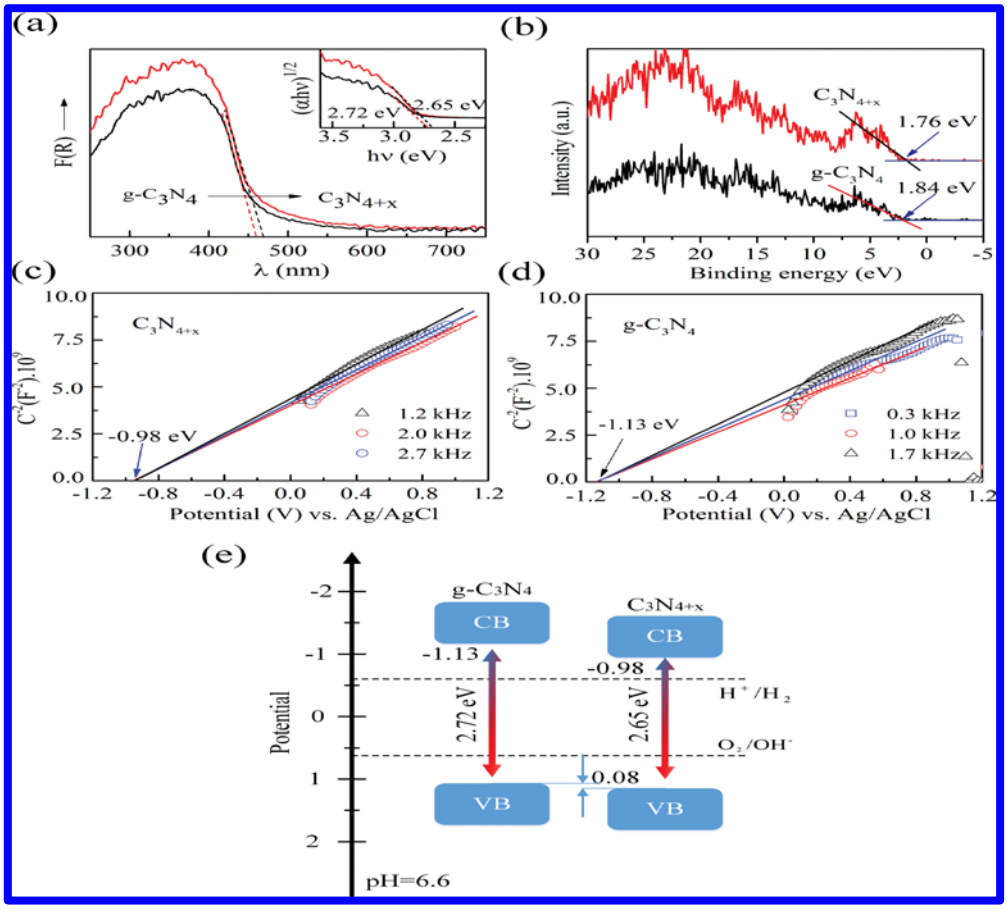

Fig. 2.6 UV-vis DRS (a) and XPS band analysis (b) of C_3N_{4+x} and g-C_3N_4; Mott–Schottky plots of C_3N_{4+x} (c) and g-C_3N_4 (d); electronic band structure (e). Inset of (a): band gap estimation.[177]

2.5.1.3 Semiconductor coupling

Coupling a semiconductor to another is a popular technique to create heterojunction for extended absorbance and improved charge separation so as to enhance the photocatalysis performance of the photocatalysts. Yan and Yang [178] reported that coupling TiO_2 to C_3N_4 can remarkably increase the photocatalytic hydrogen evolution rate due to the improved charge separation efficiency. Li et al. [179] prepared various TiO_2 nanostructures, such as 0D nanoparticles, 1D nanowires, 2D nanosheets, and 3D mesoporous nanocrystals and attached each of them onto g-C_3N_4 to create different heterojunctions. Meso-TiO_2/g-C_3N_4 demonstrated the highest activity in photodegradation of MO and phenol, with 29-37 times higher than bare g-C_3N_4. Jo and Natarajan [180] investigated the influence of TiO_2 morphology (nanoparticles and nanotubes) on the photodegradation of isoniazid and found that the Z-scheme g-C_3N_4/TiO_2 nanotube (3%-CN/TNT) exhibited enhanced photocatalysis (90.8% degradation in 4 h) than that of nanoparticles/CN (79.5%) and pure TiO_2 (56.3%) and g-C_3N_4 (13.5%).

Song et al.[181] reported the fabrication of g-C_3N_4/(0 0 1) TiO_2 composite by a solvent-free in situ method. The compact connection between g-C_3N_4 and (0 0 1) TiO_2 can facilitate the interfacial charge transfer process, as proposed in Fig. 2.7. Therefore, the photocatalytic activity was enhanced in removal of NO, with 2.4 times higher than pure (0 0 1) TiO_2 and 4.1 times higher than g-C_3N_4 under UV, respectively. Huang et al.[182] studied the effect of contact interface between (0 0 1) or (1 0 1) TiO_2 and g-C_3N_4 and found that g-C_3N_4 can efficiently remove the photo-generated electrons on (1 0 1) facets for the enhanced photocatalysis.

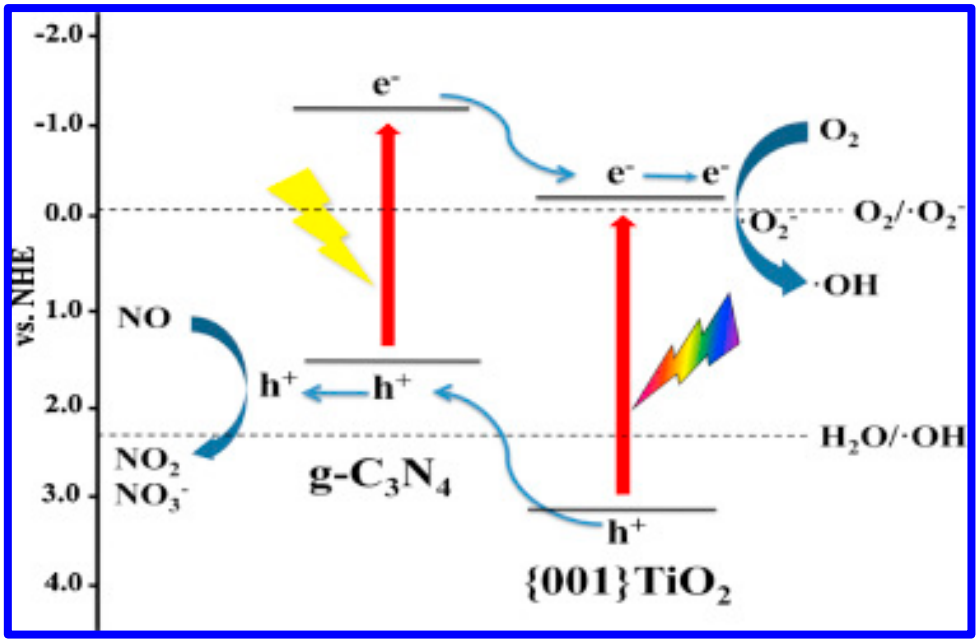

Fig. 2.7 Charge transfers of g-C_3N_4/(0 0 1) TiO_2 composite in photocatalytic reactions[181].

ZnO was used to hybridize g-C_3N_4 by a monolayer-dispersed method. The prepared hybrids showed 5 times higher photocurrent than ZnO and a photocurrent under visible light was also observed. Moreover, the photocatalytic activity under UV was enhanced by 3.5 times and the photo-corrosion of ZnO was suppressed [183]. ZnO/g-C_3N_4 composite was also prepared by a simple impregnation method for CO_2 conversion to fuels. It was found that the light-absorbance was not changed much but the heterojunction could inhibit the recombination of photo-induced charges. Therefore, the optimal ZnO/g-C_3N_4 composite showed a higher CO_2 conversion rate which are 4.9 and 6.4 times higher than pristine g-C_3N_4 and P25, respectively.

Some other metal oxides, such as α-Fe_2O_3[184], SnO_2 [185], WO_3 [186], were also used to couple with g-C_3N_4. A variety of bimetallic oxides, such as $SnNb_2O_6$ nanosheet [187], $NaNbO_3$ [188], $CuFe_2O_4$ [189], and Ag_3VO_4 [190] have been demonstrated to be effective for modification of g-C_3N_4. Besides, metal sulfides [191], metal oxohalides [192, 193], ternary compounds [194-197] and other novel materials (phosphates [198, 199], polyoxometalate [200], and zinc phthalocyanine [201]) were also able to modify g-C_3N_4 for enhanced photocatalysis.

2.5.1.4 Metal-free modification and coupling

To maintain the metal-free nature, metal free compounds were employed for modification of g-C_3N_4. Zhang et al.[202] described non-covalent modification of g-C_3N_4 with graphene and suggested that with the $\pi - \pi$ stacking interaction, the band structure of g-C_3N_4 can be modulated for enhanced photoelectrochemical properties. Graphene oxide (GO) modified g-C_3N_4 was prepared by a sonochemical approach.[203] GO was found to be of 2D sheet structure with chiffon-like ripples, which can form layer-layer structure with 2D g-C_3N_4. GO can act as a separation centre and electron acceptor and thus photodegradation of Rh B and 2,4-DCP under visible light irradiation was 3.8 and 2.08 times higher than pristine g-C_3N_4, respectively. Ge and Han [204] prepared MWCNT/g-C_3N_4 composites as efficient visible light photocatalysts for hydrogen evolution from water. At the optimal modification level of 2.0 wt%, the composite photocatalyst showed 3.7 folds higher hydrogen evolution from methanol solutions than pristine g-C_3N_4.

Grafting functional groups onto g-C_3N_4 can be obtained by copolymerization with organic compounds having amino cyano moieties. Zhang et al. [205] employed various monomer building blocks with desired compositions and electronic structures modification of g-C_3N_4. Enhanced photocatalysis was claimed on the modified photocatalyst. Chu et al.[206] reported a simple bottom-up approach to prepare g-C_3N_4 with desired band structure by incorporating electron-deficient pyromellitic dianhydride (PMDA) monomer. The modified g-C_3N_4 has a lowered VB ensuring a stronger photo-oxidation ability in degradation of MO. Moreover, the formation processes of reactive radicals were tuned by photoinduced holes other than electrons due to the band gap engineering. Some other metal-free compounds, such as polyacylonitrile (g-PAN)[207] and melem [208] were also employed to modify g-C_3N_4.

2.5.3 Carbonaceous, boron-based and elemental photocatalysts

Zhang et al.[209] reported the synthesis GO and rGO pillared by carbon nanotubes by a CVD method with acetonitrile as the carbon source. They observed that the CNT-rGO composite showed excellent photocatalytic performances in degradation of Rh B owing to the porous structure and the improved electronic properties. GO was employed

as a novel photocatalyst for photocatalytic CO_2 conversion to methanol by Hsu et al.[210] It was reported that carbon quantum dots (CQDs) can function as an efficient photocatalyst responsive to near infrared (NIR) light for selective oxidation reactions[211].

Liu et al. [212] demonstrated that inexpensive boron carbides ($B_{4.3}C$ and $B_{13}C_2$) can be functioned as visible light photocatalysts for H_2 production and the rate was about two orders of magnitude larger than that of g-C_3N_4. More recently, synthesis of a ternary semiconductor, boron nitride was developed and the photocatalyst showed excellent performances in hydrogen or oxygen evolution from water and CO_2 reduction reactions[213].

In addition to conventional photocatalysts, several novel, elemental photocatalysts have been reported [214]. For example, α-sulfur [215], red phosphorus [216], and β-rhombohedral boron [217] were all proven to be effective photocatalysts.

2.6 Conclusions and perspectives

Photocatalysis has been extensively investigated for over four decades, and demonstrated a wide variety of applications, such as water splitting for hydrogen evolution, CO_2 conversion for hydrocarbon fuels, oxidation of aqueous and gaseous pollutants, reduction of heavy metals, building materials, and chemical synthesis. The mechanism and application implications have been well elucidated. The barrier of photocatalysis is the development of photocatalyst materials.

TiO_2 and ZnO as wide band gap semiconductors have been widely employed as photocatalysts. The wide band gap energy ensures high redox potentials, which are necessary for facilitating photocatalytic reactions. But their wide band gaps can only be activated by UV, so in solar energy utilization the overall efficiency is very low. For extending the light absorbance, surface modification, doping, dye-sensitization, and semiconductor coupling have been used. On the other hand, many other metal oxides, or bimetallic oxides, and metal sulfides and nitrides were also explored for enhanced photocatalysis and visible light response. It is very common that multiple modifications

are used for modulation of the physicochemical properties of the photocatalyst materials.

The scarcity and metal toxicity of metal-based photocatalysts were raised as major concerns. Metal-free, polymeric graphitic carbon nitride (g-C_3N_4) was demonstrated as an efficient visible light photocatalyst for hydrogen evolution. It is generally prepared by a condensation approach which leads to a very low BET surface area, not higher than 10.0 m^2/g. The polymeric nature indicates a low mobility of charges leading to a low photocatalytic activity. Also the band structure of high VB minimum and high CB maximum of g-C_3N_4 determines that it has a high reduction ability but a low photooxidation activity. Therefore, various methods have been applied to modify g-C_3N_4 photocatalysts, such as creation of porosity, semiconductor coupling, carbonaceous materials coupling, metal-doping, non-metal doping, monomer modification, and sensitization. With the modifications, porosity, morphology, surface functional groups, and band structure can be modulated for enhanced photocatalytic activity and extended applications, i.e. from photoreduction to photooxidation.

Some emerging photocatalysts, such as boron nitride, boron carbide, and elemental photocatalysts (sulfur, boron and phosphorus) were also developed as novel photocatalyst materials.

So far photocatalysis is still restricted to fundamental research only, as the efficiency of the photocatalyst is not satisfactory. In future studies, based on the development of photocatalyst materials, several strategies can be applied as follows.

(i) Basal photocatalyst for modification should be cheap, non-toxic and abundant on the Earth. Photocatalyst development sometimes has gone too far beyond reality with employment of very expensive rare earth elements or highly toxic metals. This kind of research is highly likely confined at lab-scale even if a superior solar energy utilization efficiency is succeeded.

(ii) Multiple modification techniques offering both thermodynamic and kinetic controls. The photocatalysis involves photon absorption, charge formation, charge separation

and recombination, surface reactions for radical generation, and photocatalytic reactions. The final photocatalytic efficiency is literally controlled by each step, therefore multiple modifications, including changing composition, tailoring shape, and modulating surface feature, should be incorporated.

(iii) Integrated studies employing both experimental and theoretical investigations. Photocatalyst design is very complicated. For example, for a simple element doping, the experiments can involve the kind, the level and the species of the dopant. In ISI database (on 23/01/2016), when "TiO_2 and photocata* and nitrogen and dop*" is used in "TOPIC", 2,561 results were obtained. Experimental studies will never be able to screen all the possible solutions. Therefore, theoretical studies, including molecular simulations and reaction kinetics should be used for the design of photocatalyst materials.

References

[1] K.H. Solangi, M.R. Islam, R. Saidur, N.A. Rahim, H. Fayaz, A review on global solar energy policy, Renewable & Sustainable Energy Reviews, 15 (2011) 2149-2163.

[2] H.Q. Sun, S.B. Wang, Research Advances in the Synthesis of Nanocarbon-Based Photocatalysts and Their Applications for Photocatalytic Conversion of Carbon Dioxide to Hydrocarbon Fuels, Energy & Fuels, 28 (2014) 22-36.

[3] S. Mekhilef, R. Saidur, A. Safari, A review on solar energy use in industries, Renewable & Sustainable Energy Reviews, 15 (2011) 1777-1790.

[4] C.G. Granqvist, Solar energy materials, Advanced Materials, 15 (2003) 1789-1803.

[5] L.C. Sun, L. Hammarstrom, B. Akermark, S. Styring, Towards artificial photosynthesis: ruthenium-manganese chemistry for energy production, Chemical Society Reviews, 30 (2001) 36-49.

[6] A. Fujishima, K. Honda, Electrochemical photolysis of water at a semiconductor electrode, Nature, 238 (1972) 37-+.

[7] A.J. Bard, Photoelectrochemistry and heterogeneous photocatalysis at semiconductors, Journal of Photochemistry, 10 (1979) 59-75.

[8] A.L. Linsebigler, G.Q. Lu, J.T. Yates, Photocatalysis on TiO_2 surfaces - principles, mechanisms, and selected results, Chemical Reviews, 95 (1995) 735-758.

[9] J.H. Carey, J. Lawrence, H.M. Tosine, Photo-dechlorination of pcbs in presence of titanium-dioxide in aqueous suspensions, Bulletin of Environmental Contamination and Toxicology, 16 (1976) 697-701.

[10] R.I. Bickley, G. Munuera, F.S. Stone, Photoadsorption and photocatalysis at rutile surfaces .2. Photocatalytic oxidation of isopropanol, Journal of Catalysis, 31 (1973) 398-407.

[11] T. Inoue, A. Fujishima, S. Konishi, K. Honda, Photoelectrocatalytic reduction of carbon-dioxide in aqueous suspensions of semiconductor powders, Nature, 277 (1979) 637-638.

[12] S. Yamagata, S. Nakabayashi, K.M. Sancier, A. Fujishima, Photocatalytic oxidation of alcohols on tio2, Bulletin of the Chemical Society of Japan, 61 (1988) 3429-3434.

[13] M. Anpo, K. Chiba, M. Tomonari, S. Coluccia, M. Che, M.A. Fox, Photocatalysis on native and platinum-loaded TiO_2 and ZnO catalysts-origin of different reactivities

on wet and dry metal-oxides, Bulletin of the Chemical Society of Japan, 64 (1991) 543-551.

[14] E.C. Butler, A.P. Davis, Photocatalytic oxidation in aqueous titanium-dioxide suspensions - the influence of dissolved transition-metals, Journal of Photochemistry and Photobiology a-Chemistry, 70 (1993) 273-283.

[15] A. Bravo, J. Garcia, X. Domenech, J. Peral, Some aspects of the photocatalytic oxidation of ammonium ion by titanium-dioxide, Journal of Chemical Research-S, (1993) 376-377.

[16] R. Wang, K. Hashimoto, A. Fujishima, M. Chikuni, E. Kojima, A. Kitamura, M. Shimohigoshi, T. Watanabe, Light-induced amphiphilic surfaces, Nature, 388 (1997) 431-432.

[17] K. Hashimoto, H. Irie, A. Fujishima, TiO_2 photocatalysis: A historical overview and future prospects, Japanese Journal of Applied Physics Part 1-Regular Papers Brief Communications & Review Papers, 44 (2005) 8269-8285.

[18] O. Legrini, E. Oliveros, A.M. Braun, Photochemical processes for water-treatment, Chemical Reviews, 93 (1993) 671-698.

[19] P.V. Kamat, Photochemistry on nonreactive and reactive (semiconductor) surfaces, Chemical Reviews, 93 (1993) 267-300.

[20] M.A. Fox, M.T. Dulay, Heterogeneous photocatalysis, Chemical Reviews, 93 (1993) 341-357.

[21] M.R. Hoffmann, S.T. Martin, W.Y. Choi, D.W. Bahnemann, Environmental applications of semiconductor photocatalysis, Chemical Reviews, 95 (1995) 69-96.

[22] F. Kapteijn, J. RodriguezMirasol, J.A. Moulijn, Heterogeneous catalytic decomposition of nitrous oxide, Applied Catalysis B-Environmental, 9 (1996) 25-64.

[23] J.M. Herrmann, Heterogeneous photocatalysis: fundamentals and applications to the removal of various types of aqueous pollutants, Catalysis Today, 53 (1999) 115-129.

[24] J. Peral, X. Domenech, D.F. Ollis, Heterogeneous photocatalysis for purification, decontamination and deodorization of air, Journal of Chemical Technology and Biotechnology, 70 (1997) 117-140.

[25] N. Jaffrezicrenault, P. Pichat, A. Foissy, R. Mercier, Effect of deposited pt particles on the surface-charge of TiO_2 aqueous suspensions by potentiometry, electrophoresis, and labeled ion adsorption, Journal of Physical Chemistry, 90 (1986) 2733-2738.

[26] A. Sclafani, M.N. Mozzanega, P. Pichat, Effect of silver deposits on the photocatalytic activity of titanium-dioxide samples for the dehydrogenation or oxidation of 2-propanol, Journal of Photochemistry and Photobiology a-Chemistry, 59 (1991) 181-189.

[27] S. Sakthivel, M.V. Shankar, M. Palanichamy, B. Arabindoo, D.W. Bahnemann, V. Murugesan, Enhancement of photocatalytic activity by metal deposition: characterisation and photonic efficiency of Pt, Au and Pd deposited on TiO_2 catalyst, Water Research, 38 (2004) 3001-3008.

[28] H. Ross, J. Bendig, S. Hecht, Sensitized photocatalytical oxidation of terbutylazine, Solar Energy Materials and Solar Cells, 33 (1994) 475-481.

[29] Y.M. Cho, W.Y. Choi, C.H. Lee, T. Hyeon, H.I. Lee, Visible light-induced degradation of carbon tetrachloride on dye-sensitized TiO_2, Environmental Science & Technology, 35 (2001) 966-970.

[30] P.V. Kamat, M.A. Fox, Photo-sensitization of TiO_2 colloids by erythrosin-b in acetonitrile, Chemical Physics Letters, 102 (1983) 379-384.

[31] L. Spanhel, H. Weller, A. Henglein, Photochemistry of semiconductor colloids .22. electron injection from illuminated cds into attached TiO_2 and zno particles, Journal of the American Chemical Society, 109 (1987) 6632-6635.

[32] L. Wu, J.C. Yu, X.Z. Fu, Characterization and photocatalytic mechanism of nanosized CdS coupled TiO_2 nanocrystals under visible light irradiation, Journal of Molecular Catalysis a-Chemical, 244 (2006) 25-32.

[33] W.K. Ho, J.C. Yu, J. Lin, J.G. Yu, P.S. Li, Preparation and photocatalytic behavior of MoS2 and WS2 nanocluster sensitized TiO_2, Langmuir, 20 (2004) 5865-5869.

[34] D. Robert, Photosensitization of TiO_2 by MxOy and MxSy nanoparticles for heterogeneous photocatalysis applications, Catalysis Today, 122 (2007) 20-26.

[35] M. Fujihira, Y. Satoh, T. Osa, Heterogeneous photocatalytic reactions on semiconductor-materials .3. effect of ph and Cu2+ ions on the photo-fenton type reaction, Bulletin of the Chemical Society of Japan, 55 (1982) 666-671.

[36] V. Brezova, A. Blazkova, L. Karpinsky, J. Groskova, B. Havlinova, V. Jorik, M. Ceppan, Phenol decomposition using $Mn+/TiO_2$ photocatalysts supported by the sol-gel technique on glass fibres, Journal of Photochemistry and Photobiology a-Chemistry, 109 (1997) 177-183.

[37] N. Serpone, D. Lawless, J. Disdier, J.M. Herrmann, Spectroscopic, photoconductivity, and photocatalytic studies of TiO_2 colloids - naked and with the lattice doped with cr3+, fe3+, and v5+ cations, Langmuir, 10 (1994) 643-652.

[38] W.Y. Choi, A. Termin, M.R. Hoffmann, Effects of metal-ion dopants on the photocatalytic reactivity of quantum-sized TiO_2 particles, Angewandte Chemie-International Edition in English, 33 (1994) 1091-1092.

[39] U.G. Akpan, B.H. Hameed, The advancements in sol-gel method of doped-TiO_2 photocatalysts, Applied Catalysis a-General, 375 (2010) 1-11.

[40] C.H. Liang, F.B. Li, C.S. Liu, H.L. Lu, X.G. Wang, The enhancement of adsorption and photocatalytic activity of rare earth ions doped TiO_2 for the degradation of Orange I, Dyes and Pigments, 76 (2008) 477-484.

[41] A.W. Xu, Y. Gao, H.Q. Liu, The preparation, characterization, and their photocatalytic activities of rare-earth-doped TiO_2 nanoparticles, Journal of Catalysis, 207 (2002) 151-157.

[42] R. Asahi, T. Morikawa, T. Ohwaki, K. Aoki, Y. Taga, Visible-light photocatalysis in nitrogen-doped titanium oxides, Science, 293 (2001) 269-271.

[43] S. Livraghi, M.C. Paganini, E. Giamello, A. Selloni, C. Di Valentin, G. Pacchioni, Origin of photoactivity of nitrogen-doped titanium dioxide under visible light, Journal of the American Chemical Society, 128 (2006) 15666-15671.

[44] H. Irie, Y. Watanabe, K. Hashimoto, Nitrogen-concentration dependence on photocatalytic activity of TiO_2-xNx powders, Journal of Physical Chemistry B, 107 (2003) 5483-5486.

[45] T. Ihara, M. Miyoshi, Y. Iriyama, O. Matsumoto, S. Sugihara, Visible-light-active titanium oxide photocatalyst realized by an oxygen-deficient structure and by nitrogen doping, Applied Catalysis B-Environmental, 42 (2003) 403-409.

[46] C. Burda, Y.B. Lou, X.B. Chen, A.C.S. Samia, J. Stout, J.L. Gole, Enhanced nitrogen doping in TiO2 nanoparticles, Nano Letters, 3 (2003) 1049-1051.

[47] H.Q. Sun, Y. Bai, H.J. Liu, W.Q. Jin, N.P. Xu, Photocatalytic decomposition of 4-chlorophenol over an efficient N-doped TiO_2 under sunlight irradiation, Journal of Photochemistry and Photobiology a-Chemistry, 201 (2009) 15-22.

[48] H.Q. Sun, Y. Bai, W.Q. Jin, N.P. Xu, Visible-light-driven TiO_2 catalysts doped with low-concentration nitrogen species, Solar Energy Materials and Solar Cells, 92 (2008) 76-83.

[49] H.Q. Sun, G.L. Zhou, S.Z. Liu, H.M. Ang, M.O. Tade, S.B. Wang, Visible light responsive titania photocatalysts codoped by nitrogen and metal (Fe, Ni, Ag, or Pt) for remediation of aqueous pollutants, Chemical Engineering Journal, 231 (2013) 18-25.
[50] H.Q. Sun, R. Ullah, S.H. Chong, H.M. Ang, M.O. Tade, S.B. Wang, Room-light-induced indoor air purification using an efficient Pt/N-TiO_2 photocatalyst, Applied Catalysis B-Environmental, 108 (2011) 127-133.
[51] Q.J. Xiang, J.G. Yu, M. Jaroniec, Nitrogen and sulfur co-doped TiO_2 nanosheets with exposed {001} facets: synthesis, characterization and visible-light photocatalytic activity, Physical Chemistry Chemical Physics, 13 (2011) 4853-4861.
[52] D.M. Chen, Z.Y. Jiang, J.Q. Geng, Q. Wang, D. Yang, Carbon and nitrogen co-doped TiO2 with enhanced visible-light photocatalytic activity, Industrial & Engineering Chemistry Research, 46 (2007) 2741-2746.
[53] S. Yin, K. Ihara, Y. Aita, M. Komatsu, T. Sato, Visible-light induced photocatalytic activity of $TiO_{(2-x)}A_{(y)}$ (A = N, S) prepared by precipitation route, Journal of Photochemistry and Photobiology a-Chemistry, 179 (2006) 105-114.
[54] S.U.M. Khan, M. Al-Shahry, W.B. Ingler, Efficient photochemical water splitting by a chemically modified n-TiO_2 2, Science, 297 (2002) 2243-2245.
[55] W.J. Ren, Z.H. Ai, F.L. Jia, L.Z. Zhang, X.X. Fan, Z.G. Zou, Low temperature preparation and visible light photocatalytic activity of mesoporous carbon-doped crystalline TiO_2, Applied Catalysis B-Environmental, 69 (2007) 138-144.
[56] J.H. Park, S. Kim, A.J. Bard, Novel carbon-doped TiO_2 nanotube arrays with high aspect ratios for efficient solar water splitting, Nano Letters, 6 (2006) 24-28.
[57] H. Irie, Y. Watanabe, K. Hashimoto, Carbon-doped anatase TiO2 powders as a visible-light sensitive photocatalyst, Chemistry Letters, 32 (2003) 772-773.
[58] C. Lettmann, K. Hildenbrand, H. Kisch, W. Macyk, W.F. Maier, Visible light photodegradation of 4-chlorophenol with a coke-containing titanium dioxide photocatalyst, Applied Catalysis B-Environmental, 32 (2001) 215-227.
[59] X. Yang, C. Cao, K. Hohn, L. Erickson, R. Maghirang, D. Hamal, K. Klabunde, Highly visible-light active C- and V-doped TiO_2 for degradation of acetaldehyde, Journal of Catalysis, 252 (2007) 296-302.
[60] L. Lin, R.Y. Zheng, J.L. Xie, Y.X. Zhu, Y.C. Xie, Synthesis and characterization of phosphor and nitrogen co-doped titania, Applied Catalysis B-Environmental, 76 (2007) 196-202.

[61] H.Q. Sun, Y. Bai, Y.P. Cheng, W.Q. Jin, N.P. Xu, Preparation and characterization of visible-light-driven carbon-sulfur-codoped TiO_2 photocatalysts, Industrial & Engineering Chemistry Research, 45 (2006) 4971-4976.
[62] H.X. Li, X.Y. Zhang, Y.N. Huo, J. Zhu, Supercritical preparation of a highly active S-doped TiO_2 photocatalyst for methylene blue mineralization, Environmental Science & Technology, 41 (2007) 4410-4414.
[63] J.C. Yu, W.K. Ho, J.G. Yu, H. Yip, P.K. Wong, J.C. Zhao, Efficient visible-light-induced photocatalytic disinfection on sulfur-doped nanocrystalline titania, Environmental Science & Technology, 39 (2005) 1175-1179.
[64] T. Umebayashi, T. Yamaki, S. Tanaka, K. Asai, Visible light-induced degradation of methylene blue on S-doped TiO_2, Chemistry Letters, 32 (2003) 330-331.
[65] R. Asapu, V.M. Palla, B. Wang, Z.H. Guo, R. Sadu, D.H. Chen, Phosphorus-doped titania nanotubes with enhanced photocatalytic activity, Journal of Photochemistry and Photobiology a-Chemistry, 225 (2011) 81-87.
[66] R.Y. Zheng, L. Lin, J.L. Xie, Y.X. Zhu, Y.C. Me, State of doped phosphorus and its influence on the physicochemical and photocatalytic properties of P-doped titania, Journal of Physical Chemistry C, 112 (2008) 15502-15509.
[67] Q. Shi, D. Yang, Z.Y. Jiang, J. Li, Visible-light photocatalytic regeneration of NADH using P-doped TiO2 nanoparticles, Journal of Molecular Catalysis B-Enzymatic, 43 (2006) 44-48.
[68] A. Zaleska, J.W. Sobczak, E. Grabowska, J. Hupka, Preparation and photocatalytic activity of boron-modified TiO_2 under UV and visible light, Applied Catalysis B-Environmental, 78 (2008) 92-100.
[69] N. Lu, X. Quan, J.Y. Li, S. Chen, H.T. Yu, G.H. Chen, Fabrication of boron-doped TiO_2 nanotube array electrode and investigation of its photoelectrochemical capability, Journal of Physical Chemistry C, 111 (2007) 11836-11842.
[70] S. In, A. Orlov, R. Berg, F. Garcia, S. Pedrosa-Jimenez, M.S. Tikhov, D.S. Wright, R.M. Lambert, Effective visible light-activated B-Doped and B,N-Codoped TiO_2 photocatalysts, Journal of the American Chemical Society, 129 (2007) 13790-+.
[71] D. Chen, D. Yang, Q. Wang, Z.Y. Jiang, Effects of boron doping on photocatalytic activity and microstructure of titanium dioxide nanoparticles, Industrial & Engineering Chemistry Research, 45 (2006) 4110-4116.

[72] H. Xu, Z. Zheng, L.Z. Zhang, H.L. Zhang, F. Deng, Hierarchical chlorine-doped rutile TiO_2 spherical clusters of nanorods: Large-scale synthesis and high photocatalytic activity, Journal of Solid State Chemistry, 181 (2008) 2516-2522.
[73] H.M. Luo, T. Takata, Y.G. Lee, J.F. Zhao, K. Domen, Y.S. Yan, Photocatalytic activity enhancing for titanium dioxide by co-doping with bromine and chlorine, Chemistry of Materials, 16 (2004) 846-849.
[74] H.Q. Sun, S.B. Wang, H.M. Ang, M.O. Tade, Q. Li, Halogen element modified titanium dioxide for visible light photocatalysis, Chemical Engineering Journal, 162 (2010) 437-447.
[75] Y. Ma, X.L. Wang, Y.S. Jia, X.B. Chen, H.X. Han, C. Li, Titanium Dioxide-Based Nanomaterials for Photocatalytic Fuel Generations, Chemical Reviews, 114 (2014) 9987-10043.
[76] H.Q. Sun, S.Z. Liu, S.M. Liu, S.B. Wang, A comparative study of reduced graphene oxide modified TiO_2, ZnO and Ta_2O_5 in visible light photocatalytic/photochemical oxidation of methylene blue, Applied Catalysis B-Environmental, 146 (2014) 162-168.
[77] S.Z. Liu, H.Q. Sun, A. Suvorova, S.B. Wang, One-pot hydrothermal synthesis of ZnO-reduced graphene oxide composites using Zn powders for enhanced photocatalysis, Chemical Engineering Journal, 229 (2013) 533-539.
[78] H.Q. Sun, X.H. Feng, S.B. Wang, H.M. Ang, M.O. Tade, Combination of adsorption, photochemical and photocatalytic degradation of phenol solution over supported zinc oxide: Effects of support and sulphate oxidant, Chemical Engineering Journal, 170 (2011) 270-277.
[79] L.W. Zhang, H.Y. Cheng, R.L. Zong, Y.F. Zhu, Photocorrosion Suppression of ZnO Nanoparticles via Hybridization with Graphite-like Carbon and Enhanced Photocatalytic Activity, Journal of Physical Chemistry C, 113 (2009) 2368-2374.
[80] H.B. Fu, T.G. Xu, S.B. Zhu, Y.F. Zhu, Photocorrosion Inhibition and Enhancement of Photocatalytic Activity for ZnO via Hybridization with C-60, Environmental Science & Technology, 42 (2008) 8064-8069.
[81] M.T. Uddin, Y. Nicolas, C. Olivier, T. Toupance, L. Servant, M.M. Muller, H.J. Kleebe, J. Ziegler, W. Jaegermann, Nanostructured SnO_2-ZnO Heterojunction Photocatalysts Showing Enhanced Photocatalytic Activity for the Degradation of Organic Dyes, Inorganic Chemistry, 51 (2012) 7764-7773.

[82] V. Stengl, S. Bakardjieva, N. Murafa, V. Houskova, K. Lang, Visible-light photocatalytic activity of TiO_2/ZnS nanocomposites prepared by homogeneous hydrolysis, Microporous and Mesoporous Materials, 110 (2008) 370-378.
[83] S.F. Chen, W. Zhao, W. Liu, S.J. Zhang, Preparation, characterization and activity evaluation of p-n junction photocatalyst p-ZnO/n-TiO_2, Applied Surface Science, 255 (2008) 2478-2484.
[84] D. Li, H. Haneda, Photocatalysis of sprayed nitrogen-containing Fe_2O_3-ZnO and WO3-ZnO composite powders in gas-phase acetaldehyde decomposition, Journal of Photochemistry and Photobiology a-Chemistry, 160 (2003) 203-212.
[85] L.L. Sun, D.X. Zhao, Z.M. Song, C.X. Shan, Z.H. Zhang, B.H. Li, D.Z. Shen, Gold nanoparticles modified ZnO nanorods with improved photocatalytic activity, Journal of Colloid and Interface Science, 363 (2011) 175-181.
[86] C.L. Ren, B.F. Yang, M. Wu, J.A. Xu, Z.P. Fu, Y. Lv, T. Guo, Y.X. Zhao, C.Q. Zhu, Synthesis of Ag/ZnO nanorods array with enhanced photocatalytic performance, Journal of Hazardous Materials, 182 (2010) 123-129.
[87] P. Pawinrat, O. Mekasuwandumrong, J. Panpranot, Synthesis of Au-ZnO and Pt-ZnO nanocomposites by one-step flame spray pyrolysis and its application for photocatalytic degradation of dyes, Catalysis Communications, 10 (2009) 1380-1385.
[88] M.J. Height, S.E. Pratsinis, O. Mekasuwandumrong, P. Praserthdam, Ag-ZnO catalysts for UV-photodegradation of methylene blue, Applied Catalysis B-Environmental, 63 (2006) 305-312.
[89] K. Rekha, M. Nirmala, M.G. Nair, A. Anukaliani, Structural, optical, photocatalytic and antibacterial activity of zinc oxide and manganese doped zinc oxide nanoparticles, Physica B-Condensed Matter, 405 (2010) 3180-3185.
[90] R. Ullah, J. Dutta, Photocatalytic degradation of organic dyes with manganese-doped ZnO nanoparticles, Journal of Hazardous Materials, 156 (2008) 194-200.
[91] K.G. Kanade, B.B. Kale, J.O. Baeg, S.M. Lee, C.W. Lee, S.J. Moon, H.J. Chang, Self-assembled aligned Cu doped ZnO nanoparticles for photocatalytic hydrogen production under visible light irradiation, Materials Chemistry and Physics, 102 (2007) 98-104.
[92] S. Rehman, R. Ullah, A.M. Butt, N.D. Gohar, Strategies of making TiO2 and ZnO visible light active, Journal of Hazardous Materials, 170 (2009) 560-569.

[93] Y. Guo, H.S. Wang, C.L. He, L.J. Qiu, X.B. Cao, Uniform Carbon-Coated ZnO Nanorods: Microwave-Assisted Preparation, Cytotoxicity, and Photocatalytic Activity, Langmuir, 25 (2009) 4678-4684.

[94] D. Li, H. Haneda, Synthesis of nitrogen-containing ZnO powders by spray pyrolysis and their visible-light photocatalysis in gas-phase acetaldehyde decomposition, Journal of Photochemistry and Photobiology a-Chemistry, 155 (2003) 171-178.

[95] Y.D. Hou, X.C. Wang, L. Wu, Z.X. Ding, X.Z. Fu, Efficient decomposition of benzene over a beta-Ga_2O_3 photocatalyst under ambient conditions, Environmental Science & Technology, 40 (2006) 5799-5803.

[96] X. Wang, Q. Xu, M.R. Li, S. Shen, X.L. Wang, Y.C. Wang, Z.C. Feng, J.Y. Shi, H.X. Han, C. Li, Photocatalytic Overall Water Splitting Promoted by an alpha-beta phase Junction on Ga_2O_3, Angewandte Chemie-International Edition, 51 (2012) 13089-13092.

[97] B.C. Faust, M.R. Hoffmann, D.W. Bahnemann, Photocatalytic oxidation of sulfur-dioxide in aqueous suspensions of alpha-Fe_2O_3, Journal of Physical Chemistry, 93 (1989) 6371-6381.

[98] G.K. Pradhan, D.K. Padhi, K.M. Parida, Fabrication of alpha-Fe_2O_3 Nanorod/RGO Composite: A Novel Hybrid Photocatalyst for Phenol Degradation, Acs Applied Materials & Interfaces, 5 (2013) 9101-9110.

[99] G. Liu, Q. Deng, H.Q. Wang, D.H.L. Ng, M.G. Kong, W.P. Cai, G.Z. Wang, Micro/nanostructured alpha-Fe_2O_3 spheres: synthesis, characterization, and structurally enhanced visible-light photocatalytic activity, Journal of Materials Chemistry, 22 (2012) 9704-9713.

[100] M. Barroso, A.J. Cowan, S.R. Pendlebury, M. Gratzel, D.R. Klug, J.R. Durrant, The Role of Cobalt Phosphate in Enhancing the Photocatalytic Activity of alpha-Fe_2O_3 toward Water Oxidation, Journal of the American Chemical Society, 133 (2011) 14868-14871.

[101] H.L. Xu, W.Z. Wang, W. Zhu, Shape evolution and size-controllable synthesis of Cu_2O octahedra and their morphology-dependent photocatalytic properties, Journal of Physical Chemistry B, 110 (2006) 13829-13834.

[102] M. Hara, T. Kondo, M. Komoda, S. Ikeda, K. Shinohara, A. Tanaka, J.N. Kondo, K. Domen, Cu_2O as a photocatalyst for overall water splitting under visible light irradiation, Chemical Communications, (1998) 357-358.
[103] T. Murase, H. Irie, K. Hashimoto, Visible light sensitive photocatalysts, nitrogen-doped Ta_2O_5 powders, Journal of Physical Chemistry B, 108 (2004) 15803-15807.
[104] L. Zhou, W.Z. Wang, H.L. Xu, S.M. Sun, M. Shang, Bi_2O_3 Hierarchical Nanostructures: Controllable Synthesis, Growth Mechanism, and their Application in Photocatalysis, Chemistry-a European Journal, 15 (2009) 1776-1782.
[105] L.S. Zhang, W.Z. Wang, J.O. Yang, Z.G. Chen, W.Q. Zhang, L. Zhou, S.W. Liu, Sonochemical synthesis of nanocrystallite Bi_2O_3 as a visible-light-driven photocatalyst, Applied Catalysis a-General, 308 (2006) 105-110.
[106] J. Kim, C.W. Lee, W. Choi, Platinized WO_3 as an Environmental Photocatalyst that Generates OH Radicals under Visible Light, Environmental Science & Technology, 44 (2010) 6849-6854.
[107] D. Chen, J.H. Ye, Hierarchical WO_3 hollow shells: Dendrite, sphere, dumbbell, and their photocatalytic properties, Advanced Functional Materials, 18 (2008) 1922-1928.
[108] Z.G. Zou, J.H. Ye, K. Sayama, H. Arakawa, Direct splitting of water under visible light irradiation with an oxide semiconductor photocatalyst, Nature, 414 (2001) 625-627.
[109] Q. Liu, Y. Zhou, J.H. Kou, X.Y. Chen, Z.P. Tian, J. Gao, S.C. Yan, Z.G. Zou, High-Yield Synthesis of Ultralong and Ultrathin Zn_2GeO_4 Nanoribbons toward Improved Photocatalytic Reduction of CO_2 into Renewable Hydrocarbon Fuel, Journal of the American Chemical Society, 132 (2010) 14385-14387.
[110] J.W. Tang, Z.G. Zou, J.H. Ye, Photocatalytic decomposition of organic contaminants by Bi_2WO_6 under visible light irradiation, Catalysis Letters, 92 (2004) 53-56.
[111] J.W. Tang, Z.G. Zou, J.H. Ye, Efficient photocatalytic decomposition of organic contaminants over $CaBi_2O_4$ under visible-light irradiation, Angewandte Chemie-International Edition, 43 (2004) 4463-4466.
[112] J.W. Tang, Z.G. Zou, J.H. Ye, Photophysical and photocatalytic properties of $AgInW_2O_8$, Journal of Physical Chemistry B, 107 (2003) 14265-14269.

[113] R. Ullah, H.Q. Sun, S.B. Wang, H.M. Ang, M.O. Tade, Wet-Chemical Synthesis of InTaO4 for Photocatalytic Decomposition of Organic Contaminants in Air and Water with UV-vis Light, Industrial & Engineering Chemistry Research, 51 (2012) 1563-1569.

[114] R. Ullah, H.Q. Sun, H.M. Ang, M.O. Tade, S.B. Wang, Visible light photocatalytic degradation of organics on nanoparticles of bi-metallic oxides, Separation and Purification Technology, 89 (2012) 98-106.

[115] R. Ullah, H.Q. Sun, H.M. Ang, M.O. Tade, S.B. Wang, Photocatalytic oxidation of water and air contaminants with metal doped $BiTaO_4$ irradiated with visible light, Catalysis Today, 192 (2012) 203-212.

[116] H. Yamashita, K. Mori, S. Shironita, Y. Horiuchi, Applications of single-site photocatalysts to the design of unique surface functional materials, Catalysis Surveys from Asia, 12 (2008) 88-100.

[117] M. Anpo, T.H. Kim, M. Matsuoka, The design of Ti-, V-, Cr-oxide single-site catalysts within zeolite frameworks and their photocatalytic reactivity for the decomposition of undesirable molecules-The role of their excited states and reaction mechanisms, Catalysis Today, 142 (2009) 114-124.

[118] M. Anpo, J.M. Thomas, Single-site photocatalytic solids for the decomposition of undesirable molecules, Chemical Communications, (2006) 3273-3278.

[119] N.Z. Bao, L.M. Shen, T. Takata, K. Domen, Self-templated synthesis of nanoporous CdS nanostructures for highly efficient photocatalytic hydrogen production under visible, Chemistry of Materials, 20 (2008) 110-117.

[120] T. Aruga, K. Domen, S. Naito, T. Onishi, K. Tamaru, The role of sulfite anion as a hole scavenger in the photocatalytic hydrogen formation from water on cds semiconductor under illumination of visible-light, Chemistry Letters, (1983) 1037-1040.

[121] X. Zong, G.P. Wu, H.J. Yan, G.J. Ma, J.Y. Shi, F.Y. Wen, L. Wang, C. Li, Photocatalytic H-2 Evolution on MoS_2/CdS Catalysts under Visible Light Irradiation, Journal of Physical Chemistry C, 114 (2010) 1963-1968.

[122] X.W. Wang, G. Liu, Z.G. Chen, F. Li, L.Z. Wang, G.Q. Lu, H.M. Cheng, Enhanced photocatalytic hydrogen evolution by prolonging the lifetime of carriers in ZnO/CdS heterostructures, Chemical Communications, (2009) 3452-3454.

[123] G.S. Li, D.Q. Zhang, J.C. Yu, A New Visible-Light Photocatalyst: CdS Quantum Dots Embedded Mesoporous TiO_2, Environmental Science & Technology, 43 (2009) 7079-7085.

[124] H. Park, W. Choi, M.R. Hoffmann, Effects of the preparation method of the ternary CdS/TiO_2/Pt hybrid photocatalysts on visible light-induced hydrogen production, Journal of Materials Chemistry, 18 (2008) 2379-2385.

[125] Z. Yu, B.S. Yin, F.Y. Qu, X. Wu, Synthesis of self-assembled CdS nanospheres and their photocatalytic activities by photodegradation of organic dye molecules, Chemical Engineering Journal, 258 (2014) 203-209.

[126] L. Zhu, Z.D. Meng, K.Y. Cho, W.C. Oh, Synthesis of CdS/CNT-TiO_2 with a high photocatalytic activity in the photodegradation of methylene blue, New Carbon Materials, 27 (2012) 166-174.

[127] M. Hamity, R.H. Lema, C.A. Suchetti, H.E. Gsponer, UV-vis photodegradation of dyes in the presence of colloidal Q-CdS, Journal of Photochemistry and Photobiology a-Chemistry, 200 (2008) 445-450.

[128] J.S. Hu, L.L. Ren, Y.G. Guo, H.P. Liang, A.M. Cao, L.J. Wan, C.L. Bai, Mass production and high photocatalytic activity of ZnS nanoporous nanoparticles, Angewandte Chemie-International Edition, 44 (2005) 1269-1273.

[129] H. Fujiwara, H. Hosokawa, K. Murakoshi, Y. Wada, S. Yanagida, Surface characteristics of ZnS nanocrystallites relating to their photocatalysis for CO_2 reduction, Langmuir, 14 (1998) 5154-5159.

[130] H.R. Pouretedal, H. Motamedi, A. Amiri, Aromatic compounds photodegradation catalyzed by ZnS and CdS nanoparticles, Desalination and Water Treatment, 44 (2012) 92-99.

[131] M. El-Kemary, H. El-Shamy, Fluorescence modulation and photodegradation characteristics of safranin O dye in the presence of ZnS nanoparticles, Journal of Photochemistry and Photobiology a-Chemistry, 205 (2009) 151-155.

[132] Y.G. Li, Y.L. Li, C.M. Araujo, W. Luo, R. Ahuja, Single-layer MoS_2 as an efficient photocatalyst, Catalysis Science & Technology, 3 (2013) 2214-2220.

[133] Y.H. Sang, Z.H. Zhao, M.W. Zhao, P. Hao, Y.H. Leng, H. Liu, From UV to Near-Infrared, WS_2 Nanosheet: A Novel Photocatalyst for Full Solar Light Spectrum Photodegradation, Advanced Materials, 27 (2015) 363-369.

[134] H.X. Guo, Y.C. Ke, D.F. Wang, K.L. Lin, R.X. Shen, J.H. Chen, W. Weng, Efficient adsorption and photocatalytic degradation of Congo red onto hydrothermally synthesized NiS nanoparticles, Journal of Nanoparticle Research, 15 (2013).

[135] M. Basu, A.K. Sinha, M. Pradhan, S. Sarkar, Y. Negishi, Govind, T. Pal, Evolution of Hierarchical Hexagonal Stacked Plates of CuS from Liquid-Liquid Interface and its Photocatalytic Application for Oxidative Degradation of Different Dyes under Indoor Lighting, Environmental Science & Technology, 44 (2010) 6313-6318.

[136] Z.D. Meng, T. Ghosh, L. Zhu, J.G. Choi, C.Y. Park, W.C. Oh, Synthesis of fullerene modified with Ag2S with high photocatalytic activity under visible light, Journal of Materials Chemistry, 22 (2012) 16127-16135.

[137] I. Tsuji, Y. Shimodaira, H. Kato, H. Kobayashi, A. Kudo, Novel Stannite-type Complex Sulfide Photocatalysts A(2)(I)-Zn-A(IV)-S-4 (A(I) = Cu and Ag; A(IV) = Sn and Ge) for Hydrogen Evolution under Visible-Light Irradiation, Chemistry of Materials, 22 (2010) 1402-1409.

[138] L. Zheng, Y. Xu, Y. Song, C.Z. Wu, M. Zhang, Y. Xie, Nearly Monodisperse CuInS2 Hierarchical Microarchitectures for Photocatalytic H-2 Evolution under Visible Light, Inorganic Chemistry, 48 (2009) 4003-4009.

[139] Q. Li, H. Meng, P. Zhou, Y.Q. Zheng, J. Wang, J.G. Yu, J.R. Gong, Zn1-xCdxS Solid Solutions with Controlled Bandgap and Enhanced Visible-Light Photocatalytic H-2-Production Activity, Acs Catalysis, 3 (2013) 882-889.

[140] G. Hitoki, A. Ishikawa, T. Takata, J.N. Kondo, M. Hara, K. Domen, Ta3N5 as a novel visible light-driven photocatalyst (lambda < 600 nm), Chemistry Letters, (2002) 736-737.

[141] S.S.K. Ma, T. Hisatomi, K. Maeda, Y. Moriya, K. Domen, Enhanced Water Oxidation on Ta_3N_5 Photocatalysts by Modification with Alkaline Metal Salts, Journal of the American Chemical Society, 134 (2012) 19993-19996.

[142] Y.G. Lee, T. Watanabe, T. Takata, M. Hara, M. Yoshimura, K. Domen, Effect of high-pressure ammonia treatment on the activity of Ge3N4 photocatalyst for overall water splitting, Journal of Physical Chemistry B, 110 (2006) 17563-17569.

[143] Q.S. Gao, C. Giordano, M. Antonietti, Controlled Synthesis of Tantalum Oxynitride and Nitride Nanoparticles, Small, 7 (2011) 3334-3340.

[144] T. Hisatomi, K. Teramura, J. Kubota, K. Domen, Characterization of Spinel Zinc Titanium Nitride Oxide as a Visible Light Driven Photocatalyst, Bulletin of the Chemical Society of Japan, 81 (2008) 1647-1656.
[145] Y. Tian, T. Tatsuma, Mechanisms and applications of plasmon-induced charge separation at TiO_2 films loaded with gold nanoparticles, Journal of the American Chemical Society, 127 (2005) 7632-7637.
[146] X. Chen, H.Y. Zhu, J.C. Zhao, Z.T. Zheng, X.P. Gao, Visible-light-driven oxidation of organic contaminants in air with gold nanoparticle catalysts on oxide supports, Angewandte Chemie-International Edition, 47 (2008) 5353-5356.
[147] K. Awazu, M. Fujimaki, C. Rockstuhl, J. Tominaga, H. Murakami, Y. Ohki, N. Yoshida, T. Watanabe, A plasmonic photocatalyst consisting of sliver nanoparticles embedded in titanium dioxide, Journal of the American Chemical Society, 130 (2008) 1676-1680.
[148] P. Wang, B.B. Huang, X.Y. Zhang, X.Y. Qin, H. Jin, Y. Dai, Z.Y. Wang, J.Y. Wei, J. Zhan, S.Y. Wang, J.P. Wang, M.H. Whangbo, Highly Efficient Visible-Light Plasmonic Photocatalyst Ag@AgBr, Chemistry-a European Journal, 15 (2009) 1821-1824.
[149] C.H. An, S.N. Peng, Y.G. Sun, Facile Synthesis of Sunlight-Driven AgCl:Ag Plasmonic Nanophotocatalyst, Advanced Materials, 22 (2010) 2570-2574.
[150] J.B. Cui, Y.J. Li, L. Liu, L. Chen, J. Xu, J.W. Ma, G. Fang, E.B. Zhu, H. Wu, L.X. Zhao, L.Y. Wang, Y. Huang, Near-Infrared Plasmonic-Enhanced Solar Energy Harvest for Highly Efficient Photocatalytic Reactions, Nano Letters, 15 (2015) 6295-6301.
[151] Z.W. Liu, W.B. Hou, P. Pavaskar, M. Aykol, S.B. Cronin, Plasmon Resonant Enhancement of Photocatalytic Water Splitting Under Visible Illumination, Nano Letters, 11 (2011) 1111-1116.
[152] P. Zhang, T. Wang, J.L. Gong, Mechanistic Understanding of the Plasmonic Enhancement for Solar Water Splitting, Advanced Materials, 27 (2015) 5328-5342.
[153] S. Linic, P. Christopher, D.B. Ingram, Plasmonic-metal nanostructures for efficient conversion of solar to chemical energy, Nature Materials, 10 (2011) 911-921.
[154] H.Q. Sun, G.L. Zhou, Y.X. Wang, A. Suvorova, S.B. Wang, A New Metal-Free Carbon Hybrid for Enhanced Photocatalysis, Acs Applied Materials & Interfaces, 6 (2014) 16745-16754.

[155] M. Groenewolt, M. Antonietti, Synthesis of g-C_3N_4 nanoparticles in mesoporous silica host matrices, Advanced Materials, 17 (2005) 1789-+.
[156] X.C. Wang, K. Maeda, A. Thomas, K. Takanabe, G. Xin, J.M. Carlsson, K. Domen, M. Antonietti, A metal-free polymeric photocatalyst for hydrogen production from water under visible light, Nature Materials, 8 (2009) 76-80.
[157] J.S. Zhang, J.H. Sun, K. Maeda, K. Domen, P. Liu, M. Antonietti, X.Z. Fu, X.C. Wang, Sulfur-mediated synthesis of carbon nitride: Band-gap engineering and improved functions for photocatalysis, Energy & Environmental Science, 4 (2011) 675-678.
[158] M. Shalom, S. Inal, C. Fettkenhauer, D. Neher, M. Antonietti, Improving Carbon Nitride Photocatalysis by Supramolecular Preorganization of Monomers, Journal of the American Chemical Society, 135 (2013) 7118-7121.
[159] J.D. Hong, X.Y. Xia, Y.S. Wang, R. Xu, Mesoporous carbon nitride with in situ sulfur doping for enhanced photocatalytic hydrogen evolution from water under visible light, Journal of Materials Chemistry, 22 (2012) 15006-15012.
[160] H.J. Yan, Soft-templating synthesis of mesoporous graphitic carbon nitride with enhanced photocatalytic H-2 evolution under visible light, Chemical Communications, 48 (2012) 3430-3432.
[161] Y.W. Zhang, J.H. Liu, G. Wu, W. Chen, Porous graphitic carbon nitride synthesized via direct polymerization of urea for efficient sunlight-driven photocatalytic hydrogen production, Nanoscale, 4 (2012) 5300-5303.
[162] K.K. Han, C.C. Wang, Y.Y. Li, M.M. Wan, Y. Wang, J.H. Zhu, Facile template-free synthesis of porous g-C3N4 with high photocatalytic performance under visible light, Rsc Advances, 3 (2013) 9465-9469.
[163] T. Sano, S. Tsutsui, K. Koike, T. Hirakawa, Y. Teramoto, N. Negishi, K. Takeuchi, Activation of graphitic carbon nitride (g-C_3N_4) by alkaline hydrothermal treatment for photocatalytic NO oxidation in gas phase, Journal of Materials Chemistry A, 1 (2013) 6489-6496.
[164] P. Niu, L.L. Zhang, G. Liu, H.M. Cheng, Graphene-Like Carbon Nitride Nanosheets for Improved Photocatalytic Activities, Advanced Functional Materials, 22 (2012) 4763-4770.

[165] S. Tonda, S. Kumar, S. Kandula, V. Shanker, Fe-doped and -mediated graphitic carbon nitride nanosheets for enhanced photocatalytic performance under natural sunlight, Journal of Materials Chemistry A, 2 (2014) 6772-6780.
[166] M. Zhang, X.J. Bai, D. Liu, J. Wang, Y.F. Zhu, Enhanced catalytic activity of potassium-doped graphitic carbon nitride induced by lower valence position, Applied Catalysis B-Environmental, 164 (2015) 77-81.
[167] X.S. Rong, F.X. Qiu, J. Rong, X.L. Zhu, J. Yan, D.Y. Yang, Enhanced visible light photocatalytic activity of W-doped porous g-C_3N_4 and effect of H_2O_2, Materials Letters, 164 (2016) 127-131.
[168] Y.G. Wang, Y.Z. Wang, Y.G. Li, H.C. Shi, Y.L. Xu, H.F. Qin, X. Li, Y.H. Zuo, S.F. Kang, L.F. Cui, Simple synthesis of Zr-doped graphitic carbon nitride towards enhanced photocatalytic performance under simulated solar light irradiation, Catalysis Communications, 72 (2015) 24-28.
[169] Y. Wang, Y. Di, M. Antonietti, H.R. Li, X.F. Chen, X.C. Wang, Excellent Visible-Light Photocatalysis of Fluorinated Polymeric Carbon Nitride Solids, Chemistry of Materials, 22 (2010) 5119-5121.
[170] S.C. Yan, Z.S. Li, Z.G. Zou, Photodegradation of Rhodamine B and Methyl Orange over Boron-Doped g-C_3N_4 under Visible Light Irradiation, Langmuir, 26 (2010) 3894-3901.
[171] G. Liu, P. Niu, C.H. Sun, S.C. Smith, Z.G. Chen, G.Q. Lu, H.M. Cheng, Unique Electronic Structure Induced High Photoreactivity of Sulfur-Doped Graphitic C3N4, Journal of the American Chemical Society, 132 (2010) 11642-11648.
[172] Y.J. Zhang, T. Mori, J.H. Ye, M. Antonietti, Phosphorus-Doped Carbon Nitride Solid: Enhanced Electrical Conductivity and Photocurrent Generation, Journal of the American Chemical Society, 132 (2010) 6294-+.
[173] J.R. Ran, T.Y. Ma, G.P. Gao, X.W. Du, S.Z. Qiao, Porous P-doped graphitic carbon nitride nanosheets for synergistically enhanced visible-light photocatalytic H-2 production, Energy & Environmental Science, 8 (2015) 3708-3717.
[174] Y.P. Zhu, T.Z. Ren, Z.Y. Yuana, Mesoporous Phosphorus-Doped g-C_3N_4 Nanostructured Flowers with Superior Photocatalytic Hydrogen Evolution Performance, Acs Applied Materials & Interfaces, 7 (2015) 16850-16856.

[175] Q. Han, C.G. Hu, F. Zhao, Z.P. Zhang, N. Chen, L.T. Qu, One-step preparation of iodine-doped graphitic carbon nitride nanosheets as efficient photocatalysts for visible light water splitting, Journal of Materials Chemistry A, 3 (2015) 4612-4619.
[176] Z.F. Huang, J.J. Song, L. Pan, Z.M. Wang, X.Q. Zhang, J.J. Zou, W.B. Mi, X.W. Zhang, L. Wang, Carbon nitride with simultaneous porous network and O-doping for efficient solar-energy-driven hydrogen evolution, Nano Energy, 12 (2015) 646-656.
[177] J.W. Fang, H.Q. Fan, M.M. Li, C.B. Long, Nitrogen self-doped graphitic carbon nitride as efficient visible light photocatalyst for hydrogen evolution, Journal of Materials Chemistry A, 3 (2015) 13819-13826.
[178] H.J. Yan, H.X. Yang, TiO2-g-C3N4 composite materials for photocatalytic H-2 evolution under visible light irradiation, Journal of Alloys and Compounds, 509 (2011) L26-L29.
[179] Y.L. Li, J.S. Wang, Y.L. Yang, Y. Zhang, D. He, Q.E. An, G.Z. Cao, Seed-induced growing various TiO_2 nanostructures on g-C_3N_4 nanosheets with much enhanced photocatalytic activity under visible light, Journal of Hazardous Materials, 292 (2015) 79-89.
[180] W.K. Jo, T.S. Natarajan, Influence of TiO_2 morphology on the photocatalytic efficiency of direct Z-scheme g-C_3N_4/TiO_2 photocatalysts for isoniazid degradation, Chemical Engineering Journal, 281 (2015) 549-565.
[181] X. Song, Y. Hu, M.M. Zheng, C.H. Wei, Solvent-free in situ synthesis of g-C_3N_4/{001}TiO_2 composite with enhanced UV- and visible-light photocatalytic activity for NO oxidation, Applied Catalysis B-Environmental, 182 (2016) 587-597.
[182] Z.A. Huang, Q. Sun, K.L. Lv, Z.H. Zhang, M. Li, B. Li, Effect of contact interface between TiO_2 and g-C3N4 on the photoreactivity of g-C_3N_4/TiO_2 photocatalyst: (001) vs (101) facets of TiO_2, Applied Catalysis B-Environmental, 164 (2015) 420-427.
[183] Y.J. Wang, R. Shi, J. Lin, Y.F. Zhu, Enhancement of photocurrent and photocatalytic activity of ZnO hybridized with graphite-like C3N4, Energy & Environmental Science, 4 (2011) 2922-2929.
[184] D. Xiao, K. Dai, Y. Qu, Y.P. Yin, H. Chen, Hydrothermal synthesis of alpha-Fe_2O_3/g-C_3N_4 composite and its efficient photocatalytic reduction of Cr(VI) under visible light, Applied Surface Science, 358 (2015) 181-187.

[185] Y.P. Zang, L.P. Li, X.G. Li, R. Lin, G.S. Li, Synergistic collaboration of g-C_3N_4/SnO_2 composites for enhanced visible-light photocatalytic activity, Chemical Engineering Journal, 246 (2014) 277-286.
[186] S.F. Chen, Y.F. Hu, S.G. Meng, X.L. Fu, Study on the separation mechanisms of photogenerated electrons and holes for composite photocatalysts g-C_3N_4-WO_3, Applied Catalysis B-Environmental, 150 (2014) 564-573.
[187] Z.Y. Zhang, D.L. Jiang, D. Li, M.Q. He, M. Chen, Construction of $SnNb_2O_6$ nanosheet/g-C_3N_4 nanosheet two-dimensional heterostructures with improved photocatalytic activity: Synergistic effect and mechanism insight, Applied Catalysis B-Environmental, 183 (2016) 113-123.
[188] H.F. Shi, G.Q. Chen, C.L. Zhang, Z.G. Zou, Polymeric g-C3N4 Coupled with $NaNbO_3$ Nanowires toward Enhanced Photocatalytic Reduction of CO_2 into Renewable Fuel, Acs Catalysis, 4 (2014) 3637-3643.
[189] Y.J. Yao, F. Lu, Y.P. Zhu, F.Y. Wei, X.T. Liu, C. Lian, S.B. Wang, Magnetic core-shell $CuFe_2O_4$@C3N4 hybrids for visible light photocatalysis of Orange II, Journal of Hazardous Materials, 297 (2015) 224-233.
[190] T.T. Zhu, Y.H. Song, H.Y. Ji, Y.G. Xu, Y.X. Song, J.X. Xia, S. Yin, Y.P. Li, H. Xu, Q. Zhang, H.M. Li, Synthesis of g-C_3N_4/Ag_3VO_4 composites with enhanced photocatalytic activity under visible light irradiation, Chemical Engineering Journal, 271 (2015) 96-105.
[191] M.S. Akple, J.X. Low, S. Wageh, A.A. Al-Ghamdi, J.G. Yu, J. Zhang, Enhanced visible light photocatalytic H-2-production of g-C_3N_4/WS_2 composite heterostructures, Applied Surface Science, 358 (2015) 196-203.
[192] Y.F. Li, K. Li, Y. Yang, L.J. Li, Y. Xing, S.Y. Song, R.C. Jin, M. Li, Ultrathin g-C_3N_4 Nanosheets Coupled with $AgIO_3$ as Highly Efficient Heterostructured Photocatalysts for Enhanced Visible-Light Photocatalytic Activity, Chemistry-a European Journal, 21 (2015) 17739-17747.
[193] L.Q. Ye, J.Y. Liu, Z. Jiang, T.Y. Peng, L. Zan, Facets coupling of BiOBr-g-C_3N_4 composite photocatalyst for enhanced visible-light-driven photocatalytic activity, Applied Catalysis B-Environmental, 142 (2013) 1-7.
[194] Q. Liu, Y.R. Guo, Z.H. Chen, Z.G. Zhang, X.M. Fang, Constructing a novel ternary Fe(III)/graphene/g-C_3N_4 composite photocatalyst with enhanced visible-light

driven photocatalytic activity via interfacial charge transfer effect, Applied Catalysis B-Environmental, 183 (2016) 231-241.
[195] X.L. Ding, Y.X. Li, J. Zhao, Y.Q. Zhu, Y. Li, W.Y. Deng, C.Y. Wang, Enhanced photocatalytic H-2 evolution over CdS/Au/g-C_3N_4 composite photocatalyst under visible-light irradiation, Apl Materials, 3 (2015).
[196] J.J. Xue, S.S. Ma, Y.M. Zhou, Z.W. Zhang, X.Y. Liu, Fabrication of porous g-C3N4/Ag/Fe2O3 composites with enhanced visible light photocatalysis performance, Rsc Advances, 5 (2015) 58738-58745.
[197] S.W. Zhang, J.X. Li, X.K. Wang, Y.S. Huang, M. Zeng, J.Z. Xu, In Situ Ion Exchange Synthesis of Strongly Coupled Ag@AgCl/g-C_3N_4 Porous Nanosheets as Plasmonic Photocatalyst for Highly Efficient Visible-Light Photocatalysis, Acs Applied Materials & Interfaces, 6 (2014) 22116-22125.
[198] H. Katsumata, T. Sakai, T. Suzuki, S. Kaneco, Highly Efficient Photocatalytic Activity of g-C_3N_4/Ag_3PO_4 Hybrid Photocatalysts through Z-Scheme Photocatalytic Mechanism under Visible Light, Industrial & Engineering Chemistry Research, 53 (2014) 8018-8025.
[199] L. Liu, Y.H. Qi, J.R. Lu, S.L. Lin, W.J. An, Y.H. Liang, W.Q. Cui, A stable Ag_3PO_4@g-C_3N_4 hybrid core@shell composite with enhanced visible light photocatalytic degradation, Applied Catalysis B-Environmental, 183 (2016) 133-141.
[200] J.J. He, H.Q. Sun, S. Indrawirawan, X.G. Duan, M.O. Tade, S.B. Wang, Novel polyoxometalate@g-C_3N_4 hybrid photocatalysts for degradation of dyes and phenolics, Journal of Colloid and Interface Science, 456 (2015) 15-21.
[201] W.Y. Lu, T.F. Xu, Y. Wang, H.G. Hu, N. Li, X.M. Jiang, W.X. Chen, Synergistic photocatalytic properties and mechanism of g-C_3N_4 coupled with zinc phthalocyanine catalyst under visible light irradiation, Applied Catalysis B-Environmental, 180 (2016) 20-28.
[202] Y.J. Zhang, T. Mori, L. Niu, J.H. Ye, Non-covalent doping of graphitic carbon nitride polymer with graphene: controlled electronic structure and enhanced optoelectronic conversion, Energy & Environmental Science, 4 (2011) 4517-4521.
[203] G.Z. Liao, S. Chen, X. Quan, H.T. Yu, H.M. Zhao, Graphene oxide modified g-C3N4 hybrid with enhanced photocatalytic capability under visible light irradiation, Journal of Materials Chemistry, 22 (2012) 2721-2726.

[204] L. Ge, C.C. Han, Synthesis of MWNTs/g-C_3N_4 composite photocatalysts with efficient visible light photocatalytic hydrogen evolution activity, Applied Catalysis B-Environmental, 117 (2012) 268-274.
[205] J.S. Zhang, G.G. Zhang, X.F. Chen, S. Lin, L. Mohlmann, G. Dolega, G. Lipner, M. Antonietti, S. Blechert, X.C. Wang, Co-Monomer Control of Carbon Nitride Semiconductors to Optimize Hydrogen Evolution with Visible Light, Angewandte Chemie-International Edition, 51 (2012) 3183-3187.
[206] S. Chu, Y. Wang, Y. Guo, J.Y. Feng, C.C. Wang, W.J. Luo, X.X. Fan, Z.G. Zou, Band Structure Engineering of Carbon Nitride: In Search of a Polymer Photocatalyst with High Photooxidation Property, Acs Catalysis, 3 (2013) 912-919.
[207] F. He, G. Chen, Y.G. Yu, S. Hao, Y.S. Zhou, Y. Zheng, Facile Approach to Synthesize g-PAN/g-C_3N_4 Composites with Enhanced Photocatalytic H-2 Evolution Activity, Acs Applied Materials & Interfaces, 6 (2014) 7171-7179.
[208] S.Z. Liu, H.Q. Sun, K. O'Donnell, H.M. Ang, M.O. Tade, S.B. Wang, Metal-free melem/g-C_3N_4 hybrid photocatalysts for water treatment, Journal of Colloid and Interface Science, 464 (2016) 10-17.
[209] L.L. Zhang, Z.G. Xiong, X.S. Zhao, Pillaring Chemically Exfoliated Graphene Oxide with Carbon Nanotubes for Photocatalytic Degradation of Dyes under Visible Light Irradiation, Acs Nano, 4 (2010) 7030-7036.
[210] H.C. Hsu, I. Shown, H.Y. Wei, Y.C. Chang, H.Y. Du, Y.G. Lin, C.A. Tseng, C.H. Wang, L.C. Chen, Y.C. Lin, K.H. Chen, Graphene oxide as a promising photocatalyst for CO2 to methanol conversion, Nanoscale, 5 (2013) 262-268.
[211] H.T. Li, R.H. Liu, S.Y. Lian, Y. Liu, H. Huang, Z.H. Kang, Near-infrared light controlled photocatalytic activity of carbon quantum dots for highly selective oxidation reaction, Nanoscale, 5 (2013) 3289-3297.
[212] J.K. Liu, S.H. Wen, Y. Hou, F. Zuo, G.J.O. Beran, P.Y. Feng, Boron Carbides as Efficient, Metal-Free, Visible-Light-Responsive Photocatalysts, Angewandte Chemie-International Edition, 52 (2013) 3241-3245.
[213] C.J. Huang, C. Chen, M.W. Zhang, L.H. Lin, X.X. Ye, S. Lin, M. Antonietti, X.C. Wang, Carbon-doped BN nanosheets for metal-free photoredox catalysis, Nature Communications, 6 (2015).
[214] G. Liu, P. Niu, H.M. Cheng, Visible-Light-Active Elemental Photocatalysts, Chemphyschem, 14 (2013) 885-892.

[215] G. Liu, P. Niu, L.C. Yin, H.M. Cheng, alpha-Sulfur Crystals as a Visible-Light-Active Photocatalyst, Journal of the American Chemical Society, 134 (2012) 9070-9073.
[216] F. Wang, W.K.H. Ng, J.C. Yu, H.J. Zhu, C.H. Li, L. Zhang, Z.F. Liu, Q. Li, Red phosphorus: An elemental photocatalyst for hydrogen formation from water, Applied Catalysis B-Environmental, 111 (2012) 409-414.
[217] G. Liu, L.C. Yin, P. Niu, W. Jiao, H.M. Cheng, Visible-Light-Responsive beta-Rhombohedral Boron Photocatalysts, Angewandte Chemie-International Edition, 52 (2013) 6242-6245.

3

Chapter 3: Synthesis of graphitic carbon nitride for degradation of methylene blue and sulfachloropyridazine solutions

Abstract

As a promising metal-free photocatalyst, graphitic carbon nitride (g-C_3N_4) has been widely studied. In this chapter, a series of g-C_3N_4 samples were synthesized by a thermal condensation method using different precursors such as melamine, urea, thiourea and D-glucose. These prepared g-C_3N_4 were investigated as photocatalysts and compared in degradation of methylene blue (MB) and sulfachloropyridazine (SCP) solutions under visible-light. This study demonstrated that the g-C_3N_4 prepared by melamine (heated at 550 ℃, 2 h) was the most stable and effective photocatalyst in degradation of 10 ppm MB solution. It also showed the highest efficiency in degradation in 20 ppm SCP solutions. This work indicated that the easily obtained g-C_3N_4 from the precursor of melamine is the most effective for degradation of organic pollutants.

3.1 Introduction

In recent years, graphitic carbon nitride (g-C_3N_4) has attracted much more attention in photocatalyts for many applications, such as water splitting [1], CO_2 reduction [2], decomposition of organic pollutants [3], organic synthesis [4] and bacterial disinfection [5]. At present, g-C_3N_4 has been considered as one of the most promising metal-free photocatalysts due to its unique merits, for example, low cost, earth abundance and stability and non-toxicity [6, 7] which lead to versatile applications in fields of energy conversion and environmental remediation.

A variety of attempts have been carried out in order to obtain g-C_3N_4 with a high thermal stability and photocatalytic activity, such as top-down strategy, template approach, supramolecular preorganization and solvothermal method.[7] Using different synthesis method or different precursors might be able to control the properties of g-C_3N_4. It was reported that several precursors have been employed, including melamine, urea, thiourea, cyanamide and dicyandiamide.[6, 8-11]

Melamine, urea, thiourea and their mixtures, as the non-toxic and low-cost nitrogen-rich precursors, can be used to simply synthesise pristine g-C_3N_4 via the thermal condensation method [6].Therefore, this study aims to investigate the effect of these cost-efficient precursors on the photocatalytic activity of g-C_3N_4 prepared.

3.2 Experimental section

3.2.1 Chemicals and materials

Melamine (99%), thiourea (99%) and urea (99%) were received from Sigma-Aldrich. D-glucose (99.5%) was obtained from Sigma. And ethanol (99.9%) was purchased from Chem Supply. Methylene blue (MB, 99%) and sulfachloropyridazine (SCP, 99%) were obtained from Sigma. All the chemicals were used directly without any further purification.

3.2.2 Synthesis of photocatalysts

3.2.2.1 Synthesis of graphitic carbon nitride (g-C_3N_4)

All the graphitic carbon nitrides (g-C_3N_4) samples were synthesized by a thermal condensation method. The first group of g-C_3N_4 was prepared via pure melamine. In this method, 5 g melamine was put into a 30 mL crucible with a cover and then the

crucible was transferred into a muffle furnace to heat in the static air at 550 ℃ for 2 h. The heating rate was 10 ℃/min. After that, the muffle furnace was naturally cooled down to room temperature. The g-C_3N_4 sample was then obtained and labelled as g-C_3N_4 (P).

The second sample was synthesized via the similar route with introducing ethanol as a solvent. Firstly, 5 g melamine was dissolved into 50 mL ethanol, and then the solution was kept magnetically stirring on a hotplate at 60 ℃ with 400 rpm for 6 h until the solution became pasty. Then, the pasty mixture was dried in an oven at 60 ℃ over 12 h. After that the dried material was grinded into powders and then heated at a muffle furnace at 550 ℃ for 2 h. The sample received was labelled as g-C_3N_4 (M).

The rest six g-C_3N_4 samples were synthesized by a modified way as that involving ethanol. But these g-C_3N_4 samples were synthesized by the different ratio of precursors, including melamine, urea, thiourea and D-glucose. Specifically, three samples were prepared by 4 g melamine and 1 g urea (g-C_3N_4 (4 g M + 1 g U)), 4 g melamine and 1 g thiourea (g-C_3N_4 (4 g M + 1 g T)), 4 g melamine and 1 g D-glucose (g-C_3N_4 (4 g M + 1 g D)), respectively. And another three samples were synthesized by 4 g melamine, 0.5 g urea and 0.5 g thiourea (g-C_3N_4 (4 g M + 0.5 g U + 0.5 g T)), 4 g melamine, 0.5 g urea and 0.5 g D-glucose (g-C_3N_4 (4 g M + 0.5 g U + 0.5 g D)), 4 g melamine, 0.5 g thiourea and 0.5 g D-glucose (g-C_3N_4 (4 g M + 0.5 g T + 0.5 g D)), respectively.

3.2.3 Characterization of materials

Powder X-ray diffraction (XRD) was employed to analyze all the crystalline structures of g-C_3N_4 samples. The XRD was carried out on a Bruker D8 Advance X-ray instrument using Cu Kα radiation with λ at 1.5418 Å with the 2 theta range of 5 to 70 ℃. A Micromeritics Tristar 3000 apparatus was used to measure the Brunauer-Emmett-Teller (BET) surface area and pore size under the circumstance of liquid nitrogen temperature. Thermogravimetric-differential thermal analysis (TG-DTA) was performed in an air flow. The heating rate was kept at 10 ℃/min and α-Al_2O_3 was the reference material.

3.2.4 Photocatalyst activity tests

3.2.4.1 Photodegradation of MB solutions

The photocatalytic activity of these g-C_3N_4 samples was tested in an aqueous methylene blue solution under UV-visible light irradiations. A 300 W Newport Oriel Universal Xenon arc lamp performed as the light source. Specifically, 100 mg photocatalyst was added into 200 mL, 10 ppm methylene blue solution. A double-jacket cylindrical reactor and a water bath were used to control the reaction temperature at 25 ℃. A magnetically stirrer was used to ensure the photocatalyst to disperse homogeneously into the MB solution during the whole process of reaction. Firstly, the reaction system was kept in dark for 30 min to achieve adsorption-desorption equilibrium, then the first 4 mL sample solution was taken into a centrifuge tube by a syringe. Afterwards, each 4 mL sample solution was taken at each time interval under the light source. The whole reaction process ran in 180 min. At last, the centrifuged sample solutions were analyzed by an UV-visible spectrophotometer (λ = 664 nm).

3.2.4.2 Photodegradation of SCP solutions

The activity of these samples was then studied in degradation of aqueous SCP solutions, similar to the degradation of MB solutions. In details, 100 mg photocatalyst was put into 200 mL of 20 ppm SCP solution. After adsorption in dark for 30 min, the light irradiation was turned on. At each time interval, 4 mL sample solution was taken with a syringe and then 1 mL sample solution was filtered through a 0.45μm Nylon film into an utra-fast high performance liquid chromatography (UHPLC) vial. The whole reaction process ran in 240 min. The concentration of sample solution was analyzed by the UHPLC, with an UV detector set at λ = 270 nm.

3.3 Results and discussion

3.3.1 Characterization of samples

3.3.1.1 XRD studies

Fig. 3.1 shows XRD patterns of the samples. In the sample that was obtained from directly heated melamine (g-C_3N_4 (P)), a sharp peak was observed at 27.4 ℃ and another peak was found at 13.0 ℃, suggesting a typical graphitic structure [12]. While for the rest of samples, only one obvious peak was observed at 27.4 ℃. This indicates

that different precursors or different pre-treatment parameters might affect the crystal phase. Solvent (ethanol) treatment appeared to significantly change the condensation procedure and led to a less crystalline structure.

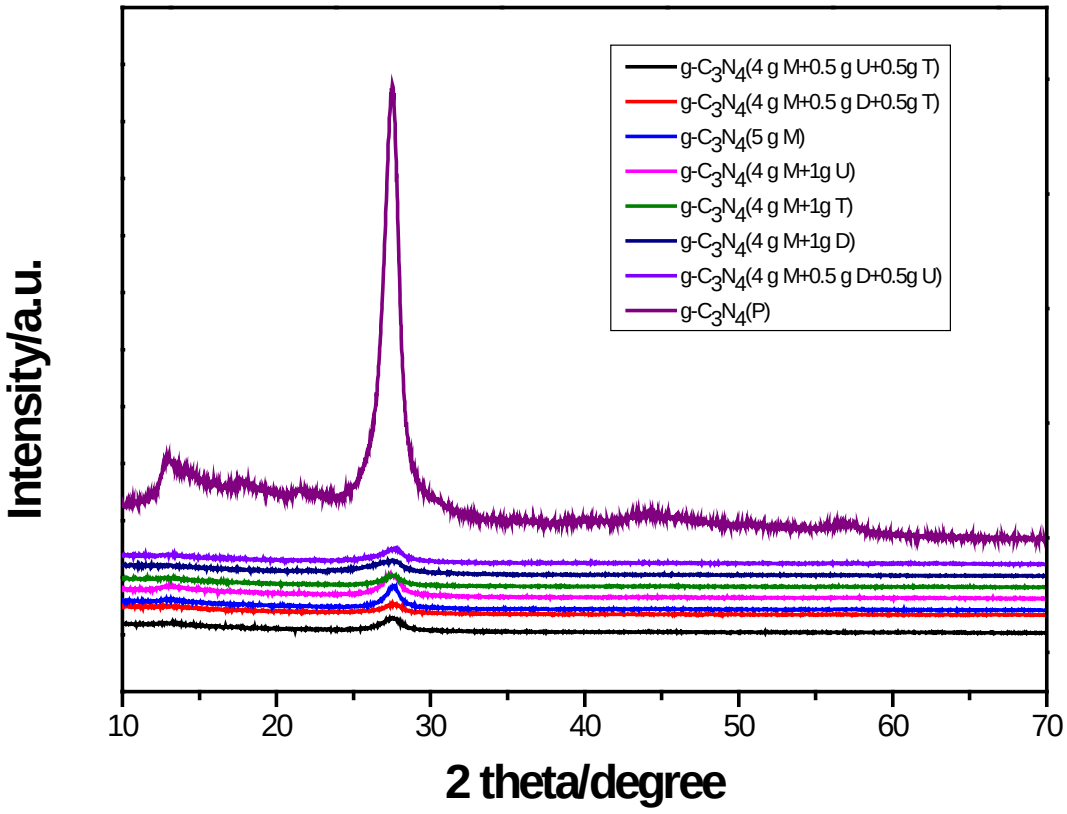

Fig. 3.1 XRD patterns of g-C_3N_4 samples.

3.3.1.2 Thermal analysis

Fig. 3.2 displays the thermal investigation of the samples. As shown in Fig. 3.2A, the two samples prepared using melamine as the precursor have the highest thermal stability in static air, and a quick weight loss occurred between 600 ℃ and 680 ℃. While the sample obtained from melamine and urea was stable up to 500 ℃, which has the lowest stability among all of these samples. The TGA curves of the rest five samples are similar which can endure the temperature around 550 ℃. This indicates that the preparation temperature determines the thermal stability of graphitic carbon nitrides to great degrees [13]. Fig. 3.2B depicts the exothermic peak of g-C_3N_4(P) is 659 ℃, while the sample g-C_3N_4 (4 g M + 0.5 g D + 0.5 g T) has the lowest thermal stability at 561 ℃.

(A)

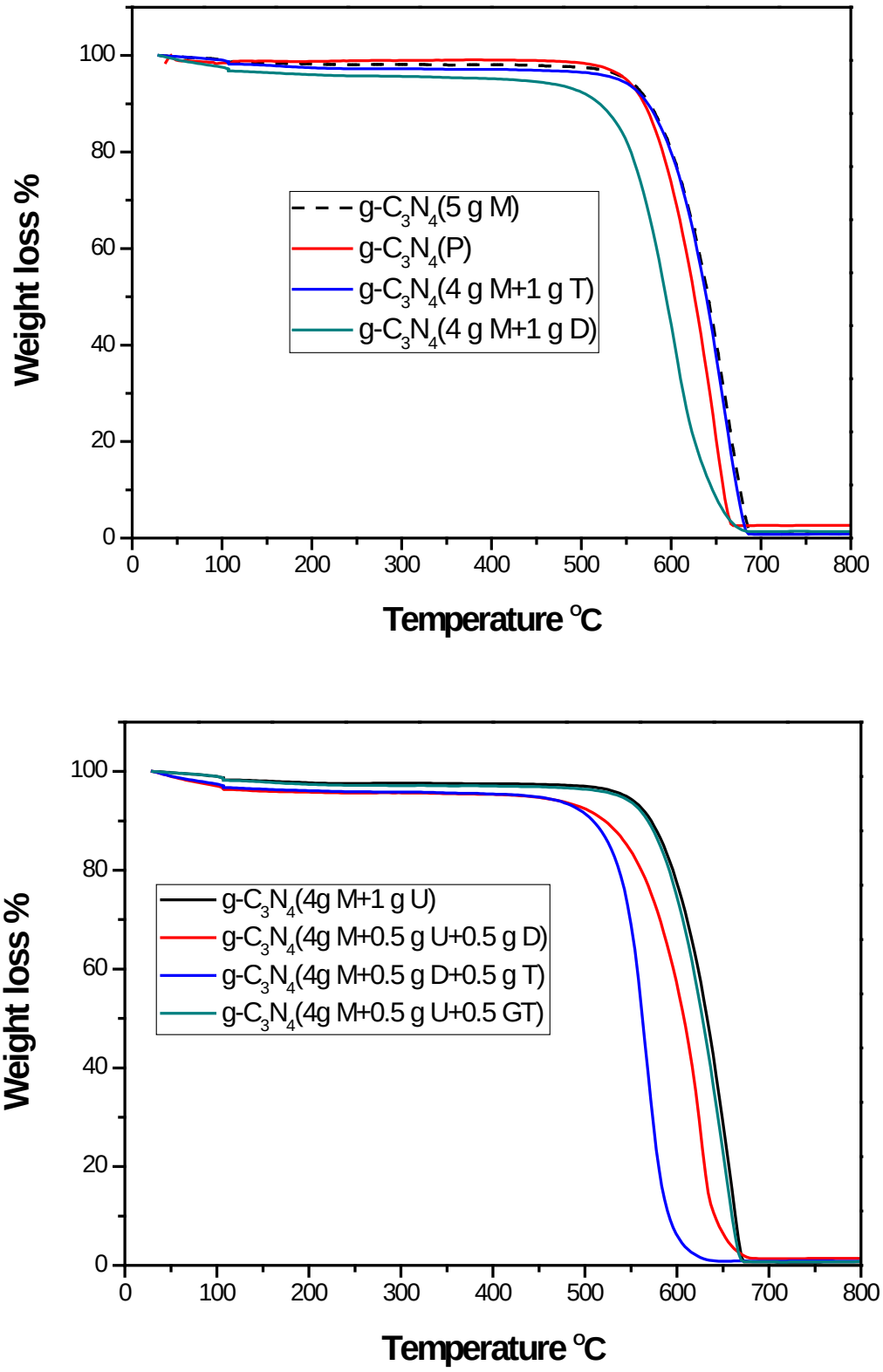

Fig 3.2 A TGA profiles of g-C_3N_4 samples.

(B)

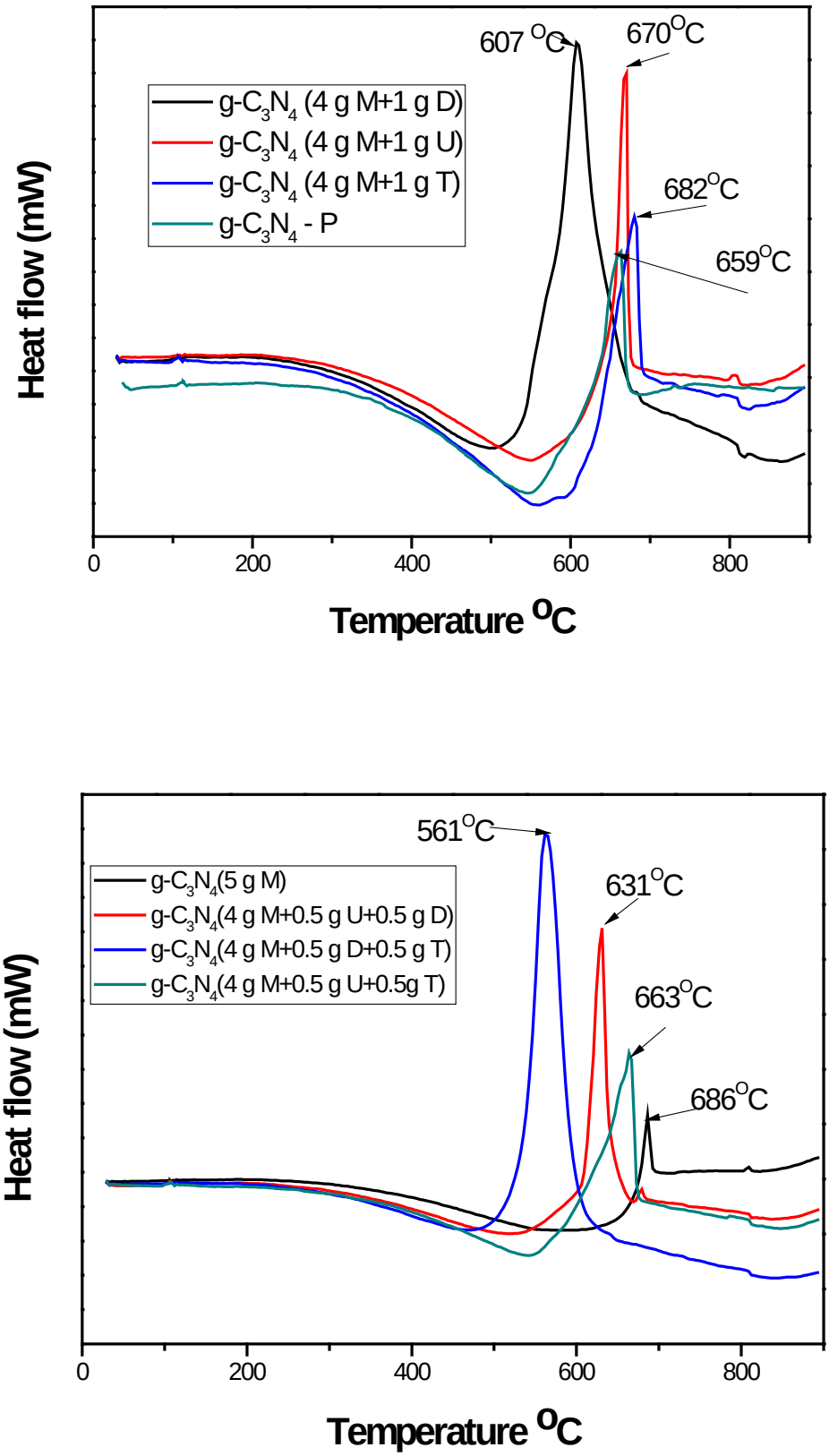

Fig. 3.2 B DSC profiles of g-C_3N_4 samples.

3.3.1.3 Nitrogen isotherms

Table 3.1 Specific surface areas (SSA) of g-C_3N_4

Catalyst	SSA (m^2/g)
g-C_3N_4-P	13
g-C_3N_4(5 g M)	15
g-C_3N_4(4 g M+1 g U)	13
g-C_3N_4(4 g M+1 g D)	24
g-C_3N_4(4 g M+1 g T)	10
g-C_3N_4(4 g M+0.5 g U+0.5 g D)	28
g-C_3N_4(4 g M+05 g U+0.5 g T)	2.6
g-C_3N_4(4 g M+0.5 g D+0.5 g T)	9.8

Table 3.1 and Fig. 3.3 illustrate the specific surface areas and nitrogen sorption isotherms, pore size distributions of these graphitic carbon nitride samples. From Table 3.1, it can be seen that g-C_3N_4 (4 g M+0.5 g U+0.5 g D) has the largest SSA while the sample g-C_3N_4 (4 g M+0.5 g U+0.5 g T) has the smallest SSA. Comparing the g-C_3N_4-P and g-C_3N_4 (5 g M), no obvious difference of SSA was observed in Table 3.1, however, the pore size of g-C_3N_4 (5 g M) is bigger than g-C_3N_4-P.

(A)

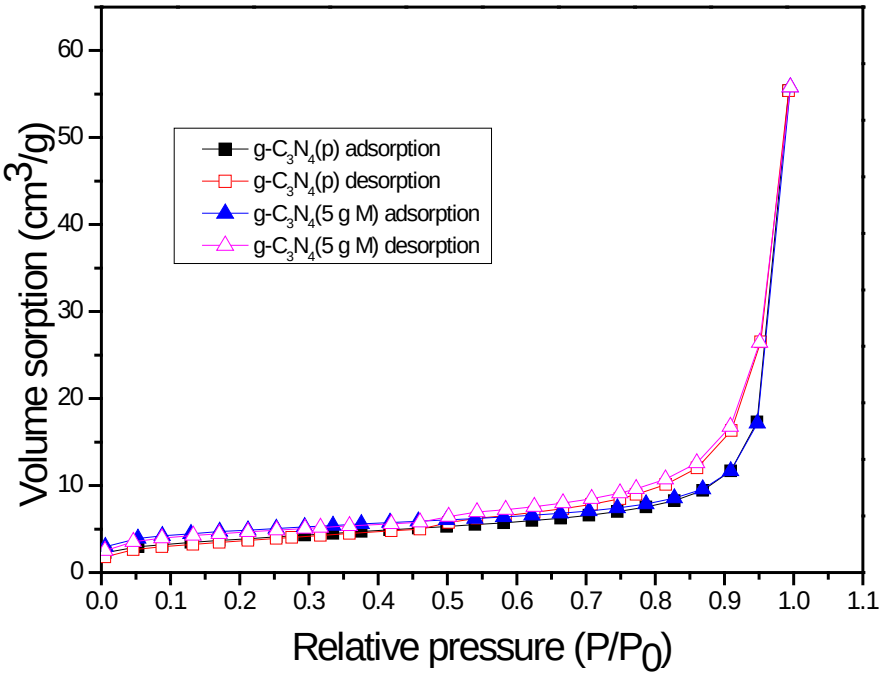
g-C3N4(p) adsorption
g-C3N4(p) desorption
g-C3N4(5 g M) adsorption
g-C3N4(5 g M) desorption
Volume sorption (cm3/g)
Relative pressure (P/P0)
0
10
20
30
40
50
60
0.0
0.1
0.2
0.3
0.4
0.5
0.6
0.7
0.8
0.9
1.0
1.1

(B)

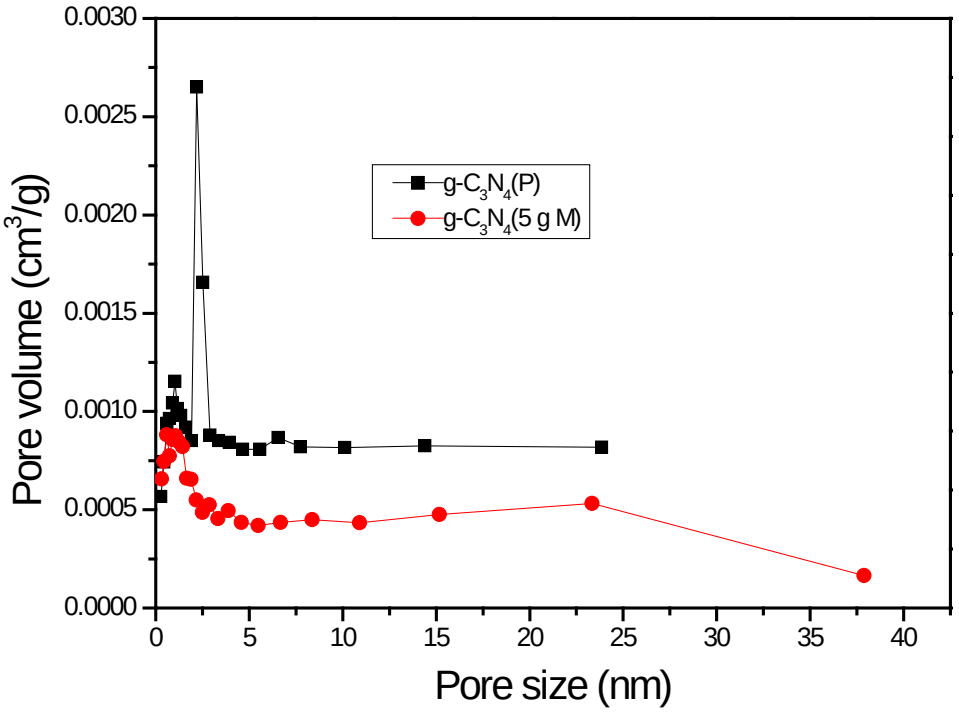
g-C3N4(P)
g-C3N4(5 g M)
Pore volume (cm3/g)
Pore size (nm)
0.0000
0.0005
0.0010
0.0015
0.0020
0.0025
0.0030
0
5
10
15
20
25
30
35
40

(C)

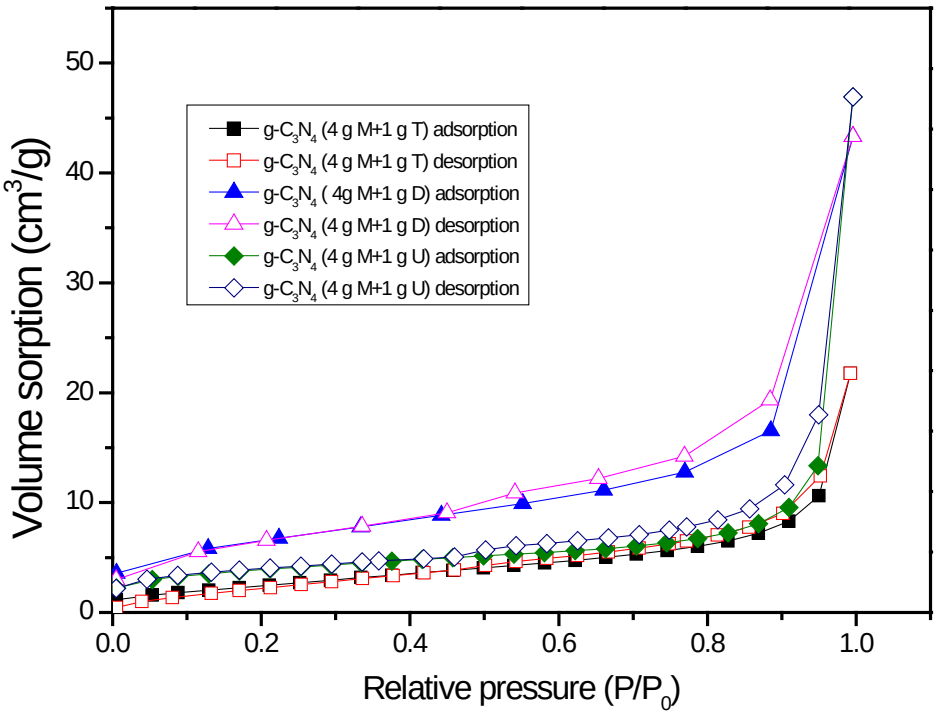

(D)

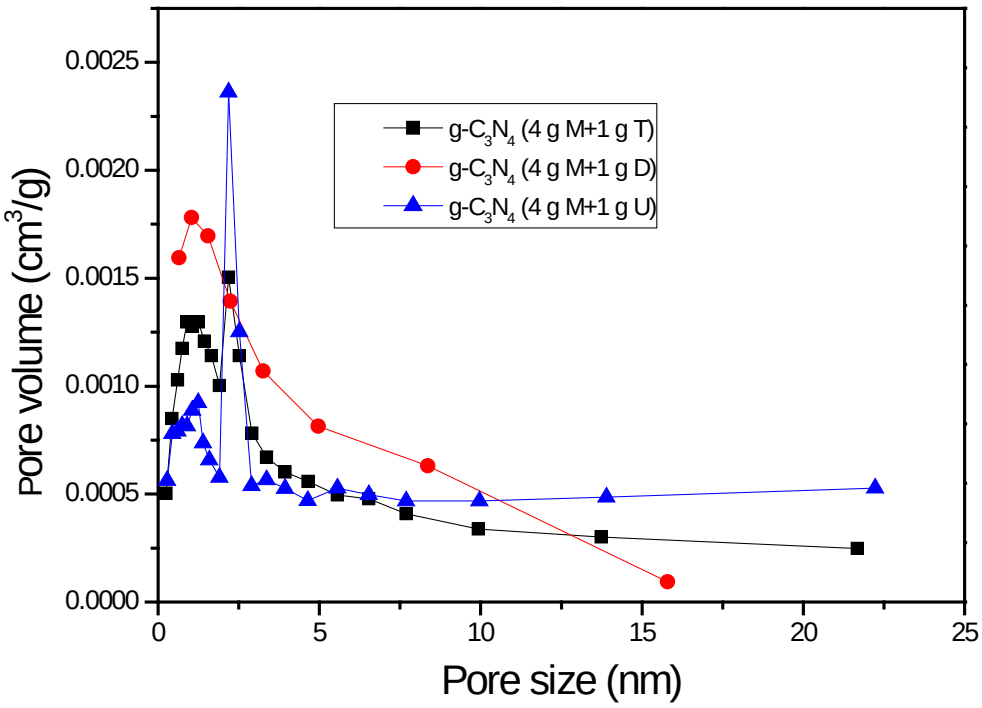

Fig. 3.3 Nitrogen sorption isotherms and pore size distributions.

3.3.2 Photodegradation tests

3.3.2.1 Photodegradation of MB solutions

Fig. 3.4 illustrates the photocatalytic activity of the samples for MB degradation under UV-vis light irradiations. It can be seen that g-C_3N_4 (M) has the highest activity, 45% of MB was degraded in 180 min. And the pristine g-C_3N_4 (P) held the second position which degraded 40% of MB within 180 min. In the meantime, around 25 to 30% of MB was degraded by the rest of samples. The results indicated that the g-C_3N_4 prepared by the precursor of melamine demonstrated a higher activity than the g-C_3N_4 obtained from the mixed precursors.

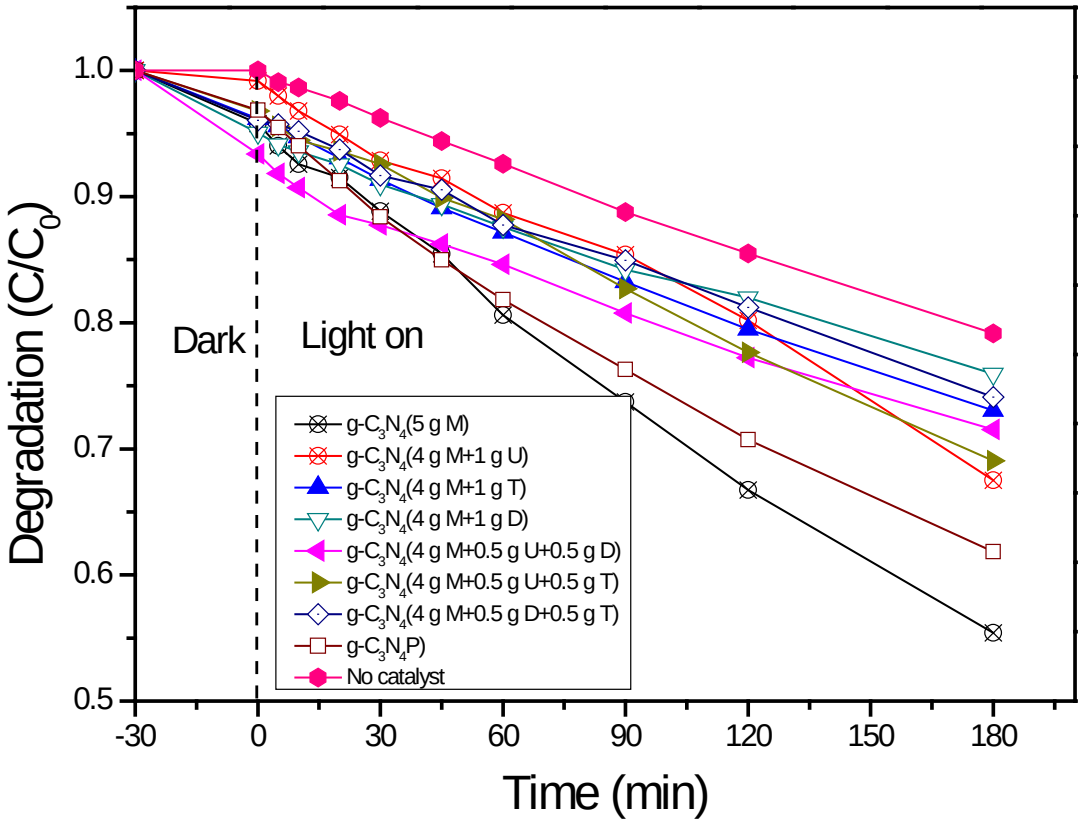

Fig. 3.4 Photodegradation of MB solution [catalyst: 0.5 g/L, MB initial concentration: 10 ppm]

3.3.2.2 Photodegradation of SCP solutions

In order to further evaluate photocatalytic activity of these samples, photodegradation of SCP was employed under the similar reaction system with test of MB. Fig. 3.5 shows that the sample (g-C_3N_4 (M)) prepared by the precursor of melamine with ethanol still has the highest activity than others. g-C_3N_4 (4 g M + 1g D) showed a similar

performance for SCP degradation. It was seen that the orders of the samples were not exactly the same as those for MB photodegradation, indicating different degradation mechanism in degradation of different organic pollutants.

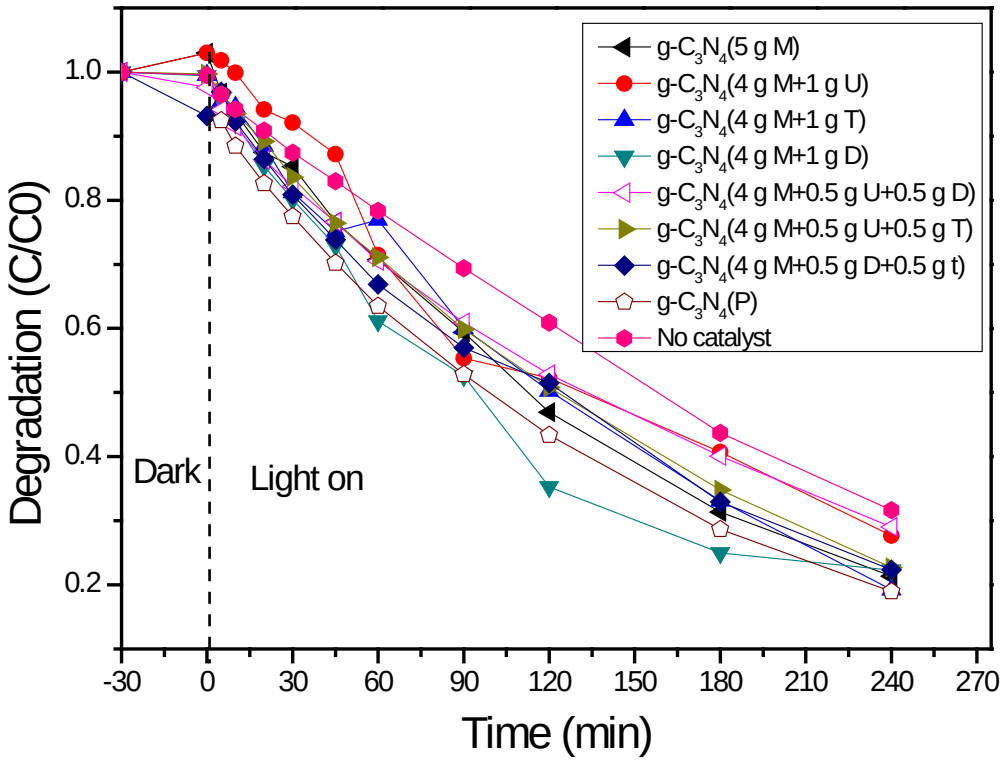

Fig 3.5 Photodegradation of SCP solution [catalyst: 0.5 g/L, SCP initial concentration: 20 ppm]

3.4 Conclusions

In summary, a series of metal-free graphitic carbon nitride photocatalysts were synthesized via a thermal condensation method using different precursors. The photocatalytic performances of these samples were investigated in photodegradation of both MB and SCP solutions. This study indicated that graphitic carbon nitride obtained from the precursor of melamine with ethanol as a solvent presents the highest photocatalytic performance than other samples. This study presents a feasible method to prepare graphitic carbon nitride and demonstrates the effect of the precursors on photocatalytic performance.

References

[1] D.J. Martin, P.J.T. Reardon, S.J.A. Moniz, J. Tang, Visible Light-Driven Pure Water Splitting by a Nature-Inspired Organic Semiconductor-Based System, Journal of the American Chemical Society, 136 (2014) 12568-12571.

[2] J. Lin, Z. Pan, X. Wang, Photochemical Reduction of CO_2 by Graphitic Carbon Nitride Polymers, Acs Sustainable Chemistry & Engineering, 2 (2014) 353-358.

[3] J. Yu, S. Wang, J. Low, W. Xiao, Enhanced photocatalytic performance of direct Z-scheme g-C_3N_4-TiO_2 photocatalysts for the decomposition of formaldehyde in air, Physical Chemistry Chemical Physics, 15 (2013) 16883-16890.

[4] J. Liu, J. Huang, H. Zhou, M. Antonietti, Uniform Graphitic Carbon Nitride Nanorod for Efficient Photocatalytic Hydrogen Evolution and Sustained Photoenzymatic Catalysis, Acs Applied Materials & Interfaces, 6 (2014) 8434-8440.

[5] J. Huang, W. Ho, X. Wang, Metal-free disinfection effects induced by graphitic carbon nitride polymers under visible light illumination, Chemical Communications, 50 (2014) 4338-4340.

[6] S.W. Cao, J.X. Low, J.G. Yu, M. Jaroniec, Polymeric Photocatalysts Based on Graphitic Carbon Nitride, Advanced Materials, 27 (2015) 2150-2176.

[7] Y. Zheng, L.H. Lin, B. Wang, X.C. Wang, Graphitic Carbon Nitride Polymers toward Sustainable Photoredox Catalysis, Angewandte Chemie-International Edition, 53 (2015) 12868-12884.

[8] S.C. Yan, Z.S. Li, Z.G. Zou, Photodegradation Performance of g-C_3N_4 Fabricated by Directly Heating Melamine, Langmuir, 25 (2009) 10397-10401.

[9] F. Dong, Z.Y. Wang, Y.J. Sun, W.K. Ho, H.D. Zhang, Engineering the nanoarchitecture and texture of polymeric carbon nitride semiconductor for enhanced visible light photocatalytic activity, Journal of Colloid and Interface Science, 401 (2013) 70-79.

[10] K. Maeda, X.C. Wang, Y. Nishihara, D.L. Lu, M. Antonietti, K. Domen, Photocatalytic Activities of Graphitic Carbon Nitride Powder for Water Reduction and Oxidation under Visible Light, Journal of Physical Chemistry C, 113 (2009) 4940-4947.

[11] H.H. Ji, F. Chang, X.F. Hu, W. Qin, J.W. Shen, Photocatalytic degradation of 2,4,6-trichlorophenol over g-C_3N_4 under visible light irradiation, Chemical Engineering Journal, 218 (2013) 183-190.

[12] X.C. Wang, K. Maeda, A. Thomas, K. Takanabe, G. Xin, J.M. Carlsson, K. Domen, M. Antonietti, A metal-free polymeric photocatalyst for hydrogen production from water under visible light, Nature Materials, 8 (2009) 76-80.
[13] H.Q. Sun, G.L. Zhou, Y.X. Wang, A. Suvorova, S.B. Wang, A New Metal-Free Carbon Hybrid for Enhanced Photocatalysis, Acs Applied Materials & Interfaces, 6 (2014) 16745-16754.

4

Chapter 4: Solvothermal synthesis of hybrids of graphitic carbon nitride and nanodiamonds for photocatalysis and photoelectrochemical applications

Abstract

Graphitic carbon nitride (g-C_3N_4) has been considered as a feasible, cost-effective and eco-friendly metal-free photocatalyst for various applications. However, its photocatalytic efficiency is still low. Great efforts have been made to improve the activity of g-C_3N_4 in recent years. Herein, a series of hybrids of g-C_3N_4 (GCN) and nanodiamonds (NDs) were synthesized using a solvothermal method. The photocatalytic activity of the GCN/NDs was investigated in photodegradation of methylene blue (MB) solutions. Photocurrent density under UV-visible light irradiations was also measured to demonstrate the potential application in the field of photoelectrochemistry. In this study, 0.1 g GCN/0.05 g NDs displayed the best photocatalytic activity and the strongest photocurrent density.

4.1 Introduction

In modern society, the increasing water pollution that caused by rapid industrialization and expanding civilization has attracted worldwide concerns[1]. A variety of methods and technologies have been made to cope with water treatment. In the meantime, photocatalysis, as a green technology, has demonstrated a great potential in removal of organic pollutants from contaminated water because it is cost-effective, clean and sustainable [2-4]. The application of metal-based photocatalysts has resulted in secondary contamination from metal leaching into water [5]. More recently, the breakthrough of development in metal-free photocatalysts has shown a capability to overcome this drawback [6].

Graphitic carbon nitride, as a green, metal-free photocatalyst, has been widely employed for hydrogen production, CO_2 reduction and removal of organic pollutants owing to its unique structure and physicochemical properties [4, 7-9]. However, the photocatalytic efficiency of g-C_3N_4 still remains at a low level because of the low specific surface area (SSA) (usually below 10 m^2 g^{-1}), high recombination rate, slow charge mobility and relatively short absorption range [10, 11]. Currently, great efforts have been made to enhance g-C_3N_4 photocatalytic activity, while coupling with other nanocarbons attracts more attention because the metal-free nature is still remained [2].

In recent years, nanodiamonds (NDs), as a non-toxic carbonaceous material, have attracted more scientific interests because they have large surface areas, unique optical and chemical properties.[12] As a result, NDs have been applied for fabrication of hybrids in composite materials, for example, nanodiamonds-TiO_2 [13-15] and nanodiamonds-graphene oxide.[16] Jang et al. also reported that the composite of nanodiamonds-rGO had high and stable photoelectrochemical activity under visible light.[17]

In this study, a series of novel hybrid photocatalysts, nanodiamonds-g-C_3N_4, were synthesized via a solvothermal route. The photocatalytic efficiency of the hybrids was investigated in photodegradation of aqueous methylene blue (MB) solutions under UV-vis light irradiations. And the photoelectrochemical activity was evaluated in an electrochemical cell under irradiations.

4.2 Experimental section

4.2.1 Materials and chemicals

Nanodiamonds (particle size below 10 nm) and melamine (99.9%) were purchased from Sigma-Aldrich. Methylene blue (99.9%) and N, N-dimethylformamide (DMF) were obtained from Sigma. Ethanol (99.9%) was received from Chem Supply. All the chemicals and materials were used as received without any further purification.

4.2.2 Synthesis of catalysts

4.2.2.1 Synthesis of graphitic carbon nitride

Graphitic carbon nitride was prepared by using the precursor of melamine via a thermal condensation method. In details, 5 g melamine was put into a crucible with a loose cover and then heated at 550 ℃ for 2 h in a muffle furnace with a heating rate of 10 ℃/min. When the temperature cooled down to room temperature, the solid pristine g-C_3N_4 was obtained and then grinded into powder for further use.

4.2.2.2 Synthesis of g-C_3N_4/NDs

0.1 g g-C_3N_4 and 0.05 g NDs were put into 80 mL N, N-dimethylformamide (DMF). The mixed solution was kept magnetically stirring for 30 min and then underwent ultrasonication for 30 min to ensure that g-C_3N_4 and NDs were dispersed homogeneously into DMF solution. After that, the mixture was transferred into a stainless steel autoclave and heated in an oven at 150 ℃ for 24 h. When the autoclave was cooled down to room temperature, the mixture was separated by a centrifuge at 7500 rpm for 20 min. Then the solid was washed with ethanol and pure water each for twice. After washed thoroughly, the hybrid photocatalyst was dried in an oven at 60 ℃ for over 24 h. The 0.1 g g-C_3N_4/0.05 g NDs was obtained.

In a same way, 0.1 g g-C_3N_4-DMF and the composites of 0.1 g g-C_3N_4/0.01 g NDs, 0.1 g g-C_3N_4/0.075 g NDs and 0.1 g g-C_3N_4/0.1 g NDs were also prepared.

4.2.3 Characterization of materials

Powder X-ray diffraction (XRD) was used to analyze the crystalline structure of g-C_3N_4/NDs on a Germany Bruker D8-X-ray diffractometer with Cu Kα radiation (λ = 1.5418 Å). The XRD results were obtained from 2 theta range of 10 to 70^o. A

Micromeritics 3000 was employed to evaluate the specific surface area (SSA) and pore size distribution of the g-C_3N_4/NDs samples by liquid nitrogen sorption at -196 ^oC. The thermal analysis of these photocatalysts was performed on a Mettler-Toledo-Star equipment under air flow with a heating rate of 10 ℃/min. The morphology of the g-C_3N_4/NDs was investigated by a scanning electron microscopy (SEM). A JASCO V670 UV-vis spectrophotometer was used to record the UV-visible diffuse spectra of these samples, and $BaSO_4$ was used as the reference material. A Varian Eclipse spectrometer instrument (wavelength = 300 nm) was employed to obtain the photoluminescence (PL) spectra.

4.2.4 Photocatalysis and photoelectrochemical performances

4.2.4.1 Photodegradation of MB solutions

The photodegradation efficiency of g-C_3N_4/NDs was tested in degradation of methylene blue (MB) solutions under UV-vis light irradiations. 10 mg photocatalyst was put into 200 mL of 10 ppm MB solution under a 300 W Newport Oriel Universal Xenon arc lamp light irradiations. Detailed procedure can be referred to Chapter 3.

4.2.4.2 Photoelectrochemical activity test

Firstly, 8 mg g-C_3N_4/NDs powders were mixed with 50 µL Nafion and 500 µL ethanol in a vial. Then the vial was ultrasonicated for 20 min to enable the samples to be dispersed thoroughly. After that, the mixed paste was smeared on a 1 cm^2 square FTO glass and then the smeared glass was dried for a few minutes in air. The dried glass was used as the working electrode. The photoelectrochemical activity of the g-C_3N_4/NDs was investigated on an electrochemical workstation (Zahner Zennium) and 0 V voltage was applied. A solar simulator (TriSOL, OAI) provided the light irradiations and a three-electrode photoelectrochemical cell system was employed, including a counter electrode (a platinum wire), a reference electrode (Ag/AgCl) and a working electrode (the prepared smeared FTO glasses). Na_2SO_4 solution (0.2 mol/L) was used as the electrolyte. The light irradiation was switched on and off in each 20 sec respectively during the measurements.

4.3 Results and discussion

4.3.1 Characterization of samples

4.3.1.1 XRD results

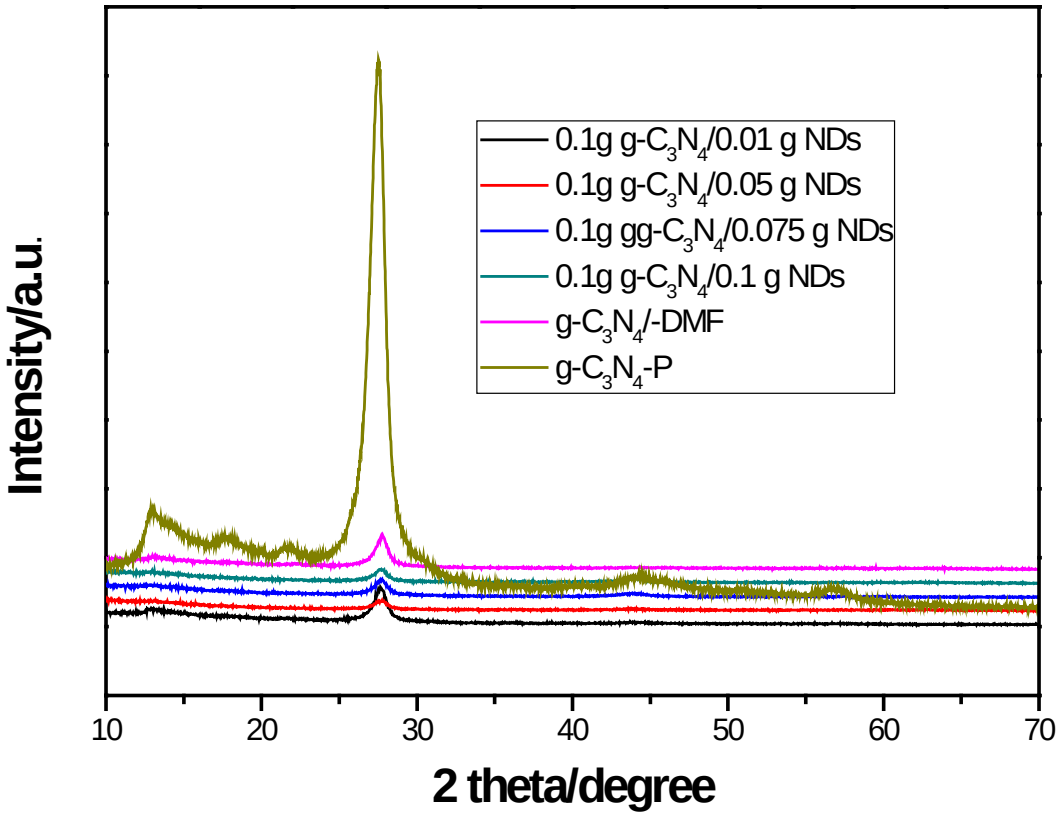

Fig. 4.1 XRD patterns of g-C_3N_4 and g-C_3N_4/NDs.

The XRD patterns of pristine g-C_3N_4 and hybrid photocatalysts are shown in Fig. 4.1. On pristine g-C_3N_4, two peaks were found at 13 and 27.4^o, which is accordance with the crystalline structures of g-C_3N_4 [18]. After solvothermal treatment with DMF, the crystalline structure appeared to be damaged at a moderate scale. Only one peak was found at around 29^o with a much lower density. It was also seen that with the increased amount of nanodiamonds, the intensity of graphitic phase declined.

4.3.1.2 Thermal analysis

Fig. 4.2 illustrates the TGA profiles of samples. It can be seen all these samples occurred a quick weight loss from 530 to 670 ℃. The significant or complete weight loss was due to the collapse of the graphitic structure and the decomposition of the

carbon nitride with oxygen into gases. The introduction of DMF (g-C_3N_4-DMF) produced porous structure and some amorphous phase in graphitic carbon nitride, and the newly formed features decreased the thermal stability of g-C_3N_4. It can be seen that the weight loss on g-C_3N_4-DMF started at around 250 ^oC. Further introduction of nanodiamonds to form a hybrid initiated earlier decomposition or oxidation of carbon nitride. Similar to weight loss of process, such effects from DMF and nanodiamonds were observed in the changes of exothermic peaks (all around at 660 ℃) between pristine g-C_3N_4 and the composites of g-C_3N_4/NDs.

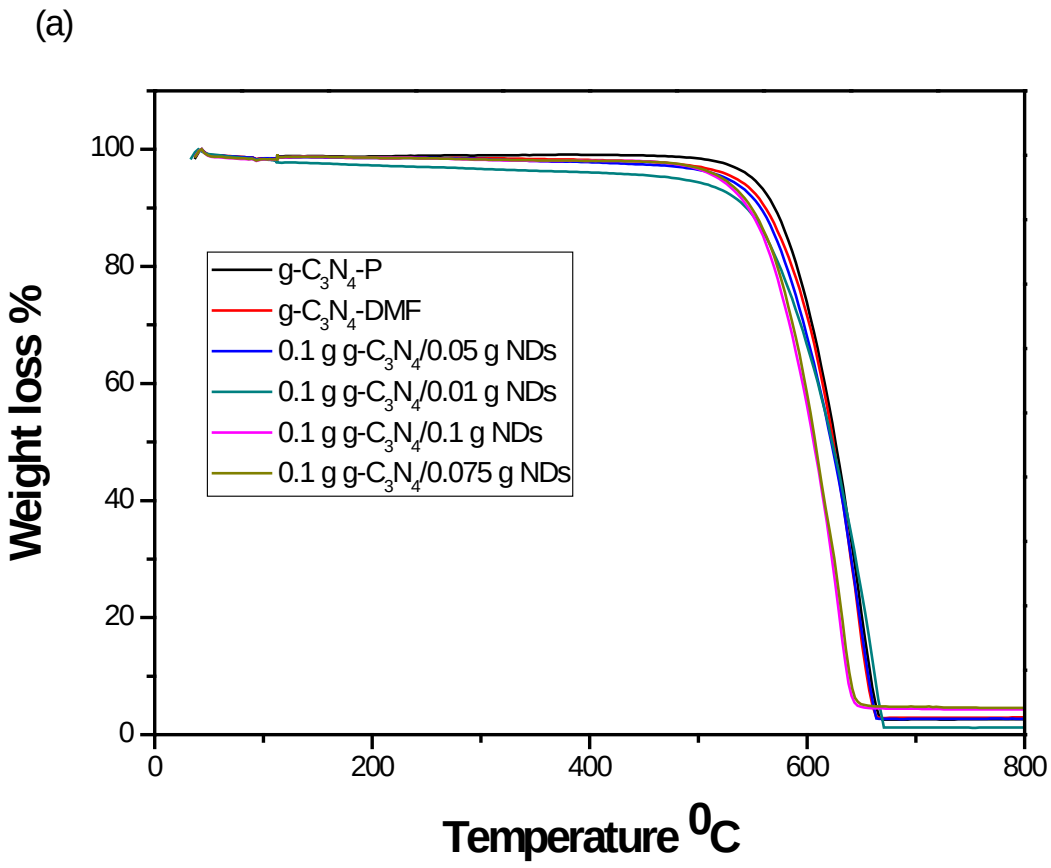

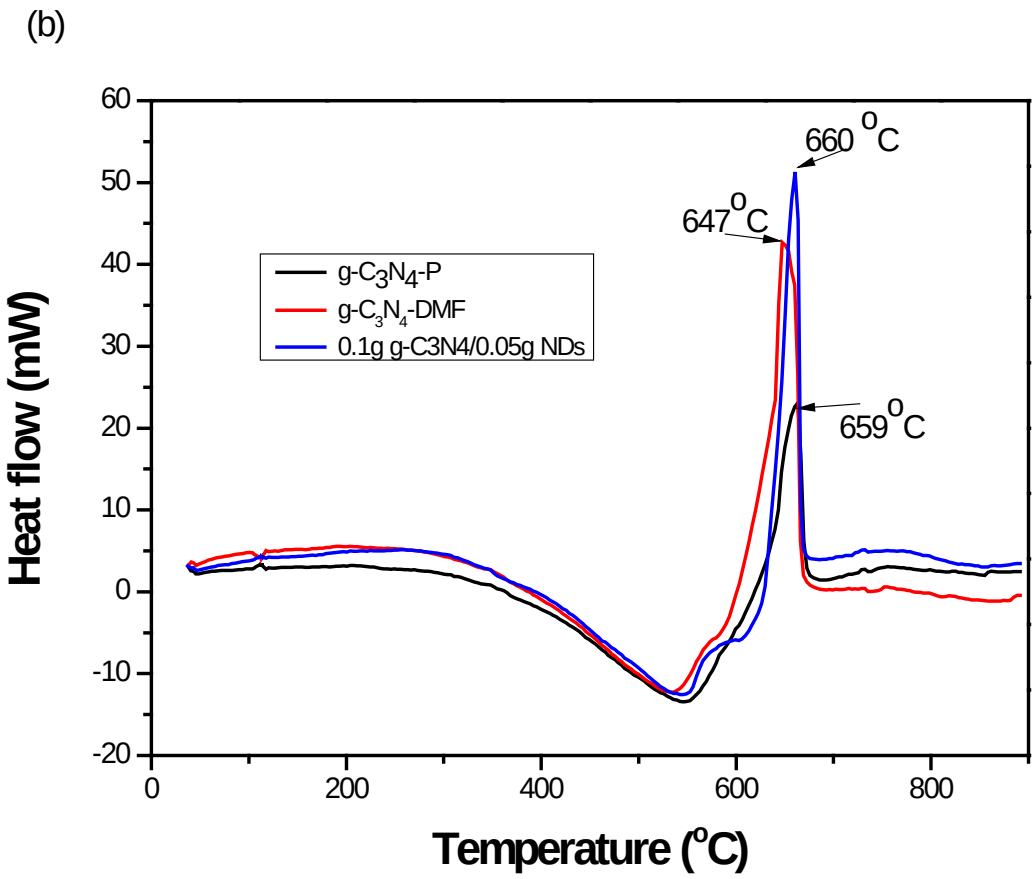

Fig 4.2 TGA (a) and DSC (b) profiles of g-C_3N_4, g-C_3N_4-DMF and g-C_3N_4/NDs.

4.3.1.3 Nitrogen isotherms

Table 4.1 Specific surface area (SSA) of g-C_3N_4-P, g-C_3N_4-DMF and g-C_3N_4/NDs.

Catalyst	SSA (m^2/g)
g-C_3N_4-P	13
g-C_3N_4-DMF	19
0.1 g g-C_3N_4/0.05 g NDs	90

The specific surface areas of g-C_3N_4, g-C_3N_4-DMF and 0.1 g g-C_3N_4/0.05 g NDs are listed in Table 4.1. As expected, the SSA of composite 0.1 g g-C_3N_4/0.05 g NDs was much larger than pristine g-C_3N_4, meanwhile, a slight SSA increase was observed after

solvothermal process between pristine g-C_3N_4 and g-C_3N_4-DMF. It was found the composites containing more NDs have larger SSAs. The reason is NDs have a larger SSA which can increase the SSA of composites. For GCN/NDs composites, some significant increases in nitrogen sorption, were observed as comparison to pristine g-C_3N_4 from Figs. 4.4 (a) and (b). In Fig. 4 (c), the mesopores were found at around 11.2 nm on all the composites GCN/NDs while 2.2 and 2.5 nm were observed on pristine g-C_3N_4 and g-C_3N_4-DMF, respectively. Compared pore size distribution of g-C_3N_4 and g-C_3N_4-DMF, we also found the mesopores on g-C_3N_4-DMF increased than pristine g-C_3N_4, in the meantime the pore size on g-C_3N_4-DMF were smaller than that of pristine g-C_3N_4. This justified the solvothermal process in DMF could affect the pore size of materials.

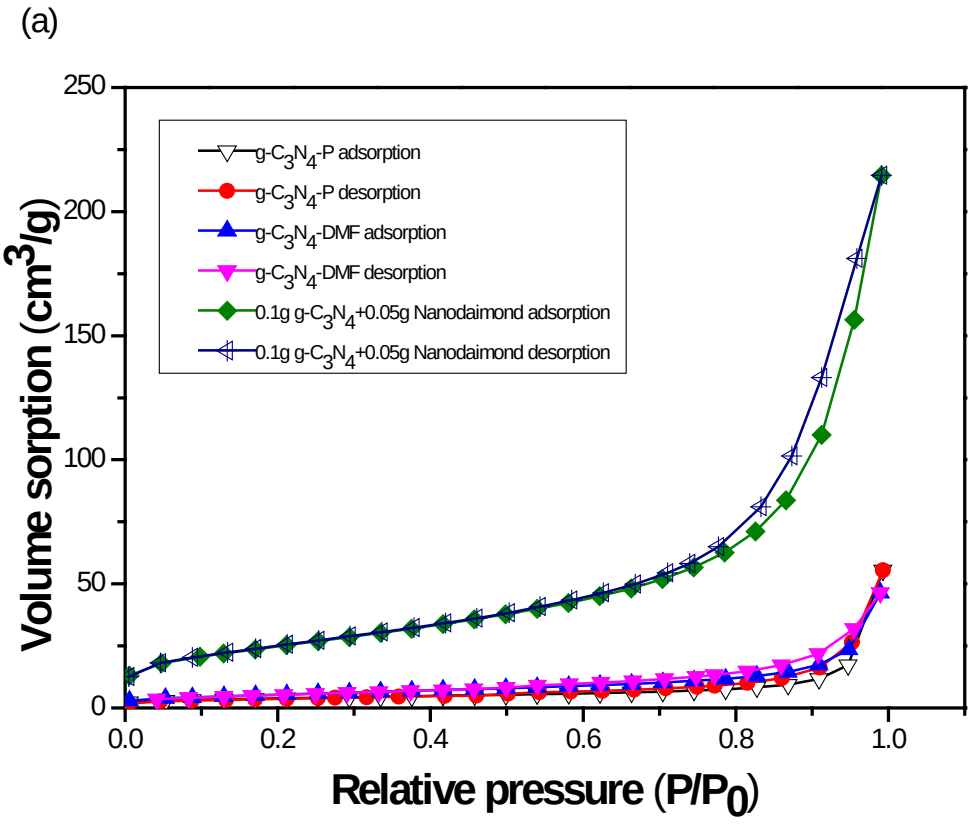

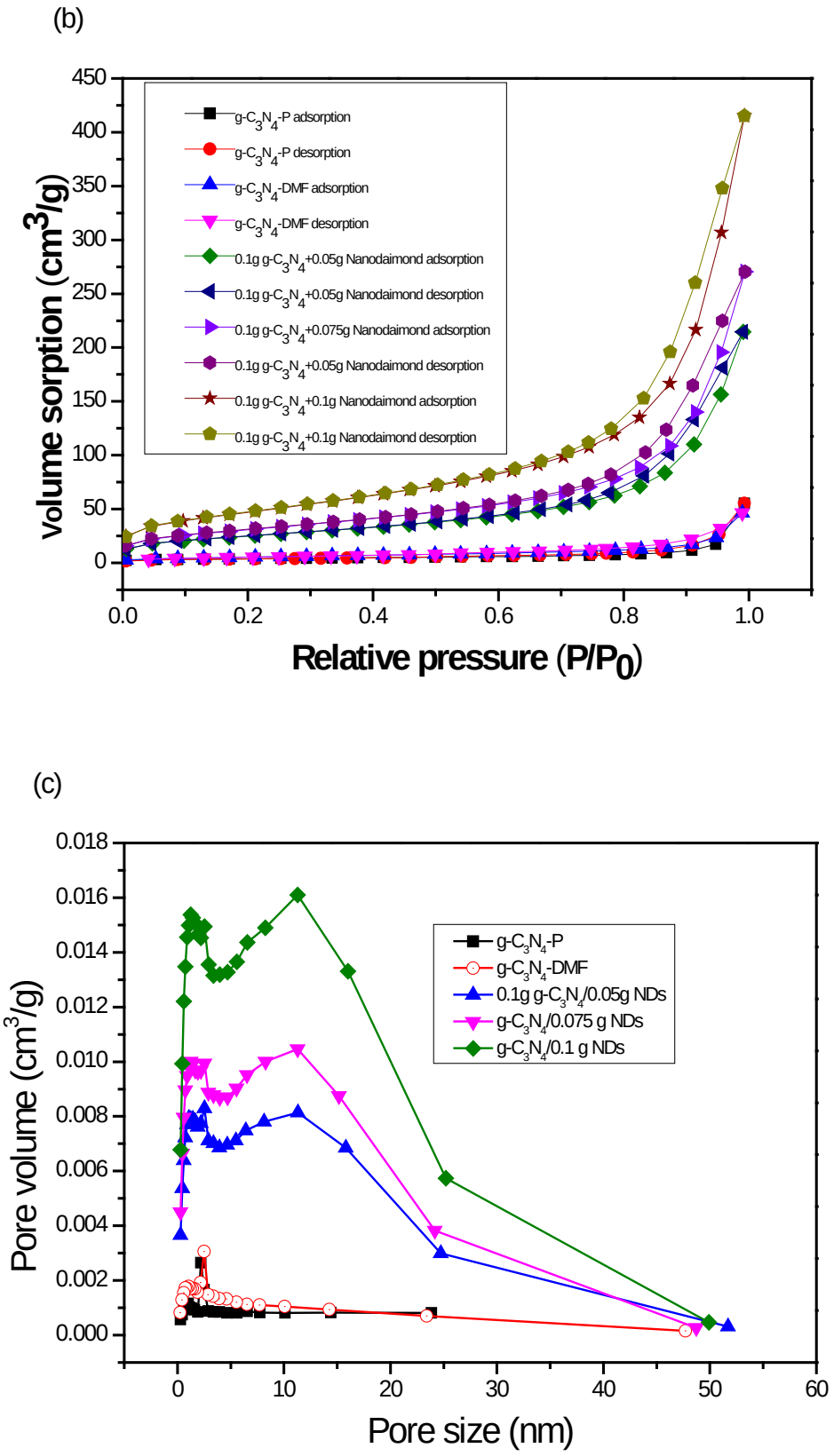

Fig. 4.4 (a) and (b) nitrogen sorption distribution of g-C_3N_4, g-C_3N_4-DMF and g-C_3N_4/NDs, and (c) pore size distribution of g-C_3N_4, g-C_3N_4-DMF and g-C_3N_4/NDs.

4.3.1.4 SEM images

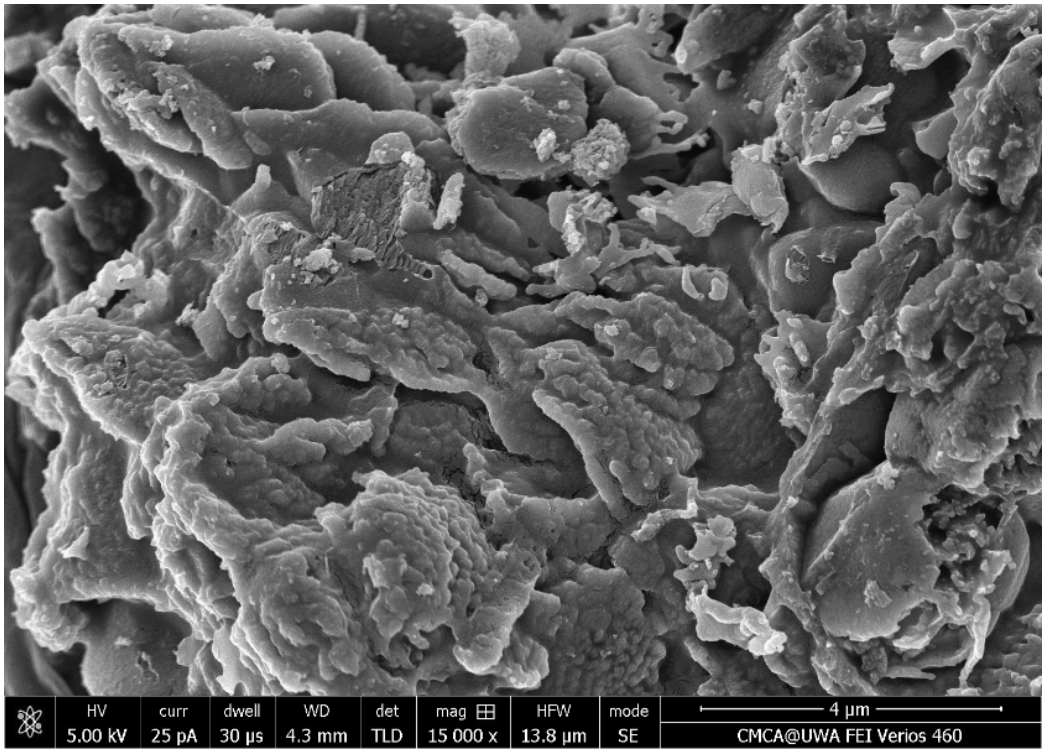

(a)

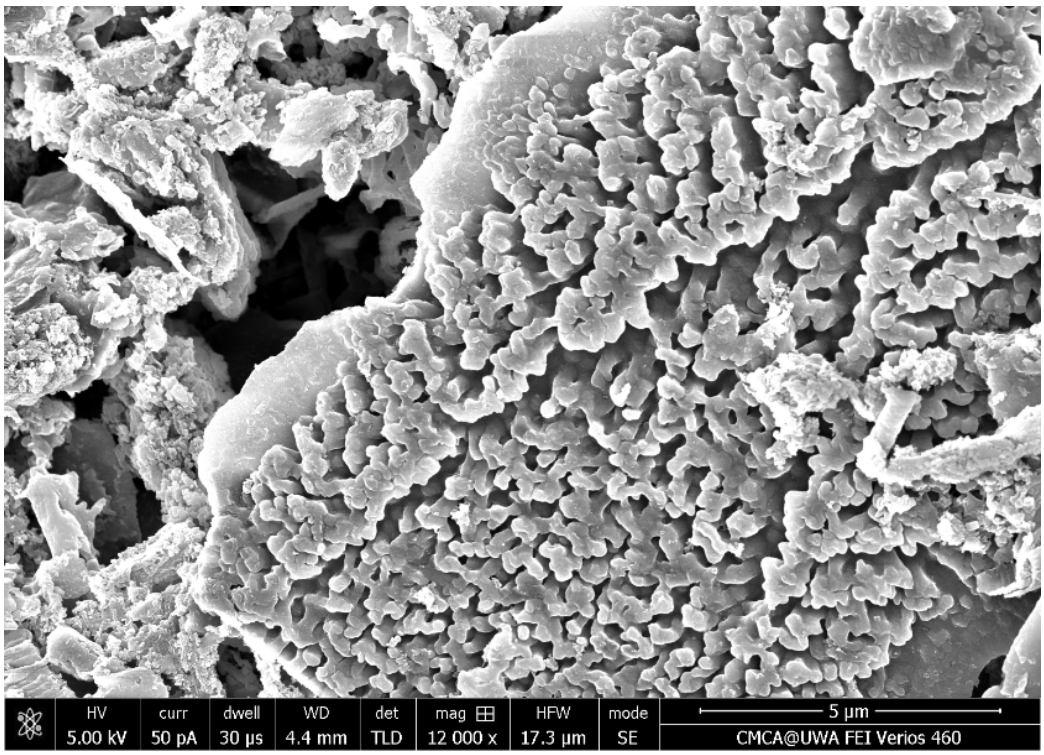

(b)

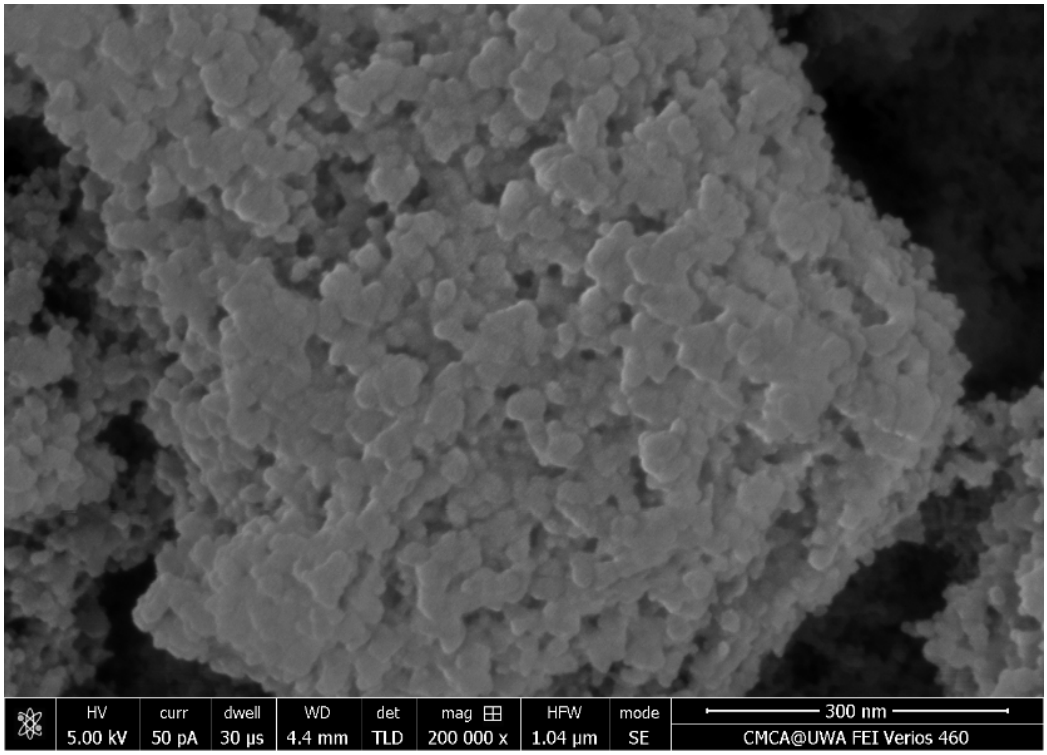

(c)

Fig. 4.5 SEM images of (a) g-C_3N_4, (b) g-C_3N_4-DMF and (c) 0.1 g g-C_3N_4/0.05 g NDs

The morphology of pristine g-C_3N_4, g-C_3N_4-DMF and 0.1 g g-C_3N_4/0.05 g NDs were investigated by SEM imaging. As shown in Fig. 4.5, pristine g-C_3N_4 prepared by direction condensation of melamine has a bulk structure and a large particle size. After solvothermal treatment with DMF, the edges become smooth and porous structure was created. The introduction of NDs did not change the morphology much and the difference between g-C_3N_4-P and 0.1 g g-C_3N_4/0.05 g NDs was similar to that of g-C_3N_4-DMF.

4.3.1.5 UV-vis DRS spectra

The UV-vis DRS spectra of g-C_3N_4, g-C_3N_4-DMF and 0.1 g g-C_3N_4/0.05 g NDs are illustrated in Fig. 4.6. The light absorption edge of pristine GCN was at about 470 nm, therefore, the band gap energy is around 2.64 eV, which is close to the reported value of 2.7 eV.[18] The absorption edge of g-C_3N_4-DMF showed a slight red-shift to 478 nm, corresponding to a band gap energy of 2.59 eV. The red-shift can be from the structural changes or the newly produced amorphous phase. Once NDs were introduced

to the sample, interestingly, blue shift was observed, due to the electrical structure of NDs. All band gap energies of these samples were below 3.1 eV, which indicated they have the ability to respond to visible light.

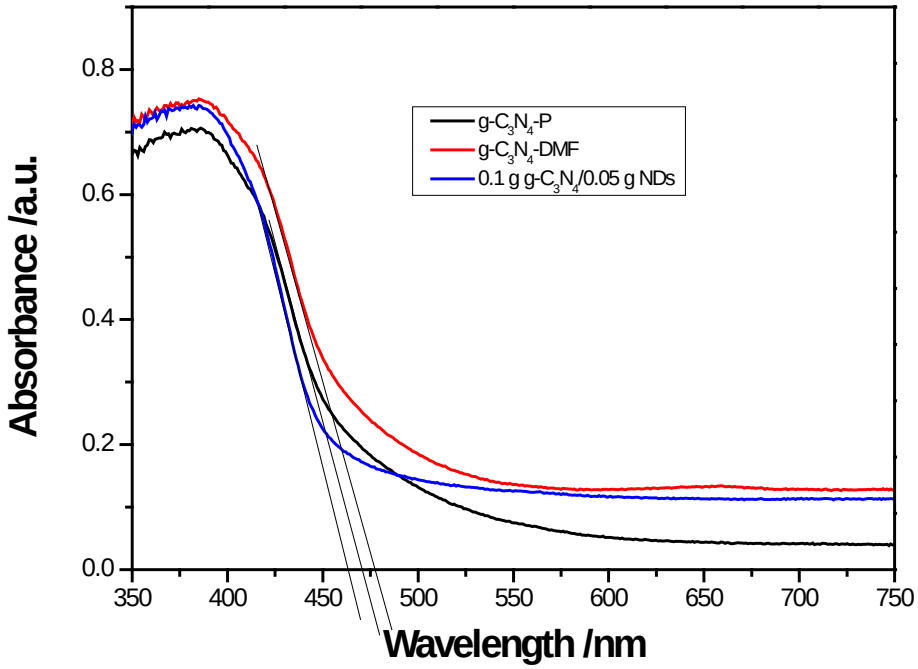

Fig. 4.6 UV-vis diffuse reflectance spectra of g-C_3N_4, g-C_3N_4-DMF and 0.1 g g-C_3N_4/0.05 g NDs.

4.3.1.6 Photoluminescence spectra (PL)

The PL spectra of pristine g-C_3N_4, g-C_3N_4-DMF and 0.1 g g-C_3N_4/0.05 g NDs are shown in Fig. 4.7. All the emission peaks of these three samples are at about 450 nm. However, 0.1 g g-C_3N_4/0.05g NDs showed the lowest emission intensity than the other two samples which could justify that it had the better separation rate of photoinduced charges.[2, 19]

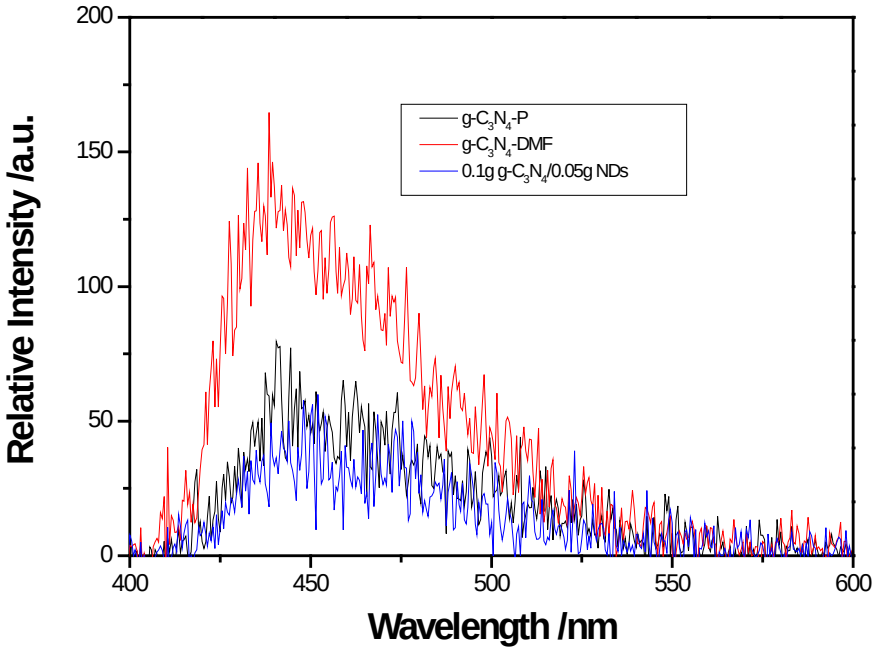

Fig. 4.7 Photoluminescence spectra of g-C_3N_4, g-C_3N_4-DMF and 0.1 g g-C_3N_4/0.05 g NDs.

4.3.2 Photocatalysis and photoelectrochemical performances

4.3.2.1 Photodegradation of MB solutions

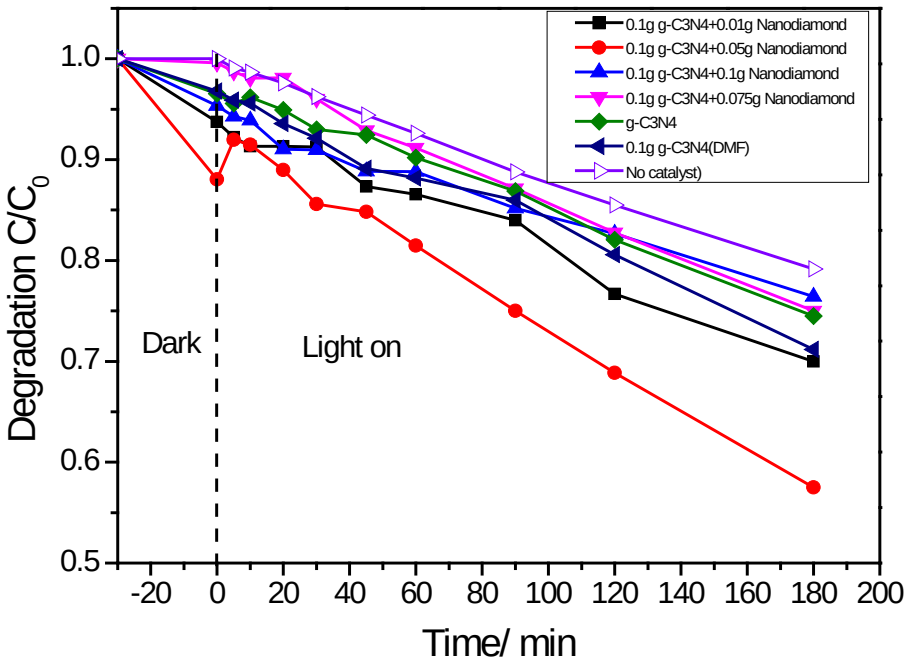

Fig. 4.8 Photodegradation of MB solutions (catalyst: 0.05 g/L, MB initial concentration: 20 ppm)

Fig. 4.8 displays the photocatalytic performance of these samples in MB solutions under UV-visible light irradiations. It was observed the composite 0.1 g g-C_3N_4/0.05 g NDs had the highest absorption rate in dark and the best photodegradation rate under visible light. In details, only about 25% of MB was degraded by pristine g-C_3N_4 within in 180 min, while more than 45% of MB was removed during the same reaction circumstance though the photocatalyst concentration was applied at a very low level (0.05 g/L). In sum, the hybrid photocatalyst can provide better performances for degradation of organic pollutants. But the content of NDs should be controlled, otherwise a higher level of NDs would result in a lower degradation than pristine g-C_3N_4 and g-C_3N_4-DMF.

4.3.2.2 Photoelectrochemical activity

Fig. 4.9 shows the transient photocurrent densities of g-C_3N_4, g-C_3N_4-DMF and 0.1 g g-C_3N_4/0.05g NDs which were response to the circle of light and dark. Similar to photocatalytic performance in MB solution, the hybrid of 0.1 g g-C_3N_4/0.05g NDs demonstrated the highest electron-transfer efficiency. The biggest gap of photocurrent densities were observed on 0.1 g g-C_3N_4/0.05g NDs between the circle of light off and on, which indicated it had the highest photoelectrochemical activity.

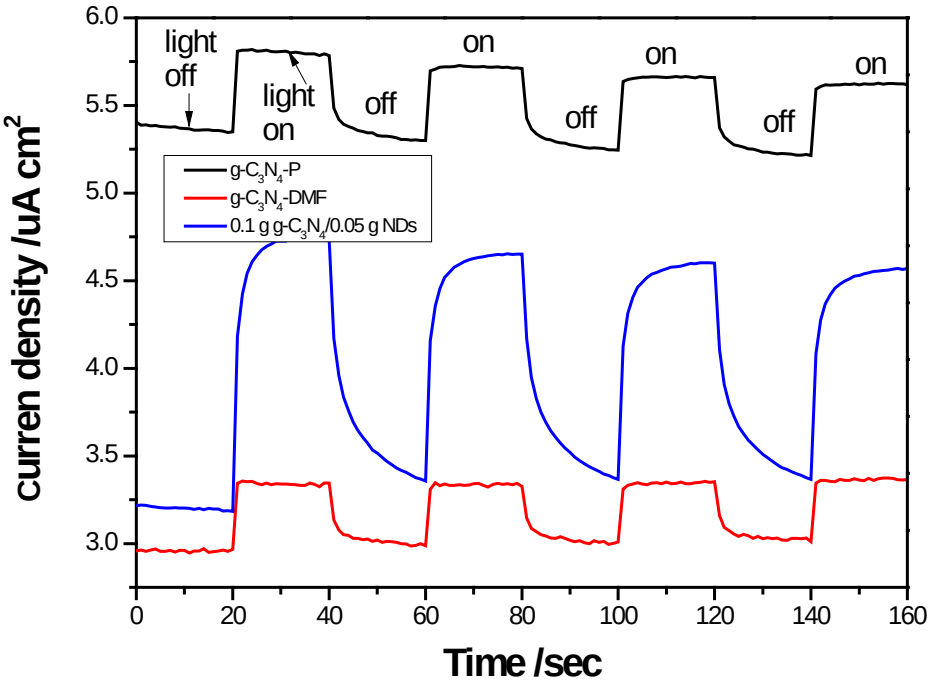

Fig. 4.9 Transient photocurrent densities of samples at 0 voltage.

4.4 Conclusions

In summary, the metal-free GCN/NDs photocatalysts were successfully synthesized using pure NDs and pristine g-C_3N_4 (obtained from thermal condensation of melamine) as the precursors via a solvothermal treatment process. The combination of NDs and g-C_3N_4 exhibited the higher efficiency in MB photodegradation, and a higher photoelectrochemical activity than g-C_3N_4. This study not only proposes a feasible strategy to develop a metal-free photocatalyst but also achieves an attempt of photoelectrochemical application based on g-C_3N_4.

References

[1] B. Ai, X.G. Duan, H.Q. Sun, X. Qiu, S.B. Wang, Metal-free graphene-carbon nitride hybrids for photodegradation of organic pollutants in water, Catalysis Today, 258 (2015) 668-675.

[2] H.Q. Sun, G.L. Zhou, Y.X. Wang, A. Suvorova, S.B. Wang, A New Metal-Free Carbon Hybrid for Enhanced Photocatalysis, Acs Applied Materials & Interfaces, 6 (2014) 16745-16754.

[3] M.R. Hoffmann, S.T. Martin, W.Y. Choi, D.W. Bahnemann, ENVIRONMENTAL APPLICATIONS OF SEMICONDUCTOR PHOTOCATALYSIS, Chemical Reviews, 95 (1995) 69-96.

[4] S.W. Cao, J.X. Low, J.G. Yu, M. Jaroniec, Polymeric Photocatalysts Based on Graphitic Carbon Nitride, Advanced Materials, 27 (2015) 2150-2176.

[5] H.Q. Sun, H.W. Liang, G.L. Zhou, S.B. Wang, Supported cobalt catalysts by one-pot aqueous combustion synthesis for catalytic phenol degradation, Journal of Colloid and Interface Science, 394 (2013) 394-400.

[6] W. Cui, Q. Liu, N.Y. Cheng, A.M. Asiri, X.P. Sun, Activated carbon nanotubes: a highly-active metal-free electrocatalyst for hydrogen evolution reaction, Chemical Communications, 50 (2014) 9340-9342.

[7] S.C. Yan, S.B. Lv, Z.S. Li, Z.G. Zou, Organic-inorganic composite photocatalyst of g-C_3N_4 and TaON with improved visible light photocatalytic activities, Dalton Transactions, 39 (2010) 1488-1491.

[8] H. Xu, J. Yan, X.J. She, L. Xu, J.X. Xia, Y.G. Xu, Y.H. Song, L.Y. Huang, H.M. Li, Graphene-analogue carbon nitride: novel exfoliation synthesis and its application in photocatalysis and photoelectrochemical selective detection of trace amount of Cu2+, Nanoscale, 6 (2014) 1406-1415.

[9] G.H. Dong, K. Zhao, L.Z. Zhang, Carbon self-doping induced high electronic conductivity and photoreactivity of g-C_3N_4, Chemical Communications, 48 (2012) 6178-6180.

[10] Z.W. Zhao, Y.J. Sun, F. Dong, Graphitic carbon nitride based nanocomposites: a review, Nanoscale, 7 (2015) 15-37.

[11] Y. Zheng, L.H. Lin, B. Wang, X.C. Wang, Graphitic Carbon Nitride Polymers toward Sustainable Photoredox Catalysis, Angewandte Chemie-International Edition, 54 (2015) 12868-12884.

[12] V.N. Mochalin, O. Shenderova, D. Ho, Y. Gogotsi, The properties and applications of nanodiamonds, Nature Nanotechnology, 7 (2012) 11-23.
[13] M.J. Sampaio, L.M. Pastrana-Martinez, A.M.T. Silva, J.G. Buijnsters, C. Han, C.G. Silva, S.A.C. Carabineiro, D.D. Dionysiou, J.L. Faria, Nanodiamond-TiO_2 composites for photocatalytic degradation of microcystin-LA in aqueous solutions under simulated solar light, Rsc Advances, 5 (2015) 58363-58370.
[14] L.M. Pastrana-Martinez, S. Morales-Torres, S.A.C. Carabineiro, J.G. Buijnsters, J.L. Faria, J.L. Figueiredo, A.M.T. Silva, Nanodiamond-TiO_2 Composites for Heterogeneous Photocatalysis, Chempluschem, 78 (2013) 801-807.
[15] K.-D. Kim, N.K. Dey, H.O. Seo, Y.D. Kim, D.C. Lim, M. Lee, Photocatalytic decomposition of toluene by nanodiamond-supported TiO_2 prepared using atomic layer deposition, Applied Catalysis a-General, 408 (2011) 148-155.
[16] T. Tung Tran, H. Ba, T.-P. Lai, J.-M. Nhut, O. Ersen, D. Begin, I. Janowska, N. Dinh Lam, P. Granger, P.-H. Cuong, A few-layer graphene-graphene oxide composite containing nanodiamonds as metal-free catalysts, Journal of Materials Chemistry A, 2 (2014) 11349-11357.
[17] D.M. Jang, Y. Myung, H.S. Im, Y.S. Seo, Y.J. Cho, C.W. Lee, J. Park, A.-Y. Jee, M. Lee, Nanodiamonds as photocatalysts for reduction of water and graphene oxide, Chemical Communications, 48 (2012) 696-698.
[18] X.C. Wang, K. Maeda, A. Thomas, K. Takanabe, G. Xin, J.M. Carlsson, K. Domen, M. Antonietti, A metal-free polymeric photocatalyst for hydrogen production from water under visible light, Nature Materials, 8 (2009) 76-80.
[19] F. He, G. Chen, Y.G. Yu, S. Hao, Y.S. Zhou, Y. Zheng, Facile Approach to Synthesize g-PAN/g-C_3N_4 Composites with Enhanced Photocatalytic H-2 Evolution Activity, Acs Applied Materials & Interfaces, 6 (2014) 7171-7179.

5

Chapter 5: Hybrid photocatalysts of graphitic carbon nitride and single-walled carbon nanotubes and their photoelectrochemical performances

Abstract

In this chapter, a series of hybrid photocatalysts derived from graphitic carbon nitride (g-C_3N_4) and single-walled carbon nanotubes (SWCNTs) were prepared for photocatalysis and photoelectrochemical applications. A variety of characterizations were applied, including X-ray diffraction (XRD), UV-vis diffusion, photoluminescence (PL), scanning electron microscopy (SEM), thermogravimetric analysis/differential temperature gradient (TGA/DTG) and nitrogen sorption isotherms. The photocatalytic efficiencies of the composites were evaluated in photodegradation of methylene blue (MB) solutions. Moreover, photoelectrochemical applications of these samples were investigated in a classic three-electrode cell by an electrochemical workstation (Zahner Zennium). It was found that the introduction of single-walled carbon nanotubes can significantly modulate the physicochemical properties of g-C_3N_4 photocatalysts.

5.1 Introduction

At present, environmental deterioration, such as water pollution and air pollution, is threatening the health of human beings[1]. Photocatalysis, an effective technology that can simultaneously addresses environmental and energy issues, has attracted considerable attention [2]. In recent years, some metal-free catalysts were widely used which demonstrated the high catalytic activity [3-4]. Graphitic carbon nitride (g-C_3N_4), as a typical metal-free photocatalyst, has been seriously considered by researchers due to its excellent properties and perspective applications [5-8]. In order to enhance the photocatalytic activity of g-C_3N_4, many strategies have been applied. Among these strategies, synthesis of hybrid photocatalyst of g-C_3N_4 and nanocarbons was reported [9].

Among the materials of nanocarbons, carbon nanotubes (CNTs) including multi-walled carbon nanotubes (MWCNTs) and single-walled nanotubes (SWCNTs), appear to attract more researchers' interests on development of photocatalysis. The composites of photocatalysts based on CNTs can improve the efficiencies in removing organic pollutants from contaminated water, such as dye and phenolics [10-13], and have been reported. As for SWCNTs, most publications focused on the synthesis of photocatalysts of the hybrids of titanium dioxide and SWCNTs [14-17]. Recently, our group found that SWCNTs could be used to promote catalytic oxidation in advanced oxidation processes[18].

In Chapter 4, g-C_3N_4/Nanodiamonds composites were chosen to improve the photocatalytic efficiency of pristine g-C_3N_4. In this chapter, SWCNTs were employed to improve the catalytic activity of graphitic carbon nitride because SWCNTs possess many excellent physical properties and chemical characteristics, such as large specific surface areas, single dimensional structure, flexible electronic property and high thermal stability [19-21]. A various samples with ratios of combination between g-C_3N_4 and SWCNTs were prepared via a solvothermal method. In photodegradation of methylene blue (MB) solutions, 0.1 g g-C_3N_4/0.05 g SWCNTs demonstrated the highest catalytic activity which was similar to g-C_3N_4/nanodiamonds described in Chapter 4.

5.2 Experimental section

5.2.1 Materials and chemicals

SWCNTs were purchased from Timesnano, Chengdu, China. Methylene blue (99.9%) and N, N-dimethylformamide (DMF) were received from Sigma. Melamine (99.0%) were obtained from Sigma-Aldrich, Na_2SO_4 (99.0%) and Nafion were purchased from Sigma-Aldrich as well. Ethanol (99.9%) were provided by Chem Supply. All the materials and chemicals were used as received.

5.2.2 Synthesis of catalysts

5.2.2.1 Synthesis of g-C_3N_4

We used the same pristine g-C_3N_4 (GCN) as described in Chapter 4. The details of preparation of g-C_3N_4 was illustrated in Chapter 4 (refer to 4.2.2.1 Synthesis of graphitic carbon nitride).

5.2.2.2 Synthesis of g-C_3N_4/SWCNTs

A solvothermal route was used to prepare the composites of g-C_3N_4/SWCNTs. In details, 0.1 g g-C_3N_4 and 0.05 g SWCNTs were transferred into a beaker, then mixed with 80 mL N, N-dimethylformamide (DMF) solution. The mixed solution was stirred for over than 30 min on a hot plate. After that, the mixture solution was sonicated for 30 min. Then, the mixed solution was poured into a Teflon-lined stainless steel autoclave. The autoclave was heated in an oven at 150 ℃ for 24 h. When the autoclave was cooled down to room temperature, the solid was obtained by centrifugation. Then it was washed by ethanol and pure water for each 3 times. The cleaned solid was put into an oven at 60 ℃ over 24 h. The dried solid was grinded into the fine powder which was referred to 0.1g g-C_3N_4/0.05 g SWCNTs.

Using the same method, the composites of g-C_3N_4-DMF, 0.1g g-C_3N_4/0.01 g SWCNTs, 0.1g g-C_3N_4/0.075 g SWCNTs and 0.1 g g-C_3N_4/0.1g SWCNTs were also synthesized.

5.2.3 Characterization of materials

The crystalline structures of these composites were investigated with X-ray diffraction (XRD) patterns. XRD was performed on a Bruker D8 diffractometer (Bruker-AXS, Karlsruhe, Germany) with Cu Kα radiation (λ = 1.5418 Å). The specific surface areas

(SSA) and pore size distribution of these prepared samples were analyzed by liquid nitrogen sorption. Thermal stability of these composites was evaluated by thermogravimetric-differential thermal analysis (TG-DTA) under air flow with a heating rate of 10 ℃/min. A scanning electron microscopy (SEM) system was employed. UV-visible diffuse spectra of these samples were obtained from a JASCO V670 UV-vis spectrophotometer, and $BaSO_4$ was used as the reference. The photoluminescence (PL) spectra of the photocatalysts were studied on a Varian Eclipse spectrometer instrument, and wavelength was set up at 300 nm.

5.2.4 Catalyst activity test

5.2.4.1 Photocatalytic decomposition of MB

The photocatalytic decomposition of methylene blue (MB) was used to evaluate the photocatalytic efficiency of these composites under UV-visible light irradiations. The light irradiation was provided by a 300 W Newport Oriel Universal Xenon arc lamp. The reactions of photodegradation were carried out in a stable temperature (25 ℃) with a 1 L double-jacket reactor and a water bath to control the temperature. Firstly, 10 mg of GCN/SWCNTs was dispersed into 200 mL of MB solution (10 ppm). In order to achieve in sorption equilibrium, the reaction system was kept in dark for 30 min, afterwards, the light was switched on. Each 4 mL sample solution was taken at each time interval during the whole process of photoreaction. The sample solution was centrifuged for 20 min by a typical centrifuge machine with 7500 rpm. At last, a UV-visible spectrophotometer (λ = 664 nm) was employed to analyze the centrifuged sample solution.

5.2.4.2 Photoelectrochemical activity test

Photoelectrochemical activity tests were conducted on an electrochemical workstation (Zahner Zennium) and 0 V voltage was applied. A traditional three-electrode cell system was employed, including the counter electrode (Pt wireless), a reference electrode (Ag/AgCl) and a working electrode. The working electrode was prepared by the 0.1 g g-C_3N_4/0.05 g SWCNTs which was coated on a piece of F-doped tin oxide (FTO) glass. The working electrode was prepared via the same way as described in Chapter 4 (refer to 4.2.4.2). Na_2SO_4 solution at 0.2 mol/L (PH=6.8) was used as the electrolyte [22].

5.3 Results and discussion

5.3.1 Characterization of samples

5.3.1.1 XRD studies

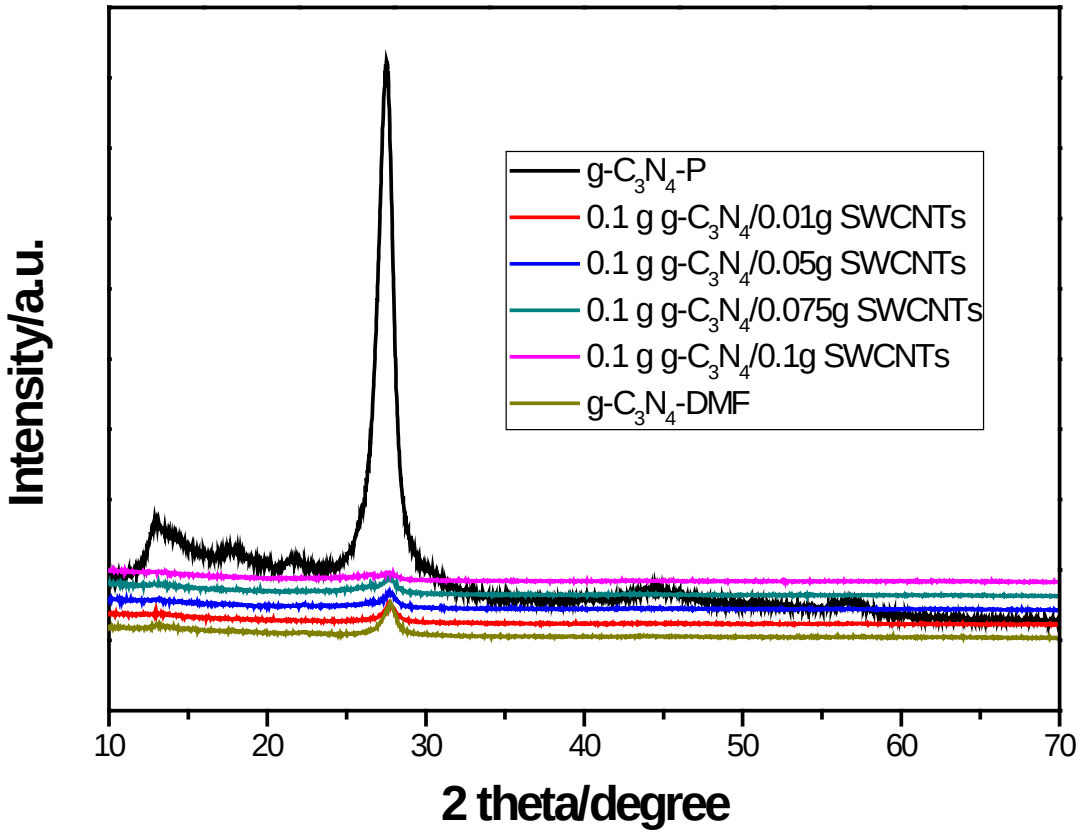

Fig. 5.1 XRD patterns of g-C_3N_4 and g-C_3N_4/SWCNTs.

Fig. 5.1 shows XRD patterns of pristine g-C_3N_4 and composites g-C_3N_4/SWCNTs. Only g-C_3N_4 shows two peaks around at 13.0 and 27.4^o, which are corresponding to the crystalline structures of pristine g-C_3N_4 [23]. On these hybrid photocatalysts, only one peak was observed around 27.5-28^o which is similar to the composites g-C_3N_4/Nanodiamonds as discussed in Chapter 4. Due to the low amount of SWCNTs, no peaks associated with them were observed.

5.3.1.2 Thermal analysis

Fig. 5.2 indicated the TGA and DSC profiles of pristine g-C_3N_4, g-C_3N_4-DMF and 0.1 g g-C_3N_4/0.05 g SWCNTs. The pristine g-C_3N_4 demonstrated the highest stability up to 600 ^{o}C. As confirmed in Chapter 4, DMF treatment decreased the thermal stability in air and weight loss starts at around 300 ^{o}C. Further introduction of SWCNTs made

the weight loss occur a bit earlier. DSC curves in Fig. 5.2 show that the weight loss was due to the decomposition of the polymeric material in air.

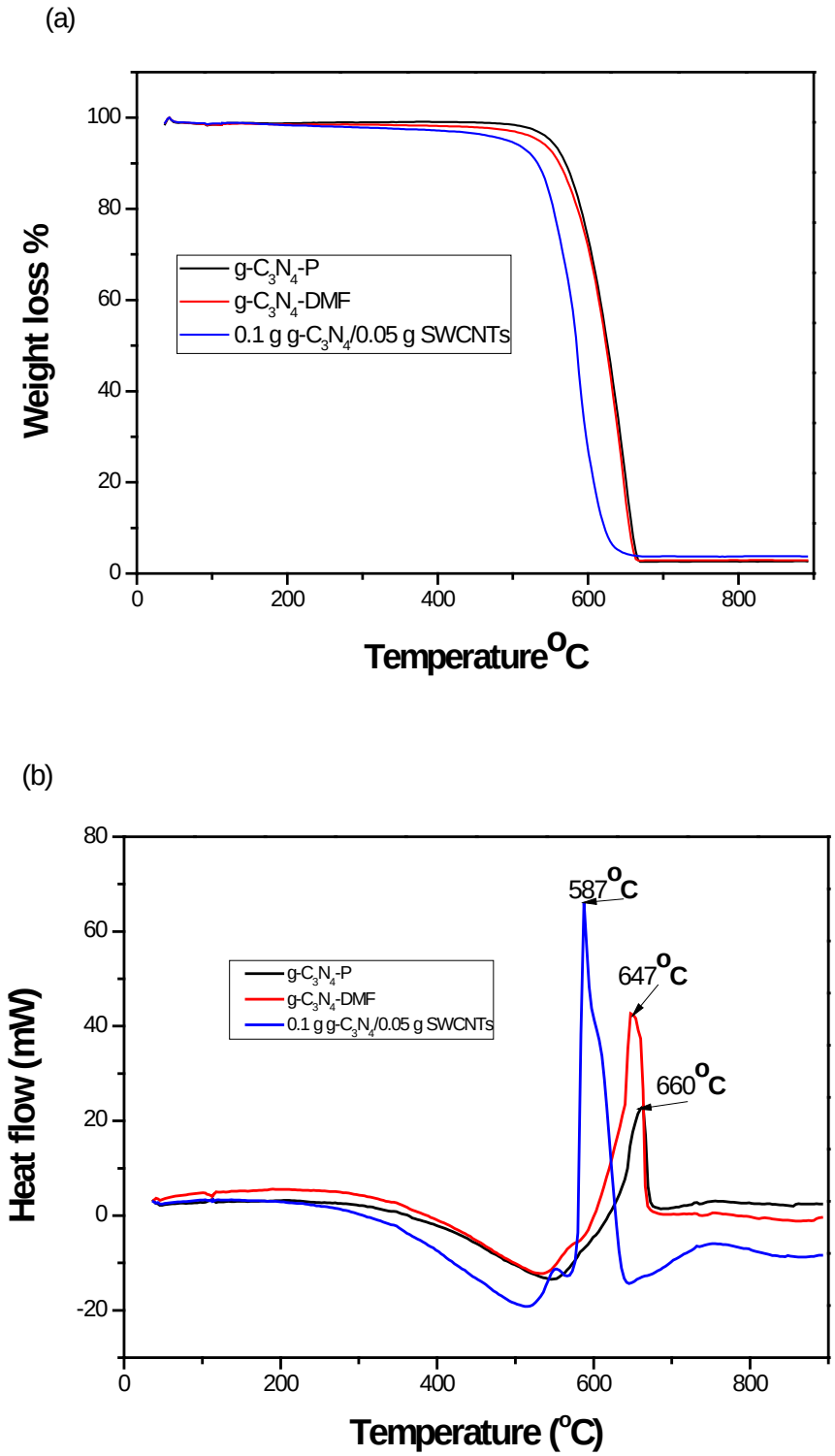

Fig. 5.2 TGA (a) and DSC (b) profiles of g-C_3N_4, g-C_3N_4-DMF and 0.1g g-C_3N_4/0.05 g SWCNTs.

5.3.1.3 Nitrogen isotherms

Table 5.1 Specific surface area (SSA) of g-C_3N_4, g-C_3N_4-DMF and g-C_3N_4/SWCNTs

Catalyst	SSA (m^2/g)
g-C_3N_4-P	13
g-C_3N_4-DMF	19
0.1 g g-C_3N_4/0.05 g SWCNTs	175

Table 5.1 shows the SSA of pristine g-C_3N_4, g-C_3N_4-DMF and 0.1 g g-C_3N_4/0.05 g SWCNTs. As expected, the SSA of GCN/SWCNTs was increased significantly to be more than 10 times of pristine g-C_3N_4. This is because that SWCNTs have a large SSA [19]. From Fig. 5.3 (a), it can be seen clearly that the nitrogen adsorption capacity of 0.1 g g-C_3N_4/0.05 g SWCNTs was higher than g-C_3N_4 and g-C_3N_4-DMF. In Fig. 5.4 (b), it was found that the pore size of composites was larger than pristine g-C_3N_4.

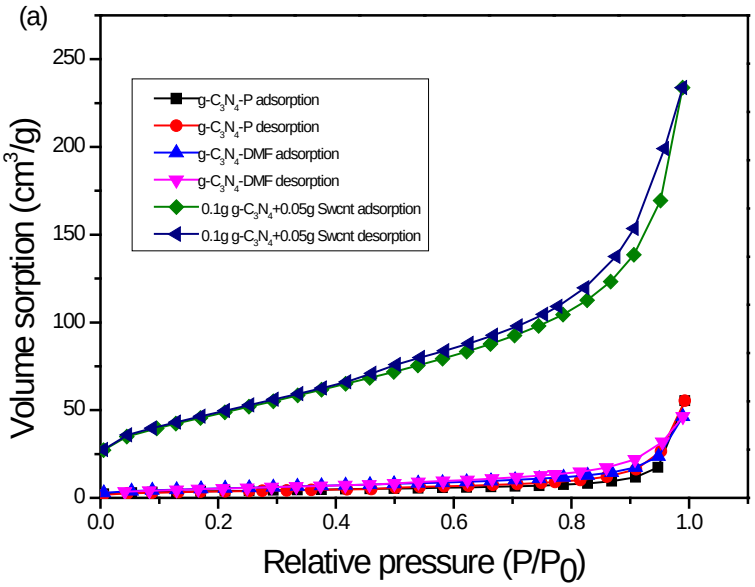

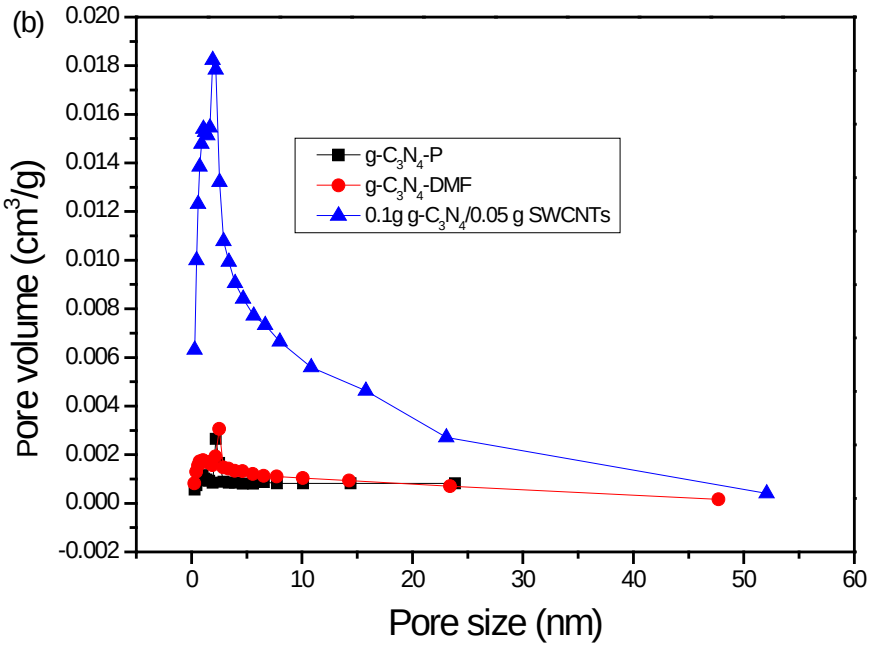

Fig. 5.3 (a) nitrogen sorption distribution, and (b) pore size distribution

5.3.1.4 SEM images

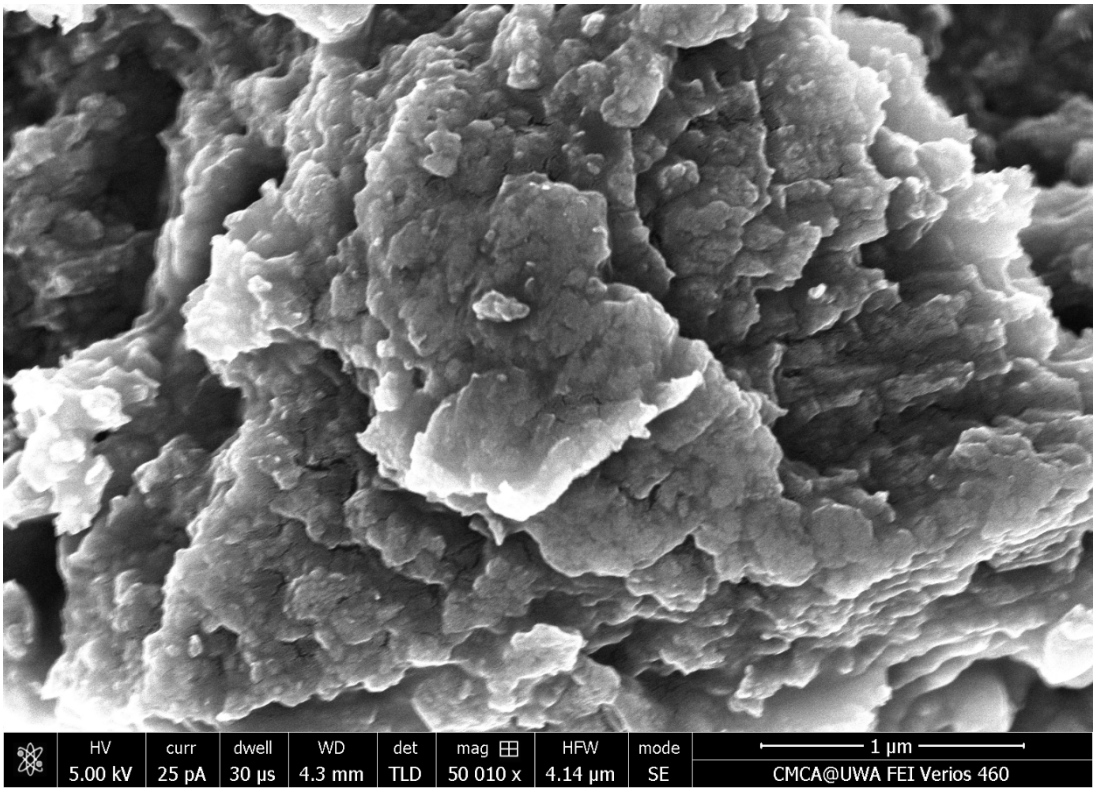

(a)

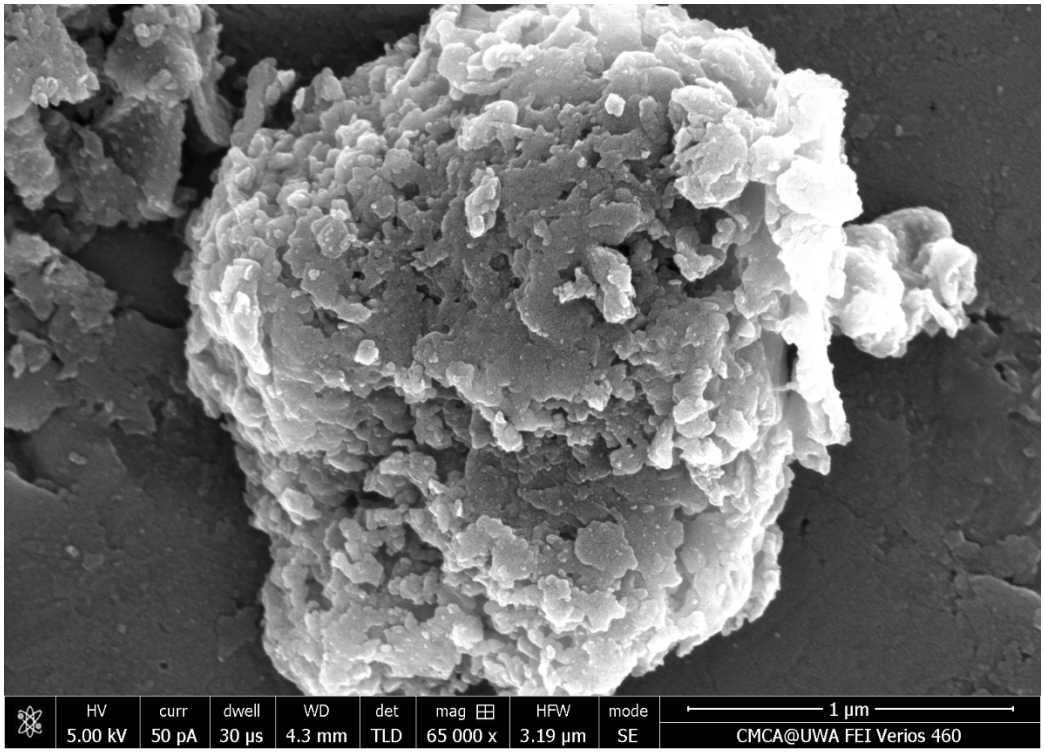

(b)

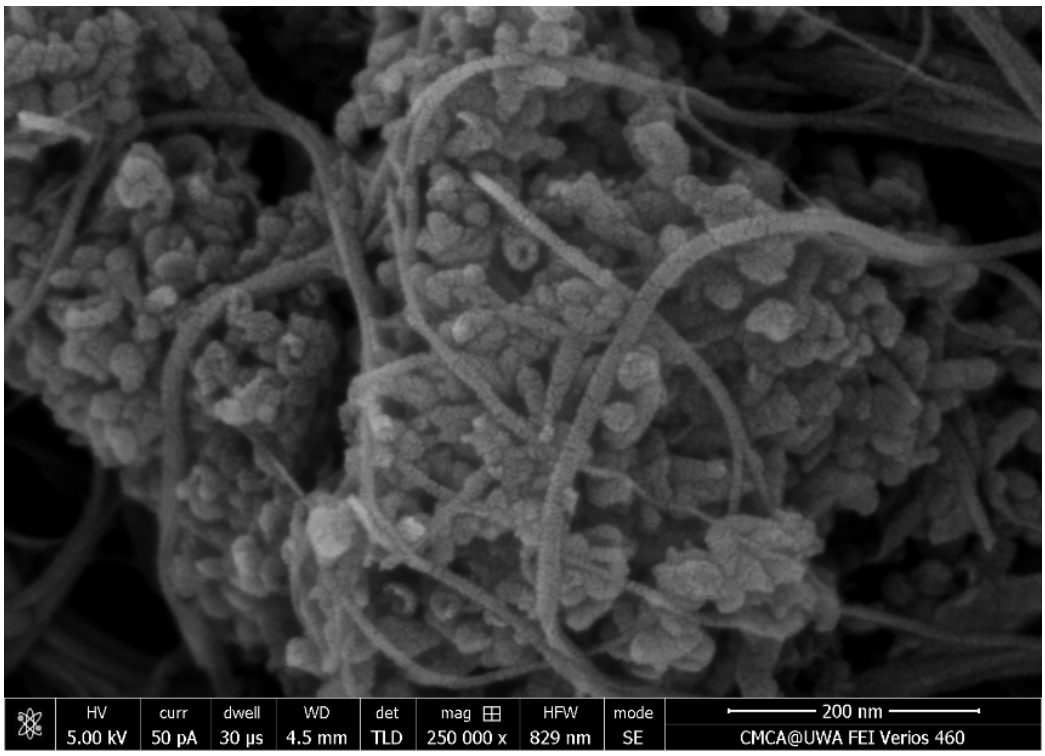

(c)

Fig. 5.4 SEM images of (a) g-C_3N_4, (b) g-C_3N_4-DMF, and (c) 0.1 g g-C_3N_4/0.05 g SWCNTs.

SEM was used to study the morphology of pristine g-C_3N_4, g-C_3N_4-DMF and 0.1 g g-C_3N_4/0.05 g SWCNTs. Fig. 5.4 (a) showed a bulk structure of pristine g-C_3N_4. Compared with pristine g-C_3N_4 in Fig. 5.4 (a), a more porous structure of g-C_3N_4-DMF was obtained after the process of solvothermal treatment in DMF as shown in Fig. 5.4 (b). From Fig. 5.4(c), it can be found that SWCNTs indicated a close interaction with particles of g-C_3N_4. We also found that the surfaces of SWCNTs and g-C_3N_4 were more porous, indicating that these two materials were corroded by DMF under temperature of 150 ℃.

5.3.1.5 UV-vis diffuse reflectance spectra (DRS)

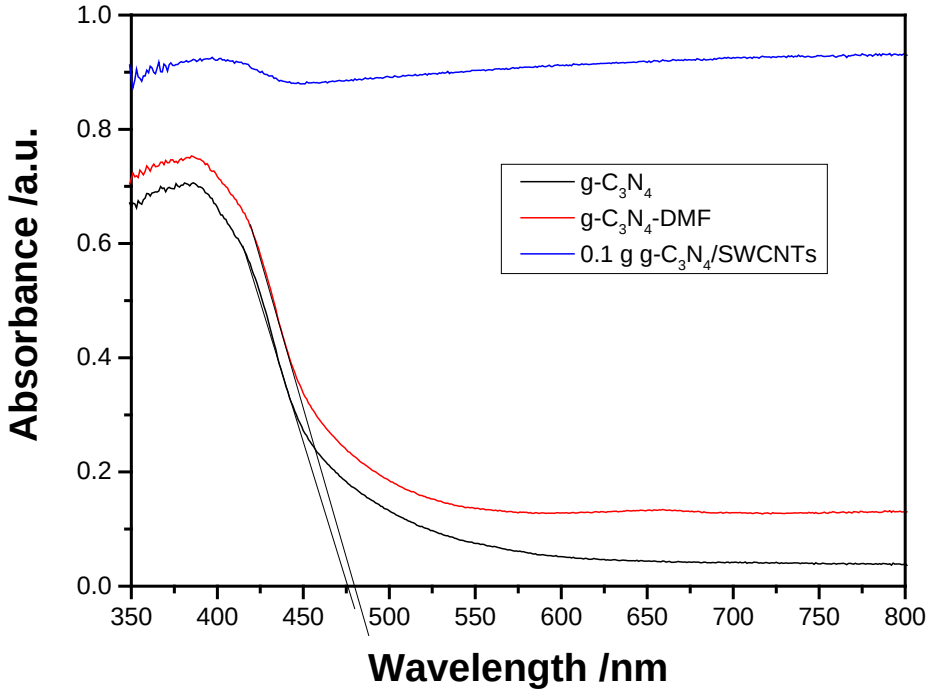

Fig. 5.5 UV-vis DRS of g-C_3N_4, g-C_3N_4-DMF and 0.1 g g-C_3N_4/0.05 g SWCNTs.

Fig. 5.5 demonstrated the UV-vis DRS of pristine g-C_3N_4 and g-C_3N_4 composites. G-C_3N_4 indicated an absorption at around 460 nm which results in a band gap energy of 2.69 eV. This band gap energy is close to the previous reported value[24]. While 0.1 g g-C_3N_4/0.05 g SWCNTs showed significant red-shift and demonstrated response to full visible light range with extending to IR. The improved optical property of the hybrid photocatalyst might promise an enhanced visible light photocatalysis.

5.3.1.6 Photoluminescence spectra (PL)

Fig. 5.6 presented the PL spectra of pristine g-C_3N_4 and g-C_3N_4 composites. Comparing the three samples, 0.1 g g-C_3N_4/0.05 g SWCNTs demonstrated the lowest intensity of photoluminescence, indicating a low recombination of carriers and a high photocatalytic efficiency [2]. The low recombination of the photoinduced electron/hole pairs might lead to a higher photocatalysis than pristine and DMF modified g-C_3N_4.

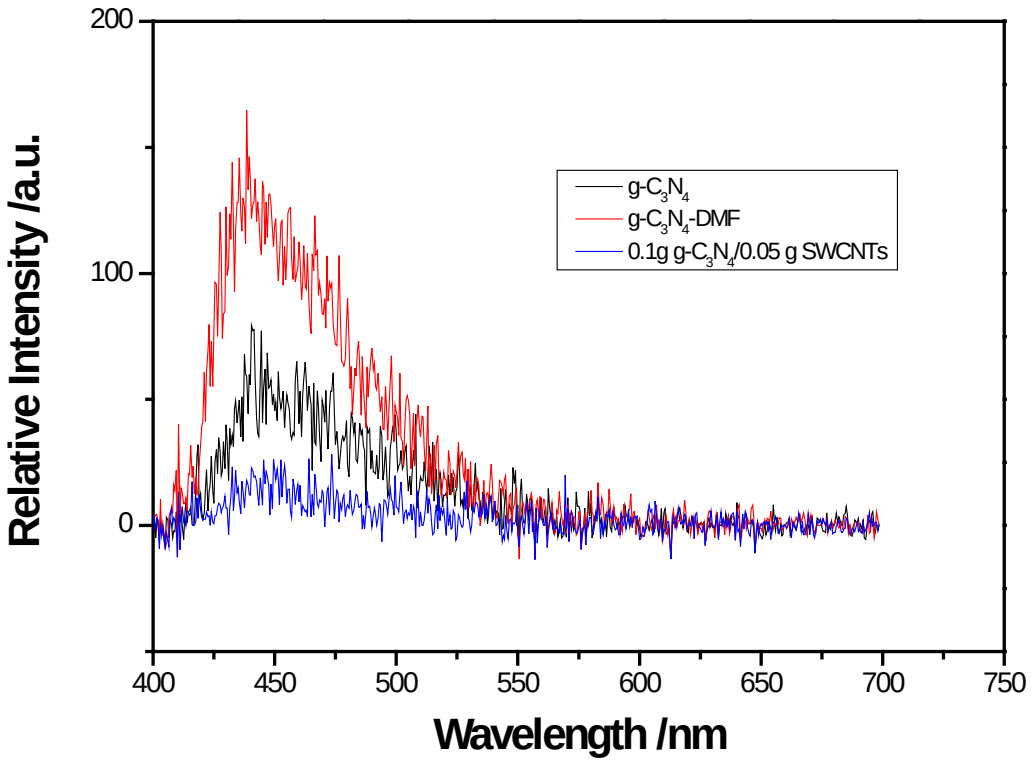

Fig. 5.6 PL spectra of g-C_3N_4, g-C_3N_4-DMF and 0.1 g g-C_3N_4/0.05 g SWCNTs.

5.3.2 Catalytic activity tests

5.3.2.1 Photodegradation of MB solutions

The photocatalytic activities of the pristine g-C_3N_4 and g-C_3N_4/SWCNTs were investigated in MB solutions under UV-vis light source, and the results were depicted in Fig. 5.7. It can be seen that 0.1 g g-C_3N_4/0.1 g SWCNTs had the highest efficiency of absorption in dark because it had the largest SSA. Comparing with all of these samples, the composite of 0.1g g-C_3N_4/0.05 g SWCNTs not only demonstrated the excellent absorptive capacity but also presented the highest photocatalytic activity.

More than 50% of MB was removed by 0.1g g-C_3N_4/0.05 g SWCNTs at a dosage of 0.05 g/L in 210 min while MB was hardly photodegraded by pristine g-C_3N_4 during the same reaction conditions though pristine g-C_3N_4 had been a notable metal-free photocatalyst [2, 5, 23]. To be concluded, the photocatalytic efficiency of composite based on g-C_3N_4 was improved dramatically.

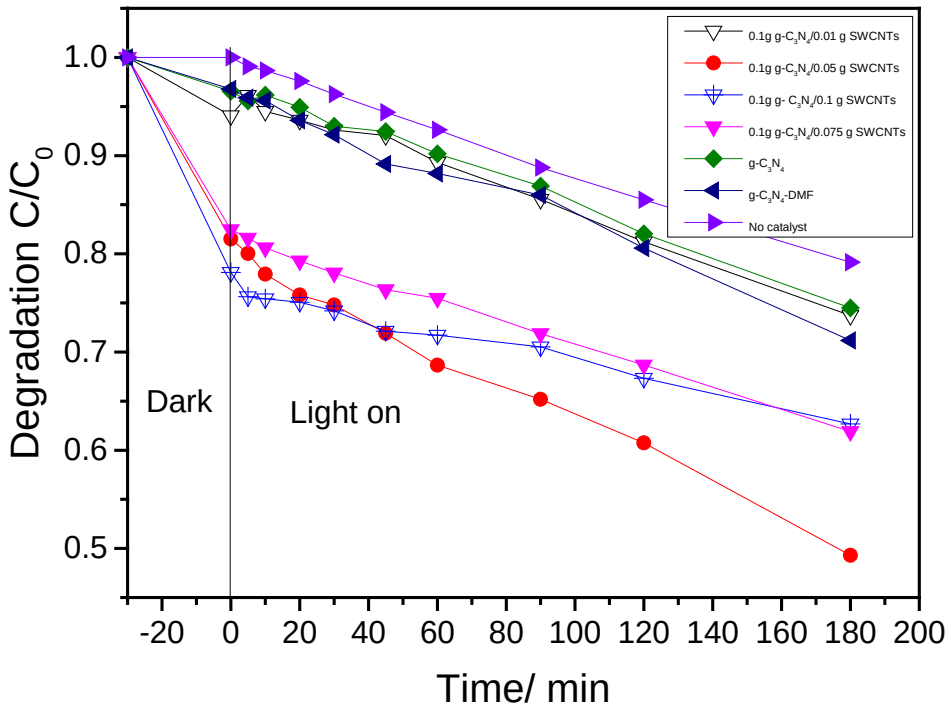

Fig. 5.7 Photodegradation of MB solutions (catalyst: 0.05 g/L, MB initial concentration: 10 ppm)

5.3.2.2 Photoelectrochemical performance evaluation

Fig. 5.8 presented the photoelectrochemical efficiencies of the pristine g-C_3N_4, g-C_3N_4-DMF and 0.1 g g-C_3N_4/0.05 g SWCNTs. Compared to the pristine g-C_3N_4 and g-C_3N_4-DMF, the hybrid photocatalyst of 0.1 g g-C_3N_4/0.05 g SWCNTs showed the larger stable gap of transient photocurrent densities during the circles of light on and off. Interestingly, 0.1 g g-C_3N_4/0.05 g SWCNTs demonstrated the opposite corresponding photocurrent, indicating the delay in generation of photocurrent. However, it still can be considered that the composite of 0.1 g g-C_3N_4/0.05 g SWCNTs had the highest photoelectrochemical activity due to the strongest density.

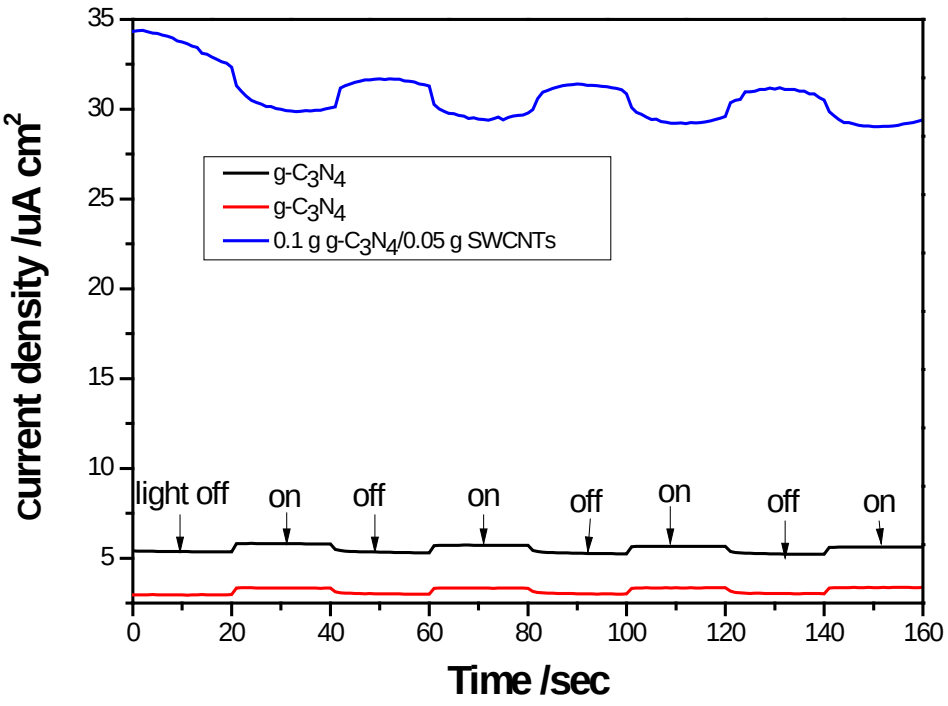

Fig. 5.8 Transient photocurrent densities of samples at 0 V voltage.

5.4 Conclusions

In conclusion, g-C_3N_4/SWCNTs hybrids were synthesized by a simple solvothermal method. Compared to the efficiencies of photodegradation of MB solutions under UV-vis light irradiations, 0.1 g g-C_3N_4/0.05 g SWCNTs exhibited an excellent photocatalytic activity. In addition, the composite of 0.1 g g-C_3N_4/0.05 g SWCNTs also presented the potential applications in photoelectrochemical field. This study proposes a feasible strategy to develop a new metal-free photocatalyst based on graphitic carbon nitride.

Reference

[1] X.G. Duan, Z.M. Ao, H.Q. Sun, L. Zhou, G.X. Wang, S.B. Wang, Insights into N-doping in single-walled carbon nanotubes for enhanced activation of superoxides: a mechanistic study, Chemical Communications, 51 (2015) 15249-15252.

[2] H.Q. Sun, G.L. Zhou, Y.X. Wang, A. Suvorova, S.B. Wang, A New Metal-Free Carbon Hybrid for Enhanced Photocatalysis, Acs Applied Materials & Interfaces, 6 (2014) 16745-16754.

[3] H.Q. Sun, S.Z. Liu, G.L. Zhou, H.M. Ang, M.O. Tade, S.B. Wang, Reduced Graphene Oxide for Catalytic Oxidation of Aqueous Organic Pollutants, Acs Applied Materials & Interfaces, 4 (2012) 5466-5471.

[4] Q.H. Liang, Z. Li, X.L. Yu, Z.H. Huang, F.Y. Kang, Q.H. Yang, Macroscopic 3D Porous Graphitic Carbon Nitride Monolith for Enhanced Photocatalytic Hydrogen Evolution, Advanced Materials, 27 (2015) 4634-4639.

[5] Y. Zheng, L.H. Lin, B. Wang, X.C. Wang, Graphitic Carbon Nitride Polymers toward Sustainable Photoredox Catalysis, Angewandte Chemie-International Edition, 54 (2015) 12868-12884.

[6] J.J. Zhu, P. Xiao, H.L. Li, S.A.C. Carabineiro, Graphitic Carbon Nitride: Synthesis, Properties, and Applications in Catalysis, Acs Applied Materials & Interfaces, 6 (2014) 16449-16465.

[7] X.C. Wang, S. Blechert, M. Antonietti, Polymeric Graphitic Carbon Nitride for Heterogeneous Photocatalysis, Acs Catalysis, 2 (2012) 1596-1606.

[8] Y. Zheng, J. Liu, J. Liang, M. Jaroniec, S.Z. Qiao, Graphitic carbon nitride materials: controllable synthesis and applications in fuel cells and photocatalysis, Energy & Environmental Science, 5 (2012) 6717-6731.

[9] R.C. Pawar, S. Kang, S.H. Ahn, C.S. Lee, Gold nanoparticle modified graphitic carbon nitride/multi-walled carbon nanotube (g-C_3N_4/CNTs/Au) hybrid photocatalysts for effective water splitting and degradation, Rsc Advances, 5 (2015) 24281-24292.

[10] W.D. Wang, P. Serp, P. Kalck, J.L. Faria, Visible light photodegradation of phenol on MWNT-TiO_2 composite catalysts prepared by a modified sol-gel method, Journal of Molecular Catalysis a-Chemical, 235 (2005) 194-199.

[11] B. Gao, G.Z. Chen, G.L. Puma, Carbon nanotubes/titanium dioxide (CNTs/TiO_2) nanocomposites prepared by conventional and novel surfactant wrapping sol-gel

methods exhibiting enhanced photocatalytic activity, Applied Catalysis B-Environmental, 89 (2009) 503-509.
[12] B.D. Wu, D.X. Zhu, S.J. Zhang, W.Z. Lin, G.Z. Wu, B.C. Pan, The photochemistry of carbon nanotubes and its impact on the photo-degradation of dye pollutants in aqueous solutions, Journal of Colloid and Interface Science, 439 (2015) 98-104.
[13] C.A. Orge, M.F.R. Pereira, J.L. Faria, Photocatalytic ozonation of model aqueous solutions of oxalic and oxamic acids, Applied Catalysis B-Environmental, 174 (2015) 113-119.
[14] Y.F. Nie, L.M. Zhang, D. Wu, Y.B. Chen, G.M. Zhang, Q. Xie, Z.F. Liu, Photocatalytic Engineering of Single-Walled Carbon Nanotubes: From Metal-to-Semiconductor Conversion to Cutting and Patterning, Small, 9 (2013) 1336-1341.
[15] A. Stevanovic, S.L. Ma, J.T. Yates, Photoexcited Electron Hopping between TiO_2 Particles: Effect of Single-Walled Carbon Nanotubes, Journal of Physical Chemistry C, 118 (2014) 23614-23620.
[16] T.Y. Gao, G.C. Sun, F.Y. Cheng, K. Dai, H. Chen, K.J. Deng, Q.Y. Huang, Enhanced visible-light-driven photoactivities of single-walled carbon nanotubes coated with N doped TiO_2 nanoparticles, Rsc Advances, 5 (2015) 28973-28979.
[17] B.K. Vijayan, N.M. Dimitrijevic, D. Finkelstein-Shapiro, J.S. Wu, K.A. Gray, Coupling Titania Nanotubes and Carbon Nanotubes To Create Photocatalytic Nanocomposites, Acs Catalysis, 2 (2012) 223-229.
[18] X.G. Duan, H.Q. Sun, J. Kang, Y.X. Wang, S. Indrawirawan, S.B. Wang, Insights into Heterogeneous Catalysis of Persulfate Activation on Dimensional-Structured Nanocarbons, Acs Catalysis, 5 (2015) 4629-4636.
[19] A. Peigney, C. Laurent, E. Flahaut, R.R. Bacsa, A. Rousset, Specific surface area of carbon nanotubes and bundles of carbon nanotubes, Carbon, 39 (2001) 507-514.
[20] A.A. Kane, K. Loutherback, B.R. Goldsmith, P.G. Collins, High temperature resistance of small diameter, metallic sngle-walled carbon nanotube devices, Applied Physics Letters, 92 (2008).
[21] R.H. Baughman, A.A. Zakhidov, W.A. de Heer, Carbon nanotubes - the route toward applications, Science, 297 (2002) 787-792.
[22] G.G. Zhang, S.H. Zang, X.C. Wang, Layered Co(OH)(2) Deposited Polymeric Carbon Nitrides for Photocatalytic Water Oxidation, Acs Catalysis, 5 (2015) 941-947.

[23] S.W. Cao, J.X. Low, J.G. Yu, M. Jaroniec, Polymeric Photocatalysts Based on Graphitic Carbon Nitride, Advanced Materials, 27 (2015) 2150-2176.
[24] B. Ai, X.G. Duan, H.Q. Sun, X. Qiu, S.B. Wang, Metal-free graphene-carbon nitride hybrids for photodegradation of organic pollutants in water, Catalysis Today, 258 (2015) 668-675.

6

Chapter 6: Conclusions and Perspective

6.1 Concluding remarks

The main objective of this research is to develop new metal-free, carbonaceous photocatalysts based on graphitic carbon nitride (g-C_3N_4) for photocatalysis and photoelectrochemical applications. A series of g-C_3N_4 photocatalysts were prepared using different ratios of pure and mixed precursors via a simple thermal condensation method. In order to enhance the photocatalytic activity of g-C_3N_4, two carbonaceous materials, nanodiamonds and SWCNTs, were applied to hybridize with pristine g-C_3N_4 in DMF via a solvothermal route. Compared to the pristine g-C_3N_4, the activities of hybrid photocatalysts were greatly improved. The photocatalytic performances of all the samples were examined in photodegradation of aqueous MB or SCP solutions, and the UV-vis light was provided by a 300 W Newport Oriel Universal Xenon arc lamp. Furthermore, the photoelectrochemical performances of the composites were also studied on an electrochemical workstation using a traditional three-electrode system. In sum, two types of novel metal-free photocatalysts, the composites of g-C_3N_4/Nanodiamonds and g-C_3N_4/SWCNTs were delivered by this study.

6.1.1 Effects of different precursors on the photocatalysis of g-C_3N_4

Various precursors were used to synthesize graphitic carbon nitride, including melamine, urea, thiourea and D-glucose. A simple thermal condensation method was employed. It was found that the graphitic carbon nitride obtained from the precursor of pure melamine exhibited an excellent thermal stability and high photocatalytic activity by a series of characterizations and photocatalytic reactions.

6.1.2 Effect of DMF on surface modification of g-C_3N_4

DMF was used as the functional medium to promote the solvothermal reaction to proceed smoothly between nanocarbons and graphitic carbon nitride. Comparing SEM images of pristine g-C_3N_4 and g-C_3N_4-DMF, it was found that g-C_3N_4-DMF exhibited more porous surfaces. Therefore, it was supposed that the surfaces of graphitic carbon nitride were modified by DMF to increase the specific surface areas. As a result, the surfaces of graphitic carbon nitride composites were modified with porous structures for enlarged surface areas.

6.1.3 Effects of nanocarbons on the physiochemical properties of g-C_3N_4

In this study, nanodiamonds and SWCNTs were employed to modify graphitic carbon nitride. After synthesis with the graphitic carbon nitride, the obtained composites still remained the metal-free merit due to the nature of the carbonaceous materials, nanodiamonds and SWCNTs. While compared to the pristine graphitic carbon nitride, the composites presented a higher performance in photocatalysis and photoelectrochemistry.

6.2 Perspectives

Photocatalysis, as a green and sustainable technology, has been widely studied by researchers. The key factor is to develop the effective photocatalysts especially with visible light response. Currently, metal oxide photocatalysts have been intensively applied. Compared to metal oxide photocatalysts, metal-free photocatalysts present more advantages, such as environmentally and ecosystem-friendly. However, the metal-free photocatalysts are suffering from low efficiency. Future study needs to focus on development of some effective novel metal-free photocatalysts based on graphitic carbon nitride to remove organic pollutants from water under UV-vis light irradiations as well as to convert and store solar energy.

Our results demonstrated a feasible strategy to obtain green, metal-free photocatalysts via surface modification and hybridization of graphitic carbon nitride. Based on this study, a variety of new metal-free photocatalysts may be discovered.

This study focused on investigation of the photodegradation of organic pollutants in aqueous solutions and potential photoelectrochemical applications using these prepared photocatalysts. In the future work, these photocatalysts may be applied in water splitting for hydrogen production, CO_2 reduction, and water oxidation.